Fatigue Resistance of Angle Shape Shear Connector used in Steel-Concrete Composite Slab

A dissertation submitted to the Graduate School of Engineering of
Nagoya University
in partial fulfillment of the requirements for
the Degree of Doctor of Engineering

By

Sung-Min CHOI

January 2011

ACKNOWLEDGEMENT

I would like to record my sincere gratitude to a number of individual who have given me help and encouragement over the period in which this dissertation was written.

Firstly, my sincere thanks go to my academic advisor, Professor Kazuo Tateishi, whose tireless supports, kind encouragement and perceptive criticism made possible the completion of this study. I wish also to express my gratitude to Professor Yoshito Itoh for his detailed comment to my research. I further extend my appreciations to Professor Minoru Kunieda and Professor Takeshi Hanji, who have read and commented on parts of this manuscript.

I am grateful to Professor Obata Makoto in Nagoya Institute of Technology for providing constructive comments and valuable time serving as my advisory committee.

I would like to extend my sincere appreciation to Dr. Daisuke Uchida, Mr. Kiyoshi Kobayashi, and Mr. Koichi Asano in Mitsui Engineering & Shipbuilding Co.,Ltd.

I am indebted to many of my colleagues in the laboratories, for their invaluable contributions throughout all phases of research.

I would like to give a particular thank to Professor Dong-Uk Lee and Professor Takeshi Mori, who gave me a precious opportunity for studying Nagoya University.

My special thanks go to my family for their loving support and encouragement.

ABSTRACT

An essential component of composite slabs is shear connection between steel bottom plate and concrete. However, the welded joint of shear connector is a possible weak point against fatigue. This dissertation investigates fatigue strength of the welded joint between angle shape shear connector and steel bottom plate in steel-concrete composite slab through fatigue tests and finite element analyses, and then proposes a simple fatigue design method. In actual composite slabs, the bond action between steel and concrete is expected. However, this study supposes the worst condition that the bond is completely lost due to the numerous repeated loads in long-term service life.

In the first part of the work, static loading tests were conducted on large-scale composite slab models with perpendicular anisotropy sections. Flexural strength and local stress behavior around angle shape shear connectors were investigated. The results revealed that the stress concentration is observed at the welded joint of angle shape shear connector due to the local bending deformation of bottom plate.

As second part of the work, fatigue strength on the welded joint of angle shape shear connector was investigated by fatigue tests. Local stress behavior around the welded joint was also identified by finite element analysis. In fatigue tests, fatigue cracks were initiated at weld toe and propagated in thickness direction. Fatigue cracks were caused by the stress concentration at weld toe due to the local bending deformation of bottom plate. In addition, the fatigue strength was assessed by using hot spot stress because it is difficult to estimate the nominal stress for the welded joint. The results presented that fatigue strength of the welded joint can be conservatively assessed by using the hot spot stress and the design curve of FAT100 recommended by IIW.

In the final part of the work, the mechanism of local stress concentration around angle shape shear connector was investigated on actual composite slab models by 3D FEA. It was confirmed that the local stress concentration at welded joints of shear connectors is considerably related to the shear stress on shear connectors. Based on the relationship between the local stress concentration and the shear stress, a simple method of fatigue assessment was suggested.

CONTENTS

LIST OF TABLES

LIST OF FIGURES

CHAPTER 1

INTRODUCTION

1.1 Background

Recently, many types of steel-concrete composite slabs have been developed and applied to long span composite bridges, which have fewer steel girders supporting a wide spanning bridge deck. The use of composite slab has been gradually increased. This tendency may be accelerated by increasing need for building bridges more economically. The composite slab consists of steel panel, concrete and reinforcements. In the steel panel, bottom plate functions as a tensile member and a formwork for concrete casting. The steel panel and the concrete are composited by shear connectors. It is well known the composite slab provides several important advantages.

- No formwork
- Lighter slab than a traditional concrete slab
- High durability, and
- High quality achieved by using steel members manufactured under controlled factory.

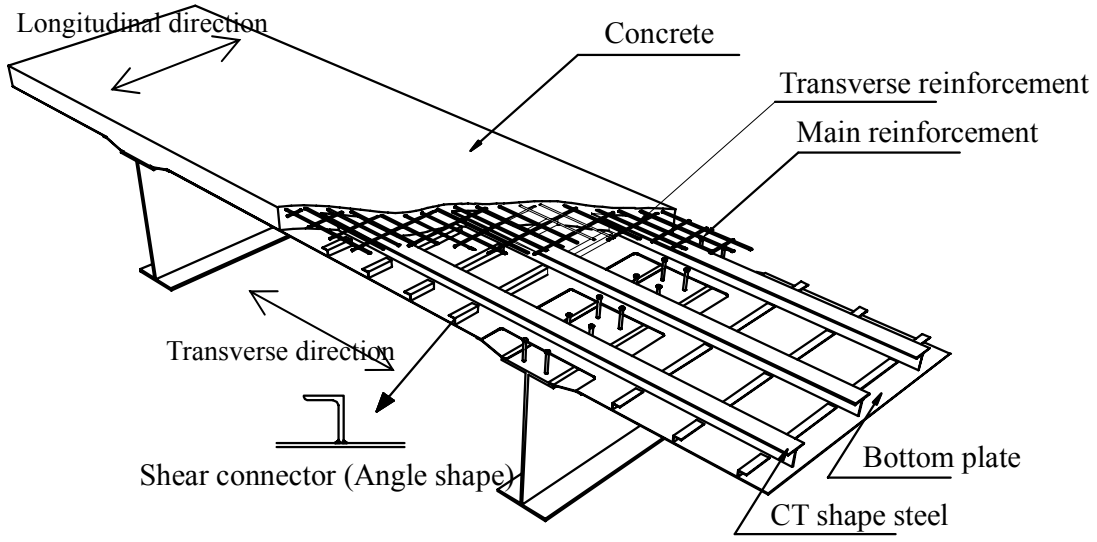

Fig. 1.1 Configuration of investigated composite bridge

There are several types of steel-concrete composite slabs proposed in Japan. Generally, the composite slab can be classified by the structure of steel panel, especially shear connector and stiffener of steel bottom plate.

Among them, this study picks up a steel-concrete composite slab shown in **Fig. 1.1**. The steel panel consists of bottom plate, CT-shape steels and angle shape steels. The bottom plate spread to entire area acts as a formwork for casting concrete and a tensile member. CT shape steels are welded on the bottom plate in transverse direction as stiffeners of bottom plate, and angle shape steels welded in longitudinal direction. The steel panel and the concrete behave together as a single body owing to angle shape steels. The advantage for using angle shape steel as shear connector is that the welding method of angle shape steel is further simple compared with stud shear connector, and the angle shape steel can act as a stiffener of bottom plate.

When a composite slab is adopted as a bridge slab, it is necessary to verify the fatigue durability because the slab is subjected to extreme cycles of traffic loading. Although composite slabs have some merits as mentioned above, mechanical behavior of the slab becomes complicated due to the interaction between steel plate and concrete. For the reason, the fatigue durability has been often examined by using a wheel trucking test in Japan. The test is carried out by loading much larger loads than actual truck wheel loads repeatedly on the slab specimen, and the fatigue durability is estimated by comparing with that of RC slab.

The Japan Society of Civil Engineers has proposed a simple formula for estimating the maximum shear stress which is primarily based on the results of wheel trucking test for some types of shear connectors. The formula has a wide application because of a coefficient which is estimated in accordance with the type of shear connector. But the foundation of the coefficient is not clear. In addition, no consideration about the local behavior of each shear connectors is included.

Some studies have been carried out for fatigue strength and shear strength of shear connectors. Unfortunately, it is difficult to apply the results to the investigated composite slab using angle shape shear connector. That will be presented in detail in the following section. Therefore, this dissertation is focused on fatigue assessment and shear strength for angle shape shear connector.

1.2 Previous research

1.2.1 Wheel trucking test on composite slab

According to the research for RC slab by Maeda et al. (1970) and Kakuta et al. (1982), in actual bridges, concrete cracks on lower surface of slab are extended to the whole slab like a grid type. As the cracks are progressed, partial concrete blocks formed by each crack are separated from the slab before the fracture of reinforcements. Whereas, in laboratory tests, radial cracks are generated below loading position, and then the fracture of reinforcements precedes the partial separation of concrete. Moreover, since the bridge deck directly supports traffic loads, the change of stress behavior with respect to moving loads has a considerable effect upon the fatigue durability.

For the reason wheel trucking test has been developed and utilized for fatigue test with full-sized slab specimens as shown in **Fig. 1.2**. The wheel trucking test is carried out under the wheel loading condition of the actual traffic vehicle while keeping a constant vertical force. In the steel-concrete composite slab, the wheel trucking test has been widely used to identify the fatigue durability as the beginning since the 1970s. The fatigue durability of composite slab proposed in Japan has been usually examined by the wheel trucking test.

Fukazawa et al. (2002) carried out the wheel trucking test on the composite slab using angle shape shear connector to clarify the performance and the applicability to

Fig. 1.2 Wheel trucking test

continuous composite steel girder bridges under moving load conditions. The results revealed that no fracture was found until 520,000 cycles under the maximum load of 392kN. Based on the results, they presented that the composite slab has sufficient fatigue durability and stiffness. On the other hand, it was observed that the bond between the steel plate and the concrete was eliminated when the load of 157kN was repeated 20,000 cycles.

1.2.2 Fatigue strength of shear connector

In composite slabs, the welded joint of shear connector is a possible weak point against fatigue. The studies on fatigue strength of shear connectors have been primarily performed on push-out shear specimens and beam specimens.

Toprac (1965) provided results of fatigue tests performed on seven steel-concrete composite beams. The 24 WF 68 steel beams and the 6 inch thick slab were connected by 1/2 and 3/4 inch diameter headed studs. The test results indicated that there is a difference (as much as 3 ksi) in fatigue strength between 1/2 and 3/4 inch studs, and the allowable stress for stud shear connectors presented in American Association of State Highway Officials (AASHO) specifications prudently could be increased by reducing the factors of safety present in use.

Slutter and Fisher (1966) were conducted fatigue tests on 35 push-out specimens with 3/4 inch stud connectors and 9 fatigue tests of push-out specimens using 4 inch×5.4lb channel connectors to examine the fatigue strength of shear connectors for steel and concrete composite beams. The test data for stud connectors were described by mathematical equations which express the fatigue life as a function of the stress range. The following equation is the result.

$$\log N = 8.072 - 0.1753 S_r \qquad (1\text{-}1)$$

where: S_r is the range of shear stress in ksi, N is the number of cycles to failure.

For the channel shear connectors, the fatigue failure was generally initiated in one of the transverse fillet welds and propagated through the weld. With the channel connectors it was obvious that the channel nearest the applied load was carrying more loads, and the fatigue failure always initiated in this connector.

Matsui et al. (1989) summarized fatigue test results on stud connectors. A multi-variable linear regression analysis was carried out to find the parameters influencing on fatigue strength. Finally, the authors found that the fatigue strength of stud connector should be expressed in the relation $R/Q_u - N$, where, R is shear force range acting on a stud connector, and Q_u is the static shear strength of the stud.

Abe et al. (1989) developed H-shape and T-shape connector and dealt with theoretical investigation of the division effect of the concrete slab, which is a variation of the rigidity of shear connectors on the stress in the slab, and the amount of slip between the slab and the upper flange of the steel girder. Also, fatigue tests were conducted on push-out specimens to develop practical flexible shear connectors. From the results, the authors presented that the flexible connectors can be applied to the shear connector.

Gattesco et al. (1997) performed low-cycle fatigue test on stud connectors. The authors assumed that the fatigue resistance of stud connector in the case of low-cycle fatigue mainly depends on the shape and amplitude of the slip history. Large-span steel and concrete composite beams subjected to repeated loads have different fatigue resistances for elastic or inelastic behavior of the connectors. The ratio between the maximum and the minimum slip is about 0.5, so that, excluding this transient phase, the slip history can be completely defined by the maximum value of the slip

Lee et al. (2005) investigated static and fatigue behavior on large stud connectors up to 30 mm diameter, which are beyond the limitation of current design codes. The results were compared with design equations. The ultimate strength of the shear connection showed that the design shear strength in Eurocode-4 and AASHTO LRFD gives conservative values for large studs. The fatigue endurance obtained from the tests was slightly lower than the current design codes in Eurocode-4.

Maleki et al. (2008) presented a study on the behavior of channel shear connectors embedded in a solid concrete material under monotonic and low-cycle fatigue loading. Material parameters of concrete were considered. The fracture mode represented the ductile behavior with a substantial displacement capacity in all specimens.

1.2.3 Shear strength of shear connector

Japan Society of Civil Engineers has proposed design rules of shear connector mainly based on stud shear connectors in Design Code for Steel Structures PART B. The limit shear strength of studs is set at 50N/mm^2 from the S-N diagrams obtained by the fatigue tests for a rotating shear force on a stud. The maximum shear force acting on shear connectors can be calculated from the following equation derived from numerical analysis by considering extreme simultaneous multiple wheel loads:

$$S = k(0.011L + 0.747)P \tag{1-1}$$

where: L is span length in meter, P is Japanese highway bridge design wheel load(98.0kN), and k is a coefficient for the type of shear connector. k is 0.5 in case of headed stud shear connector, and 1.0 when a shear connector have enough stiffness.

Matsui et al. (1986) developed an analysis model of the composite slab using stud connectors in order to estimate shear force. They assumed the steel plate and the concrete have incomplete interaction, and are bonded by stud connectors. Springs were employed in analysis where stud connectors are located. Then, the spring coefficient was estimated by coinciding with the experimental results.

Sonoda et al. (1983, 1987) estimated the shear force acting on stud shear connectors though the numerical analysis based on the elastic thin-plate theory. In the numerical model, it was supposed that steel plate and concrete are completely composited. The maximum shear force was obtained by replacing a plate with a beam. In addition, the results of numerical analysis were compared with experimental data, and a good agreement was found.

Saidi et al. (2008) investigated the relationship between transferred shear force and relative displacement on angle shape and T-shape shear connectors used in steel-concrete sandwich beam, and they developed a numerical model. In the model, the rotation at the edge of shear connectors and the horizontal movement were assumed as the boundary conditions for angle-and T-shape shear connectors.

Ros S. and Shima H. (2009) developed a new beam type test method to examine the shear force-slip relationship of angle shape shear connector. The experimental results revealed that the direction of shear force on shear connector has an effect on the shear capacity of shear connector. Moreover, the shorter shear connector caused large displacement as compared to the taller shear connector when the same level of shear force was carried.

1.2.4 Statements and problems

According to the wheel trucking test on the composite slab using angle shape shear connector, the possibility of fatigue crack occurrence on steel members is relatively low. However, if fatigue crack is generated at the welded joint of steel members in composite slabs, it is difficult to investigate the existence of fatigue crack of welded joints in service because welded joints are embedded in concrete plane. Therefore, the fatigue damage of steel members may cause the limit states of a composite slab. For the reason, engineers and researchers should pay more attention to the fatigue damage of steel members. Although endeavor has been exerted to the fatigue strength of shear connector in steel-concrete composite slabs, there are still important questions that need further investigation. Followings are some comments and discussions.

Firstly, the wheel trucking test contributes to bring a new type slab or a new technology into practical use in a short period because the test is useful to examine the comprehensive fatigue durability of a composite slab. However, in the test, since much larger wheel load than actual load is subjected to specimens by increasing the load as a step pattern to compare with fatigue durability of RC slab, the test is always quitted due to concrete damage. Therefore, even though the fatigue durability for concrete portion of composite slab can be examined by comparing with RC slab, it is not helpful to identify the fatigue durability of steel members. Also, the stress behavior of steel member can be changed by the existence of concrete damage. Therefore, in order to verify the fatigue durability of steel members, it is required to perform the wheel trucking test under the small load level which cannot lead to the concrete damage. But, it takes enormous time and cost to carry out the wheel trucking test under the small load.

Secondly, much of effort has been made by some researchers to clarify the fatigue strength of stud connector subjected to shear force, and the fatigue strength evaluation was established well. Although other types of shear connectors such as H-shape and

T-shape were studied, there has been no study that tried to indentify fatigue strength of angle shape shear connector.

Lastly, the shear connector integrating steel and concrete is directly subjected to the cyclic action by wheel load. In terms of fatigue problem, local stress concentration near shear connector is very important. However, most of the existing methods for calculating shear stress have been focused on stud connectors. Although the calculating formula of the maximum shear stress acting on shear connectors has been proposed in JSCE, it is questionable to apply the formula to the angle shape shear connector.

1.3 Research objectives

The previous section briefly introduced fatigue strength and shear strength of shear connectors used in composite slabs. The ultimate goal of this research is to develop a simple fatigue design method on angle shape shear connector, which can provide a basic data for the design of the shear connector under fluctuating load, and contribute to a rational design of the steel-concrete composite slab. **Fig. 1.3** shows the flow chart of this research.

The objectives of this study are as follow:

1) To clarify the local stress behavior around the welded joint of the angle shape shear connector, the experimental study has been conducted on large-scale plate specimens with perpendicular anisotropic sections. The validation of FE analysis has been carried out through the comparison with test results.

2) Based on the test result on large-scale plate specimen, fatigue test has been performed on push-out specimen and beam specimen to examine the fatigue strength of the angle shape shear connector.

3) To establish a simple fatigue design method for the investigated composite slab using the angle shape shear connector, endeavors should be made to clarify the relationship between HSS at welded joint and shear stress on shear connector through 3D FEA on actual composite slab model. Furthermore, to perform fatigue assessment by using the relationship, calculating methods of shear stress and bending stress has been proposed.

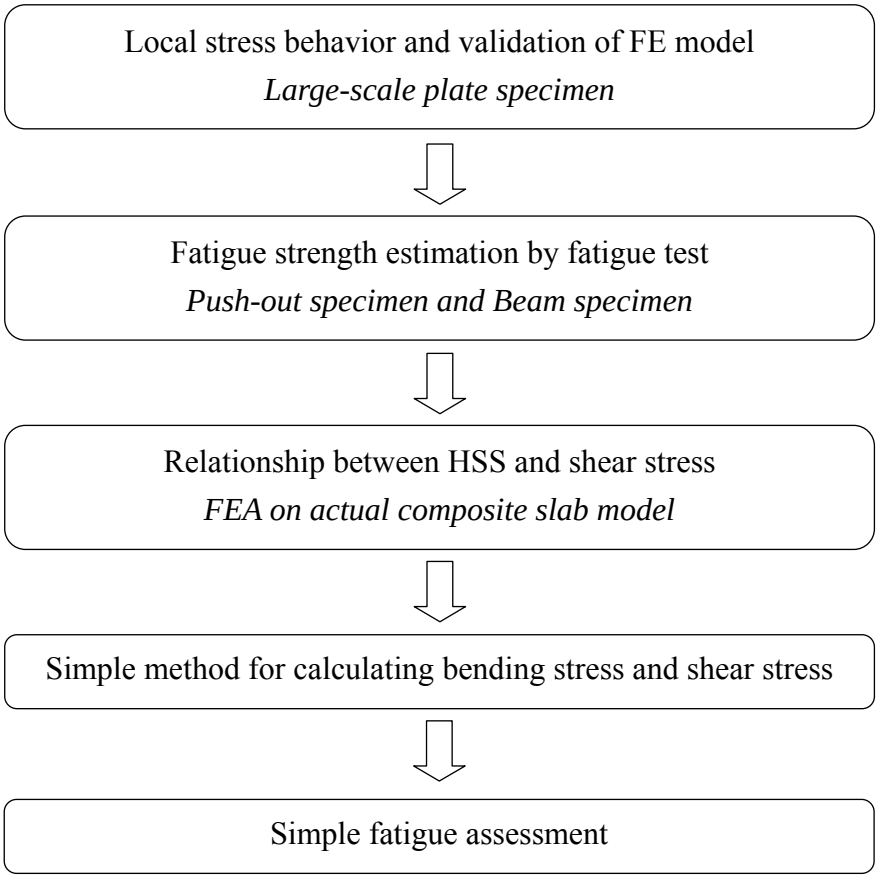

Fig. 1.3 Flow chart of this research

1.4 Structure of dissertation

In Chapter 1, background statements on the structure of composite slab using angle shape shear connector, and fatigue resistance by wheel trucking test are discussed. In addition, research objectives are mentioned and the research framework is described. Statements and problems on existing literatures for fatigue strength and shear strength of shear connector are also presented.

Chapter 2 includes the experiment and numerical study on large-scale plate specimens of composite slab. Local stress behavior and the validation for numerical analysis are examined.

Chapters 3 and 4 perform fatigue tests and numerical analysis using finite element method on push-out shear specimens and beam specimens. Fatigue damage at welded

joint of shear connector is investigated. Based on the results of fatigue test and numerical analysis, fatigue strength estimation is carried out.

Chapter 5 deals with the stress concentration mechanism around welded joints between shear connector and bottom plate through FEA on actual composite slabs. Then the relationship between hot spot stress (HSS) at welded joint and shear stress on angle shape shear connector is examined.

In Chapter 6, new calculating methods for shear stress and bending stress are presented. Finally a simple fatigue design method is proposed by applying the calculating methods to the relationship between hot spot stress and shear stress obtained in Chapter 5.

Chapter 7 presents the summaries and conclusions of this study.

CHAPTER 2

STEEL-CONCRETE COMPOSITE SLAB BEHAVIOR

2.1 Introduction

In composite slabs, it is difficult to detect fatigue cracks at welded joints at an early stage because welded joints of steel members are embedded in concrete. If the fatigue cracks occur at welded joints and penetrate bottom plate, it leads to a considerable decrement in load-carrying capacity of composite slab. Furthermore, repairing work of the fatigue cracks is not feasible due to the complicated structure. For the reasons, even though the possibility is relatively low, researchers and engineers should pay more attention to the fatigue damage of steel members.

In the investigated composite slab, a possible weak point against fatigue is the welded joint between angle shape shear connector and bottom plate. In this chapter, static test and finite element analysis (FEA) are carried out on large-scale plate specimens to verify the local stress behavior of steel members in the investigated steel-concrete composite slab. Moreover, the validation and applicability of FE model are confirmed by comparing with test results.

2.2 Test specimen and FE model

2.2.1 Test program

Large-scale plate specimens using angle shape shear connectors were manufactured and tested. Hereafter, the angle shape shear connector is called as ‘shear connector’.

Table 2.1 gives geometry dimensions of test specimens. The static test was conducted on two specimens with different interval of shear connectors for comparing flexural strength and stress behavior.

Table 2.1 Test specimens

Unit: mm

	Size	Slab thickness	Bottom plate thickness	Shear connector interval	CT shape steel interval
ST1	3,500×2,100	200	8	500	600
ST2	〃	〃	〃	833	〃

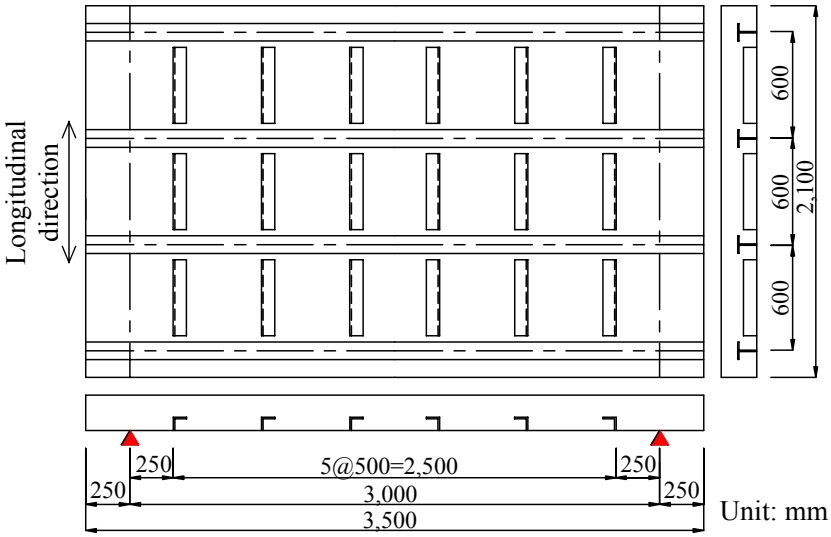

(a) ST1

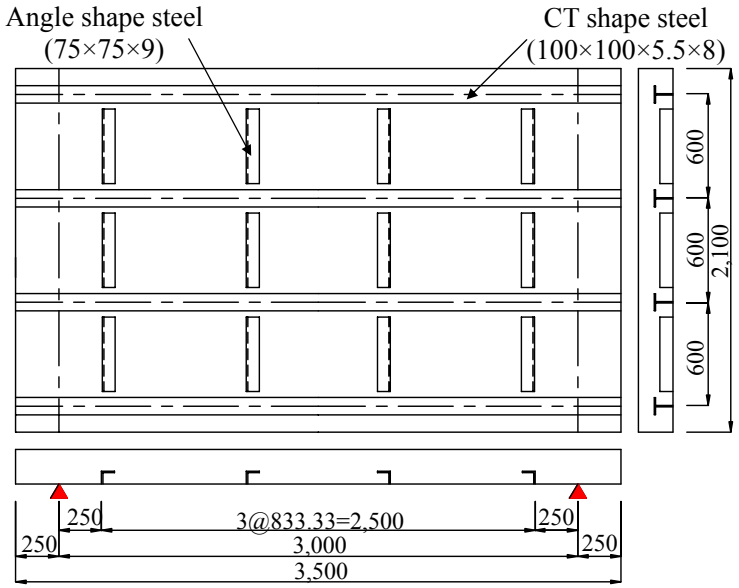

(b) ST2

Fig. 2.1 Configurations and dimensions of specimens

The configurations and dimensions of specimens are shown in **Fig. 2.1**. Three panels were designed in longitudinal direction. The specimen is 3m spanning, and the bottom plate is 8mm in thickness. Two specimens have different interval of shear connectors, 500mm and 833mm. Among them, ST1 has a typical interval of shear connectors, 500mm. Shear connectors were welded on the bottom plate in longitudinal direction and CT shape steels in transverse direction with 600mm of interval. The modulus of elasticity and compressive strength for the concrete is evaluated through compression tests. The test results of concrete are listed in **Table 2.2**, and the mechanical properties and chemical compositions of steel used in the specimens are given in **Table 2.3**.

Table 2.2 Compression test results of concrete

No.	Compressive strength (MPa)	Modulus of elasticity (MPa)	Poisson's ratio
1	36.5	3.04×10^4	0.176
2	35.9	2.67×10^4	0.188
3	36.5	2.78×10^4	0.182

Table 2.3 Mechanical properties and chemical compositions

	Mechanical properties			Chemical compositions (%)				
	Yield stress (MPa)	Ultimate strength (MPa)	Elongation (%)	C	Si	Mn	P	S
Bottom plate (SM400A)	292	445	28	0.17	0.09	0.70	0.018	0.007
Angle shape steel (SS400)	326	450	30	0.11	0.13	0.61	0.025	0.049
CT shape steel (SS400)	351	450	32	0.13	0.28	0.43	0.025	0.015

In actual composite slabs, the bond action is expected between steel and concrete. However, this study assumed the worst condition that the bond was completely lost due to the numerous repeated loads in long-term service life. This phenomenon was actually observed in the wheel trucking test on 4,500×2,800mm plate specimen when the load of 157kN was repeated 20,000 cycles (Fukazawa et al. 2002). Therefore, before casting the concrete, the remover was provided on the steel plate surfaces to eliminate the bond between the steel and the concrete. **Fig. 2.2** is the steel panel before casting concrete, and **Fig. 2.3** shows curing of concrete.

The test specimens are simply supported, and the concentrated load is applied on loading plate. The contact area is modeled as a 200×500mm^2 rectangle, which represents the contact area of a rear tire of heavy truck. A 1500kN hydraulic jack was used to apply a monotonic load at the center of plate specimen in flexural test. **Figs. 2.4** and **2.5** show an overview of test setup and loading plate, respectively.

Fig. 2.2 Steel panel (ST1)

Fig. 2.3 Curing of concrete

Fig. 2.4 Overview of test setup

Fig. 2.5 Loading plate

A number of strain gauges were applied on the inner and the outer surface of the bottom plate at the same position, and the LVDT was positioned at the mid span of specimens to monitor the vertical displacement. The arrangement of strain gauges is illustrated in **Fig. 2.6**.

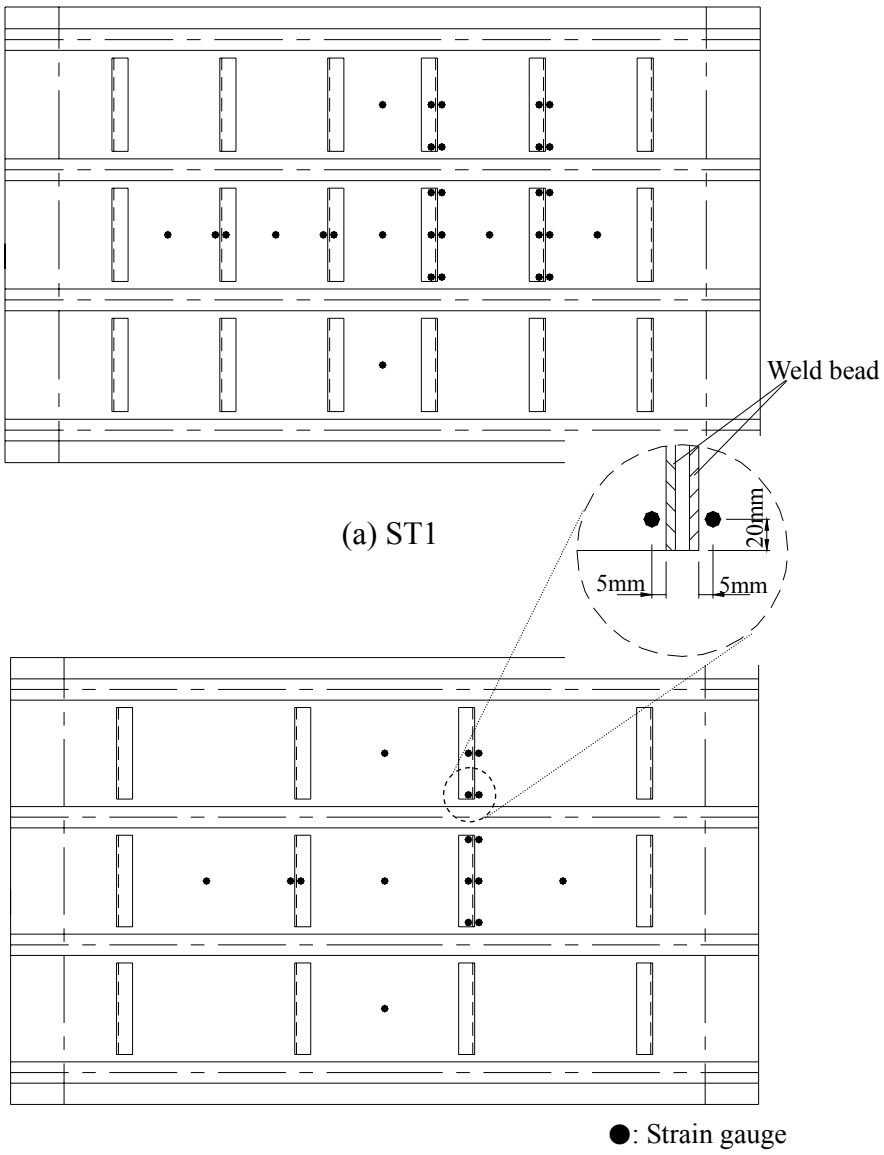

(a) ST1

(b) ST2

Fig. 2.6 Arrangement of strain gauges

2.2.2 FE model

The finite element analysis was carried out on test specimens. Analyses were carried out using ABAQUS Ver.6.7. **Fig. 2.7** gives the FE model for ST1 specimen. Taking advantage of symmetry, a quarter model was created. Solid element was employed to model not only the concrete plane but also steel members in order to create the weld bead of welded joint. In the present FE models the mesh was mainly determined to calculate the local stress of steel members. Even though the mesh size is limited around welded joints due to the specimen size and the analyzing time, it is enough to indentify the local stress behavior near the welded joint of shear connector. The minimum mesh size is 2.0×2.0×3.2mm. The contact condition was applied to the interface between the steel and the concrete so that they could behave separately.

The modulus of elasticity of steel material was applied as 206,000MPa, and the Poisson's ratio was assumed as 0.3. Yield stresses for each steel member were used the measured values listed in **Table 2.3**.

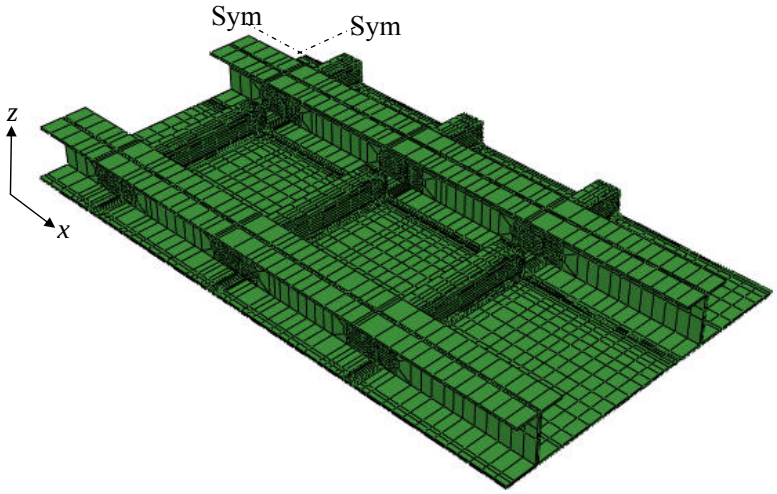

(a) Steel members

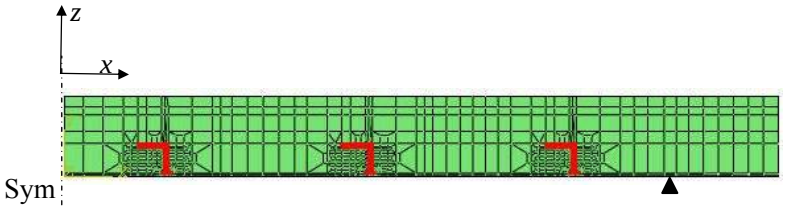

(b) Cross section of slab

Fig. 2.7 FE model

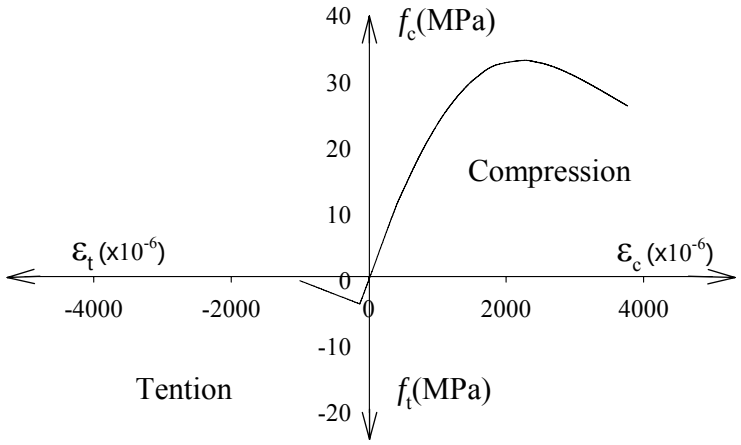

Fig. 2.8 Stress-strain curve for concrete

Concrete material properties were determined based on the results of cylinder compression tests. The modulus of elasticity and Poisson's ratio were assumed 28,300MPa and 0.182, respectively. The values are the average of three test results. **Fig. 2.8** indicates the stress-strain curve of concrete material.

The stress-strain equation suggested by Carreira and Chu has been employed to model the elastic-plastic material characteristics of concrete with strain softening as following:

$$f_c = \frac{f_c' \beta \left(\frac{\varepsilon}{\varepsilon_c'} \right)}{\beta - 1 + \left(\frac{\varepsilon}{\varepsilon_c'} \right)^{\beta}} \tag{2-1}$$

where f_c is the compressive stress in concrete, ε_c is the strain in concrete, f_c' is the compressive strength of concrete, ε_c' is the strain corresponding f_c',

$$\beta = \left(\frac{f_c'}{32.4} \right)^3 + 1.55 \tag{2-2}$$

2.3 Test and FEA results

2.3.1 Local stress behavior

Figs. 2.9 and **2.10** represent the stress distributions on bottom plate in *y*-direction when the load is applied at the center of plate specimen. The stresses were measured at 5mm away from the center-side weld toe.

It can be seen that there are stress differences between FEA and test results, especially beyond 300kN. This may be strongly relevant to the existence of concrete crack around shear connectors. According to the test results mentioned later, concrete cracks generated from the edge of shear connectors were observed. It means that these FE models cannot simulate the real concrete cracks correctly. Moreover, the stress and strain of concrete are influenced by the mesh size and shape, but in the present FE models the mesh was mainly determined to calculate the local stress of steel members.

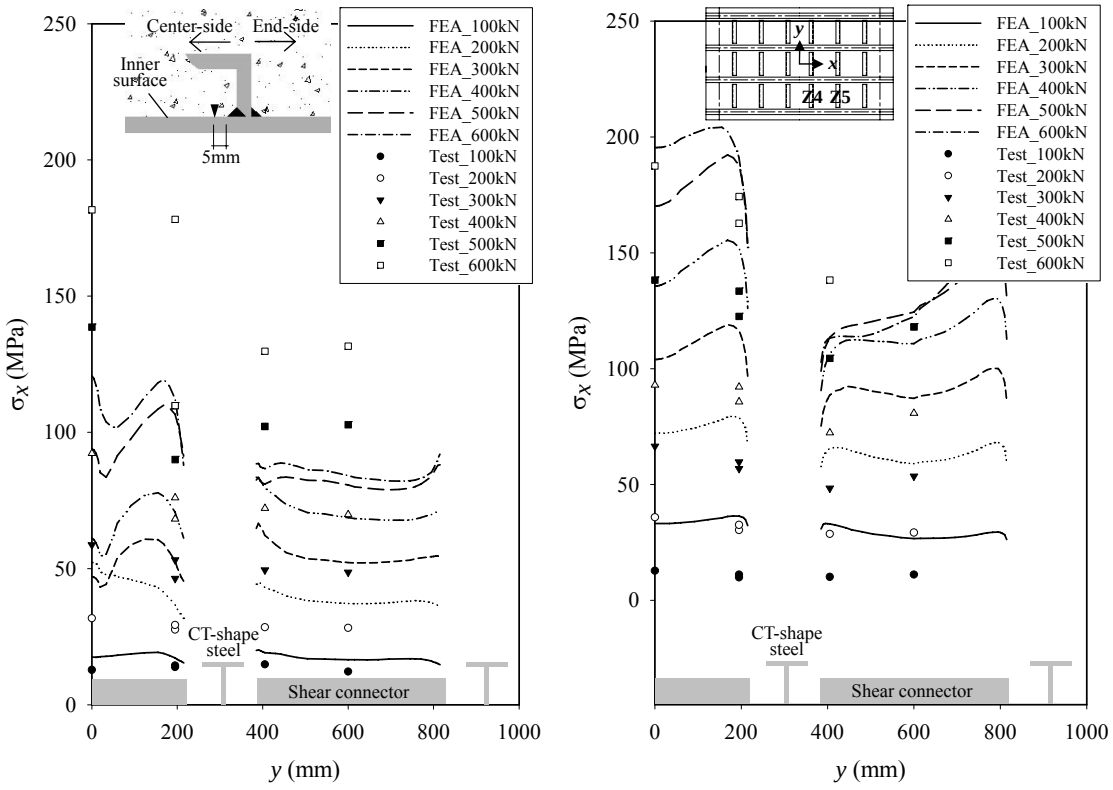

(a) near Z4 (b) near Z5

Fig. 2.9 Stress distributions on bottom plate in *y*-direction (ST1)

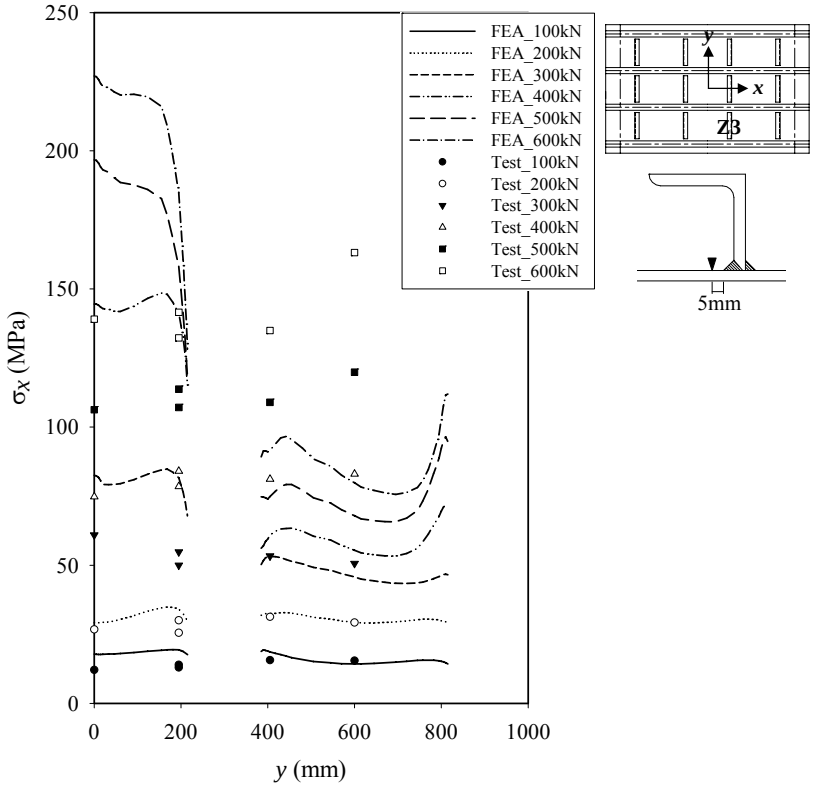

Fig. 2.10 Stress distributions on bottom plate in *y*-direction (ST2_near Z3)

In fabricating test specimen, the remover was provided on the interface between steel and concrete to simulate the no bond condition. But, it is not certain whether the bond was completely lost. Therefore, the bond condition between steel and concrete is also a possible reason of the stress difference between test and FEA results. However, below the load of 300kN, a relatively good agreement between FEA and test results can be seen. The single truck load is 100kN.

Fig. 2.11 gives the stress distribution on bottom plate in *x*-direction along the center of model (symmetric surface for *x*-*z* plane in **Fig. 2.7**) when the load of 300kN is applied at the center of specimen. Stress is suddenly changed near shear connectors except *Z*4 connector. On the inner surface contacting with the concrete, stress is sharply increased near the center-side weld toe, and suddenly decreased at the end-side weld toe. In addition, the symmetrical distribution can be seen on the outer surface of bottom plate. This unique behavior is originated by the local bending deformation of the bottom plate around the shear connector. The stress near weld toe varies very sharply, so, the measured results are very sensitive to gauge position. So, it should be noticed the test results include some errors. In ST2, the same stress manners can be observed as shown in **Fig. 2.12**. Under the other loads, similar phenomenon was also observed, and the

results were summarized in Appendix A.

From the above results, it can be found that the stress manners of FEA are almost consistent with that of tests, and the stress values of FEA and test are in good agreement below the load of 300kN. Therefore, it can be said that the FE analysis simulates well the nature of the local stress behavior below the load of 300kN in this plate specimen. Considering that the single truck load is 100kN, this FE model is useful to simulate the investigated composite slab in terms of fatigue problem.

Fig. 2.13 shows an example of the deformed shape and stress contour around the shear connector under the load of 300kN. The stress concentration is observed at the center-side welded toe due to the local bending deformation.

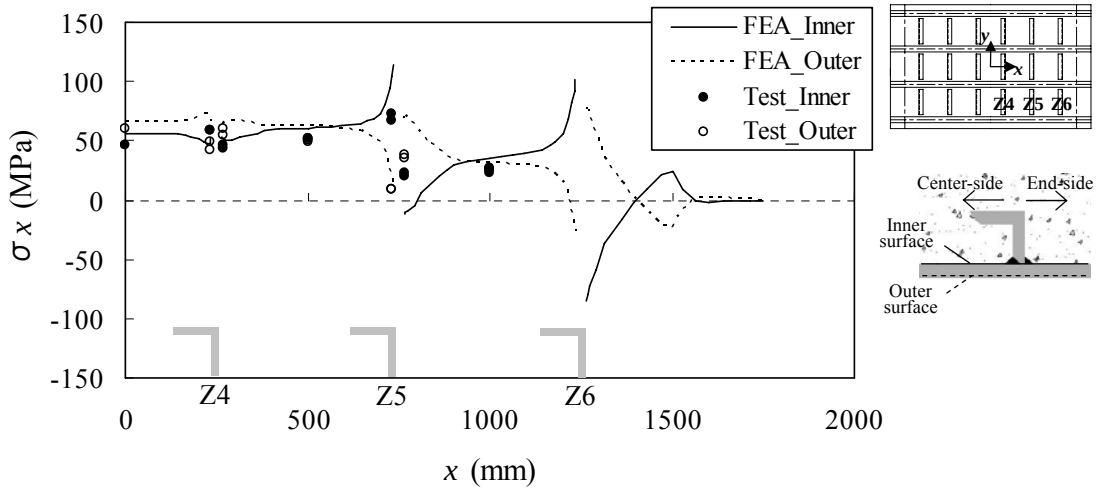

Fig. 2.11 Stress distribution on bottom plate in *x*-direction (ST1)

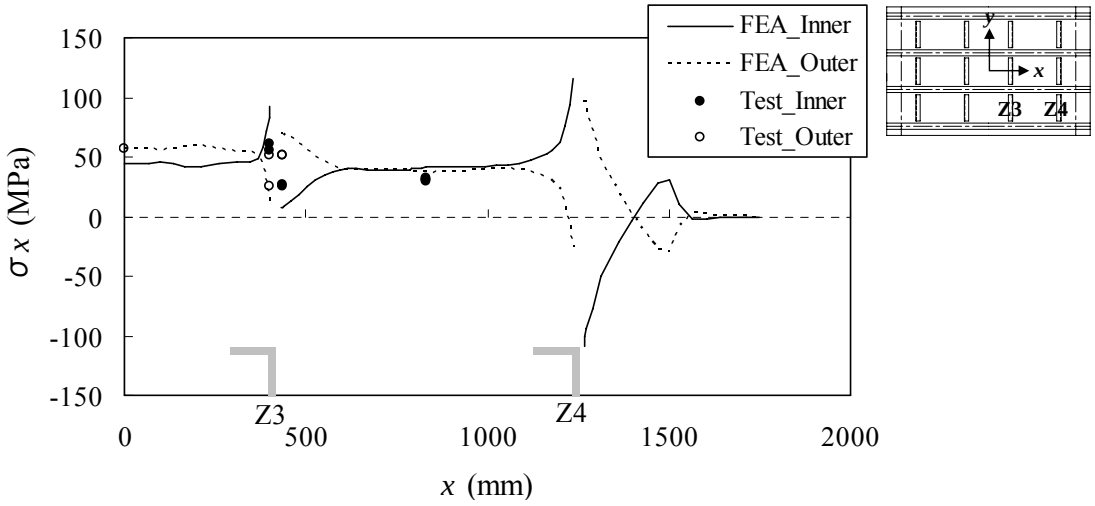

Fig. 2.12 Stress distribution on bottom plate in *x*-direction (ST2)

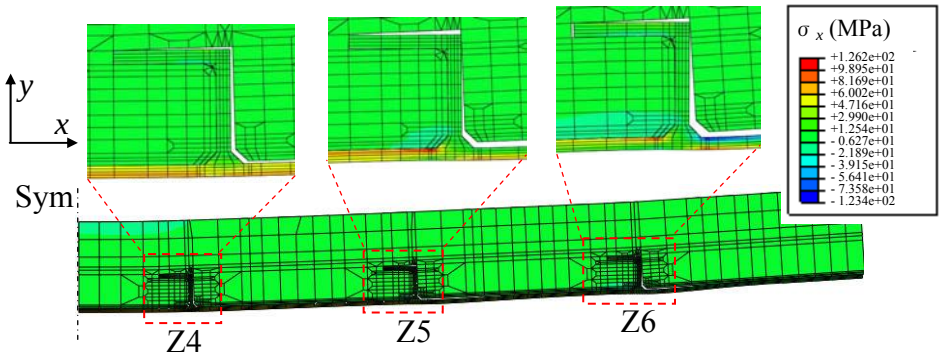

Fig. 2.13 Deformed shape and stress contour (×10)

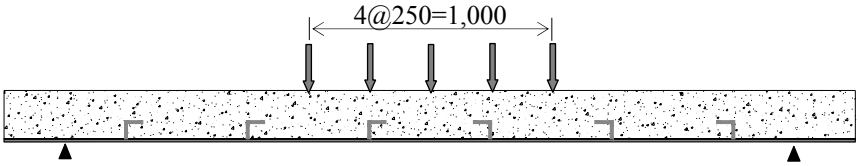

Fig. 2.14 Load cases

Unit: mm

2.3.2 Effect of loading position

In order to identify the local stress behavior in detail, the effect of loading position was investigated on both specimens by changing the loading position in 5 places as shown in **Fig. 2.14**. To prevent the concrete damage, the test was carried out with the small load of 100kN for all cases. The results were summarized by influence lines for local stresses. The stresses were measured at 5mm apart from the center-side and end-side weld toe. **Fig. 2.15** shows the influence lines in ST1. Firstly, taking attention to the stress at center-side of Z4 (**Fig.2.15 (a)**), the maximum stress occurs when the load is placed near Z3, and the stress decreases as the load is moved to the target connector (Z4). This is due to the fact that when the load is located just over the target shear connector, the vertical force acts dominantly to the shear connector compared with the shear force. The stress at the end-side represents the opposite trend. On Z5 connector, a similar phenomenon can be observed (**Fig. 2.15 (b)**). In contrast, the stress at the mid-span becomes the maximum value in the mid-span loading (**Fig. 2.15 (c)**). For other shear connectors, similar behavior was observed. Also, the same stress manner can be seen in ST2 as shown in **Fig. 2.16**. This local stress characteristic will be discussed in detail in Chapter 5. On the other hand, in the **Fig. 2.15 (c)** the design bending stress of plate specimen is 25.2kN for target position when the load is placed at mid-span. In contrast, the measured value for target position is 14.4MPa. This is strongly related to the bond condition between steel and concrete. The design bending stress was estimated under the condition of complete composite, while the bond was eliminated in plate

specimens. As mentioned later in chapter 5, in the no-bond condition, the bending stress of bottom plate between shear connectors is underestimated compared with the theory value.

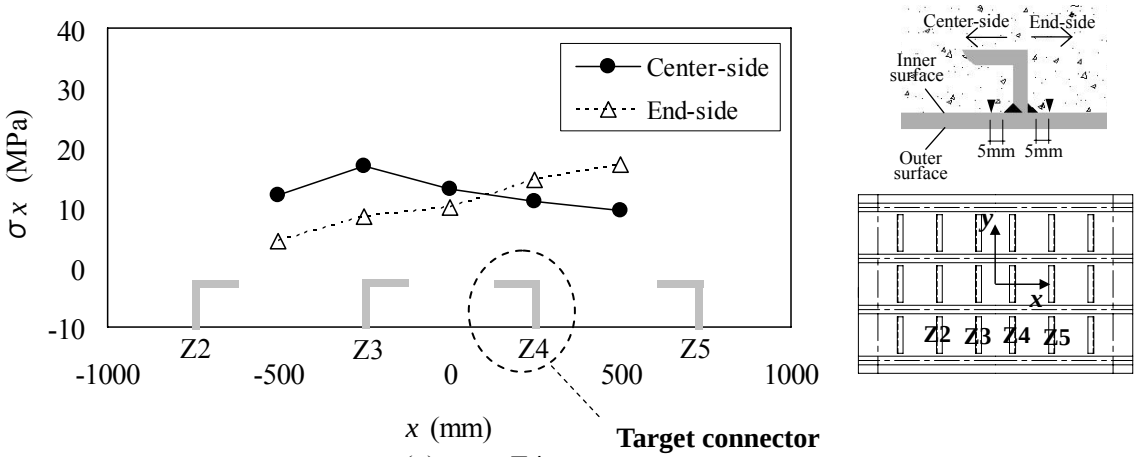

(a) near Z4

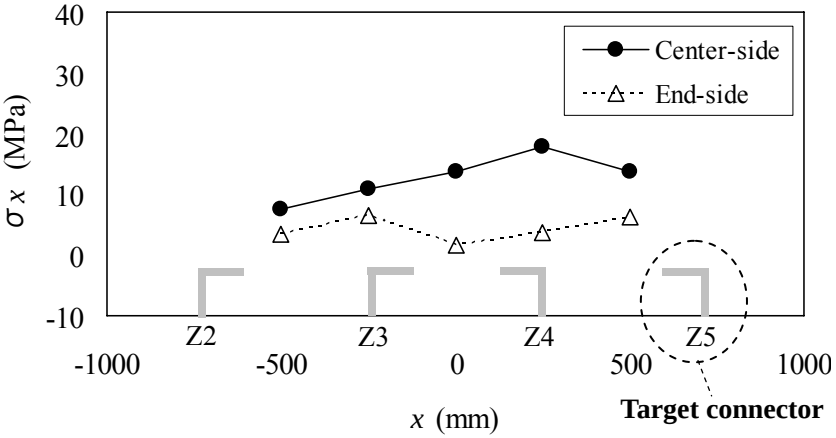

(b) near Z5

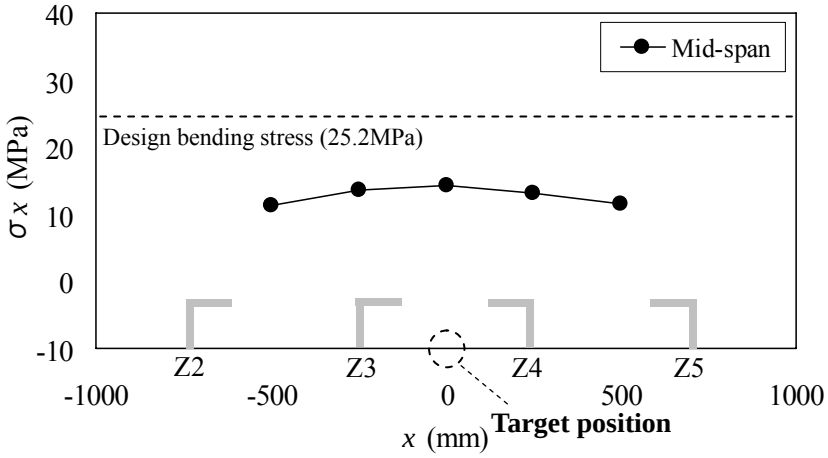

(c) at mid-span

Fig. 2.15 Influence lines (ST1)

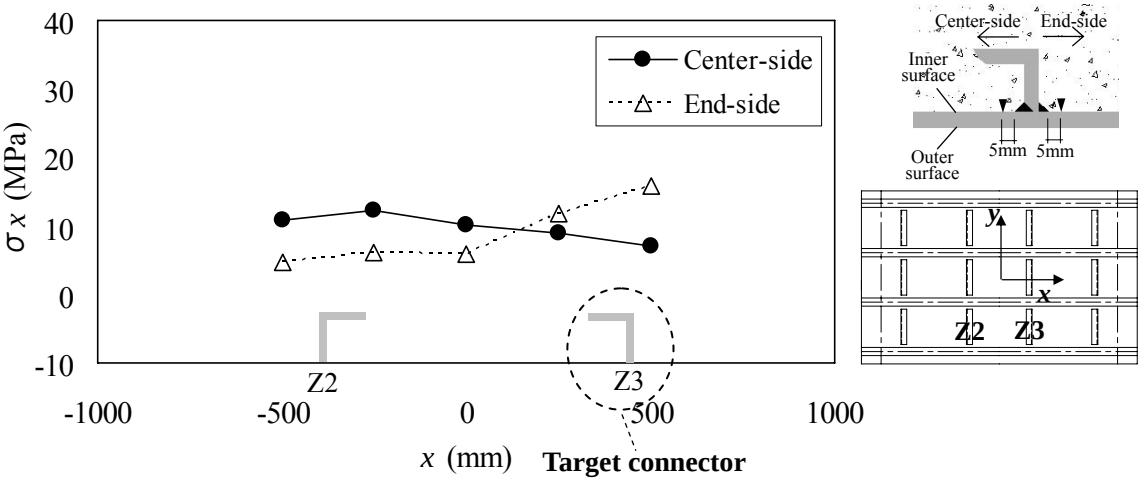

(a) near Z3

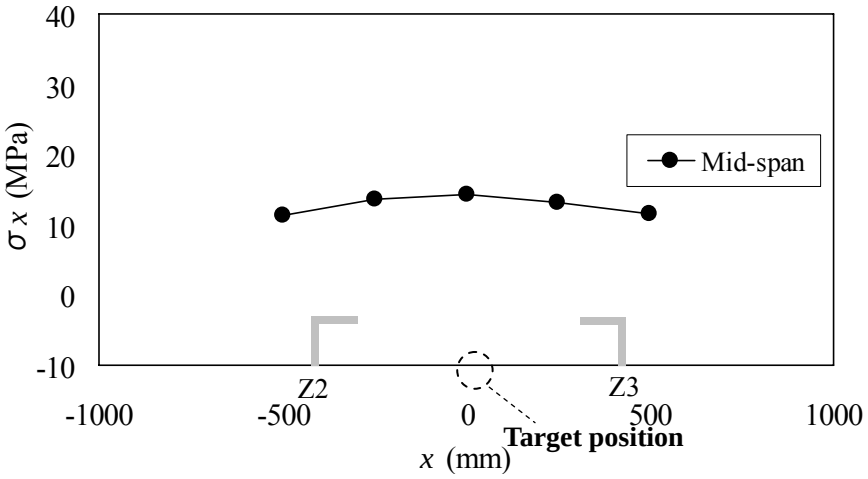

(b) at mid-span

Fig. 2.16 Influence lines (ST2)

2.4 Flexural strength

2.4.1 Load-deflection response

The comparison of the flexural strength for two specimens was carried out to investigate the effect of the interval of shear connectors. As mentioned previous section, the interval of 500mm in ST1 is a typical dimension in the investigated composite slab. The interval of shear connectors in ST2 is 833mm. Load-deflection curves obtained from static tests are represented in **Fig. 2.17**. In both specimens, deflection at center of slab increases linearly until 600kN, and then the specimens begin yielding. On the side surface of specimens, concrete cracks were observed around 600～900kN as show in **Fig. 2.18 (a)**. The cracks were initiated in the flexure zone and propagated towards the upper surface of slab, and then concrete fracture was observed near loading plate at 1050kN in ST1 and 1120kN in ST2 as shown in **Fig. 2.18 (b)**.

The design fracture load corresponding to the 3.0m spanning and 200mm of slab thickness is 760kN. This load was calculated by assuming the composite slab as a RC slab. CT shape steel and shear connector were excluded in the sectional area. In addition, the specimens were designed by supposing the worst condition that the bond between steel and concrete is lost. Therefore, it can be said that these composite slabs have enough flexural strength.

In both specimens, not only the fracture load but also the response manners are almost similar. Therefore, in terms of flexural strength, there is a possibility to diminish the number of shear connectors.

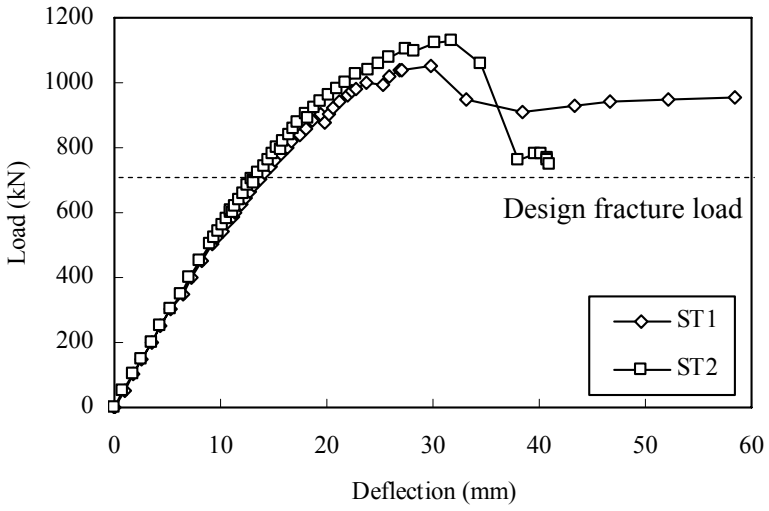

Fig. 2.17 Load-deflection curve

(a) Side surface of slab (ST2) (b) near loading plate

Fig. 2.18 Overview of concrete damage

2.4.2 Mode of failure

Fig. 2.19 illustrates the cracks on the exterior surfaces of concrete in ST1 and ST2 when the slab was fractured. As mentioned previous section, cracks initiated from the bottom of concrete were firstly observed about 600kN and propagated with increase of load, but the crack propagation was delayed about 900kN as shown in **Fig. 2.18 (a)**. After that, concrete cracks were observed near the edge of CT-shape steel, and then propagated toward the loading position near the fracture load.

In this type of composite slab, the main stiffener of bottom plate is CT-shape steel. Therefore, if the concrete plane loses its resistance, the applied load is transferred to the CT-shape steel directly. Therefore, it is considered that when concrete cracks are generated near the edge of CT-shape steel, the concrete plane has lost its durability.

After cutting the specimens, the interior cracks state of concrete was investigated as shown in **Figs. 2.20 and 2.21**. From the figures, it can be found that the composite slabs were fractured due to the punching shear failure which is the supposed failure mode of design. Generally, in case of that the sudden punching shear failure occurs, the load quickly drops in load-deflection response. However, according to the **Fig. 2.17**, this type of composite slab reveals somewhat ductile behavior due to the steel panel.

On the other hand, concrete cracks were also observed near shear connectors. The cracks were initiated from the edge of shear connectors and propagated toward the loading position. But the crack propagation delayed around reinforcements. Although the cracks did not affect directly to the fracture of composite slabs, which can be a further critical damage under fluctuating load than the punching shear failure.

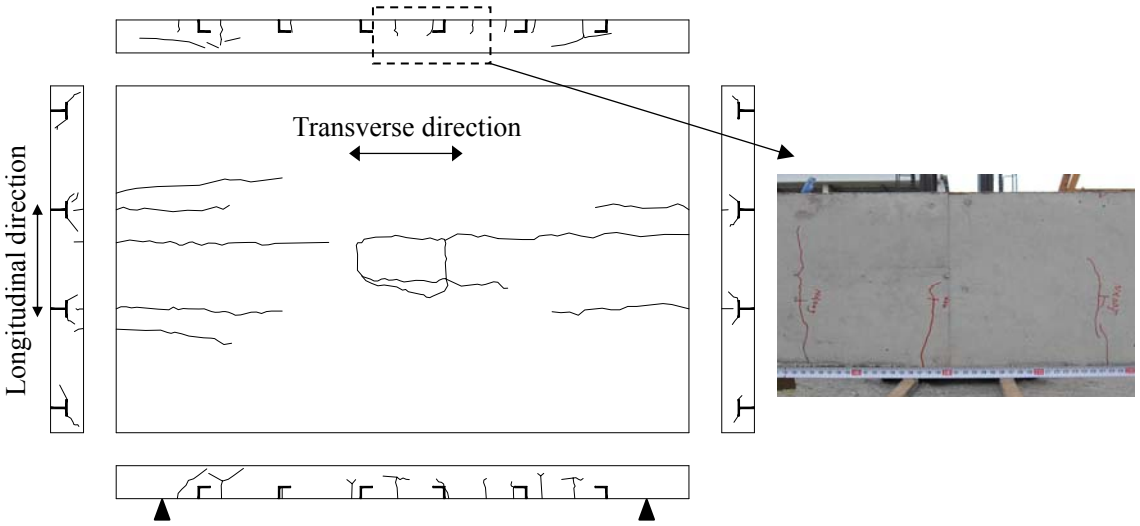

(a) ST1

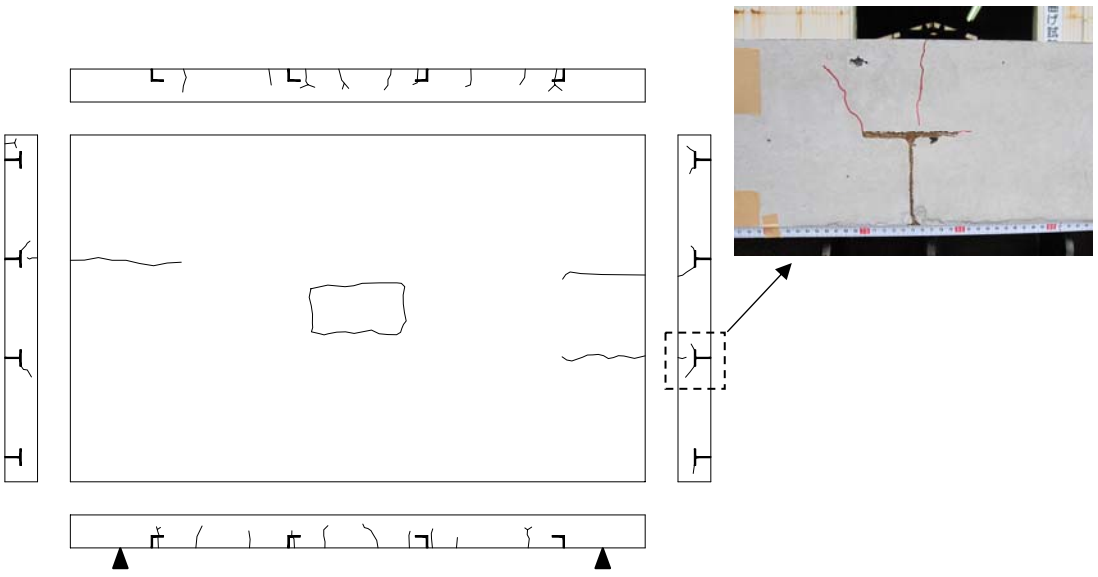

(b) ST2

Fig. 2.19 Exterior crack state

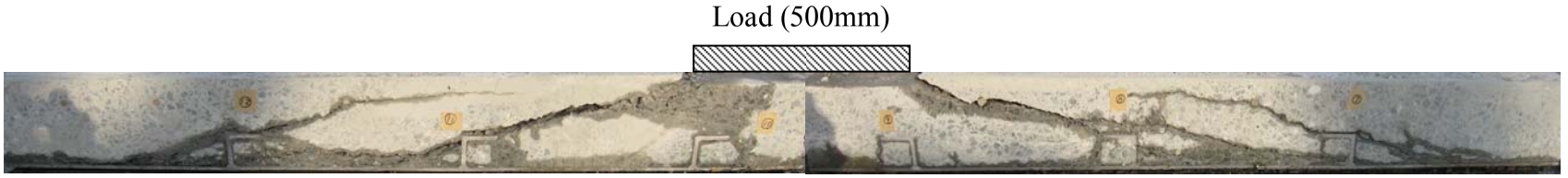

a) A-A section

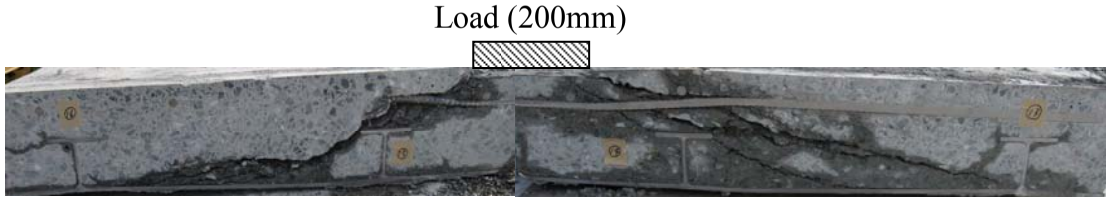

b) B-B section

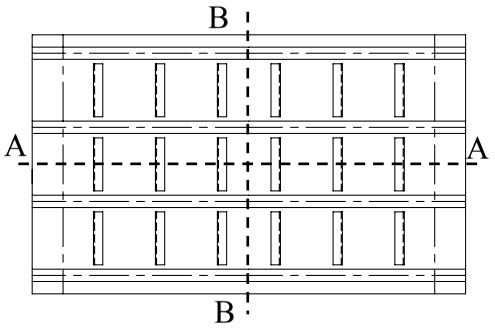

Fig. 2.20 Interior crack state (ST1)

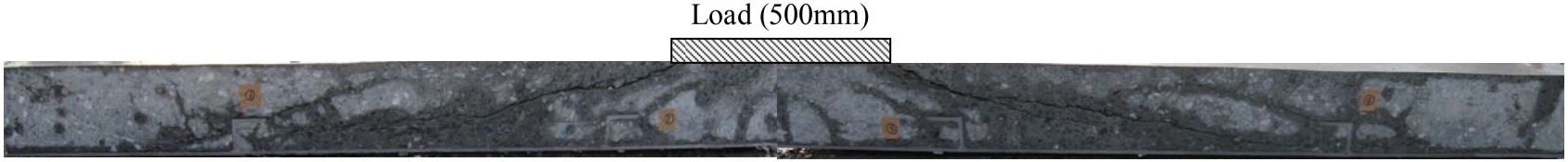

a) A-A section

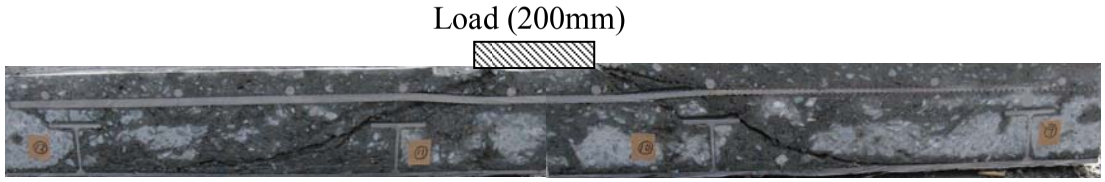

b) B-B section

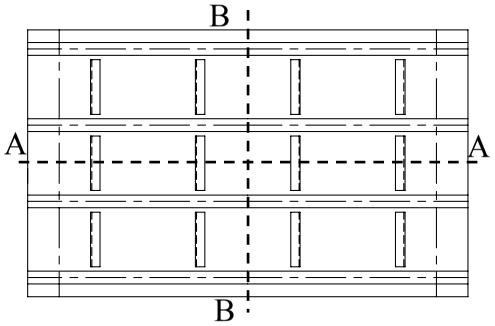

Fig. 2.21 Interior crack state (ST2)

2.5 Concluding remarks

In this chapter, the local stress behavior on the investigated steel-concrete composite slab was examined on large-scale plate specimens by static test and FEA. In addition, the effect of the interval of shear connectors to flexural strength was examined. The test and FEA were carried out under the assumption that the bond between steel and concrete is lost completely.

Following conclusions can be drawn:

1) The test and FEA results revealed that the stress concentration occurs at the welded joint due to the local bending deformation of bottom plate around welded joints of shear connectors.

2) Below the load of 300kN, a relatively good agreement between FEA and test results was identified. Since the single truck load is 100kN, it can be said that this FE model is useful to simulate the investigated composite slab in terms of fatigue problem.

3) The fracture loads of two specimens with different interval of shear connectors were almost same level as 1050kN and 1120kN, respectively. Stress behavior and fracture mode were also similar. It means that there is a possibility to extend the interval of shear connectors in terms of flexural strength.

4) Composite slabs were fractured by the punching shear failure of concrete plane. On the other hand, concrete cracks initiated from the edge of shear connectors were also observed. Even though the possibility is low that this like concrete crack occurs in actual composite slab under the service load, and the cracks had no direct influence to the fracture of large-scale plate specimens, the concrete cracks generated from the edge of shear connector can be a severe damage of composite slab against fatigue problem.

CHAPTER 3

FATIGUE TEST ON PUSH-OUT SHEAR MODEL

3.1 Introduction

The preceding chapter has provided FEA and test results on large-scale plate specimens. According to the results, the stress concentration appears near welded joints of shear connectors due to the local bending deformation of bottom plate. It means the welded joint is a potential weak point against fluctuating load. Therefore, it is needed to indentify the fatigue strength of the welded joint of shear connector. But, it takes enormous time and cost to carry out the wheel trucking test on a large-scale plate specimen under the small load level which cannot cause concrete damage.

Fig. 3.1 illustrates the load condition around shear connector in the investigated composite slab. Since the shear force is subjected to the shear connectors in transverse direction due to the deflection of slab, the effect of load position in longitudinal direction is small. Therefore, without performing the wheel trucking test on large-scale plate specimen, it is possible to identify the fatigue strength through the fatigue test on small-scale specimens which can simulate the local stress behavior around shear connector. The direction of shear force can be changed as S_1 and S_2 in **Fig. 3.1** by the loading position. In this study, however, fatigue strength of shear connector is examined for only S_1 because S_1 is considerably dominant in case that the maximum deflection is generated at mid-span.

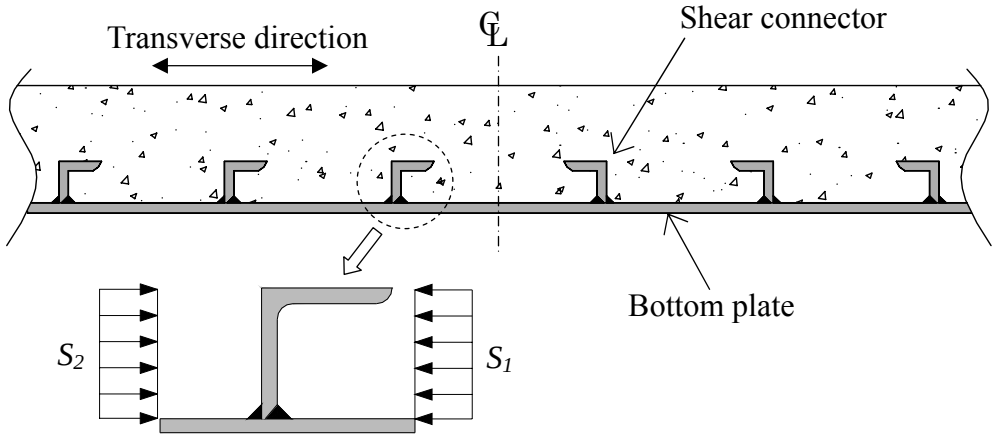

Fig. 3.1 Load condition around shear connector

Unfortunately, there has been no study that tried to verify the fatigue strength on such kind of shear connector. Therefore, regarding the load condition around shear connector, fatigue tests are performed on push-out specimens. In addition, the estimation method of fatigue strength is also examined in this chapter.

3.2 Static loading test and FEA

3.2.1 Test program

The configurations and dimensions of the specimen for push-out shear test are shown in **Fig. 3.2**. The bottom plate was 8mm in thickness. Single shear connector (75×75×9mm) was attached to the bottom plate by fillet weld through the whole cross section. Two specimens were connected together with loading ribs welded on the bottom plate. The specimens were subjected to compressive load by pushing the loading beam put on the top of the specimens. In order to apply the load uniformly, plaster was placed in the gap between specimens and the base plate, as well as rubber plate was inserted between specimens and loading beam. PC tendons connected the lower parts of

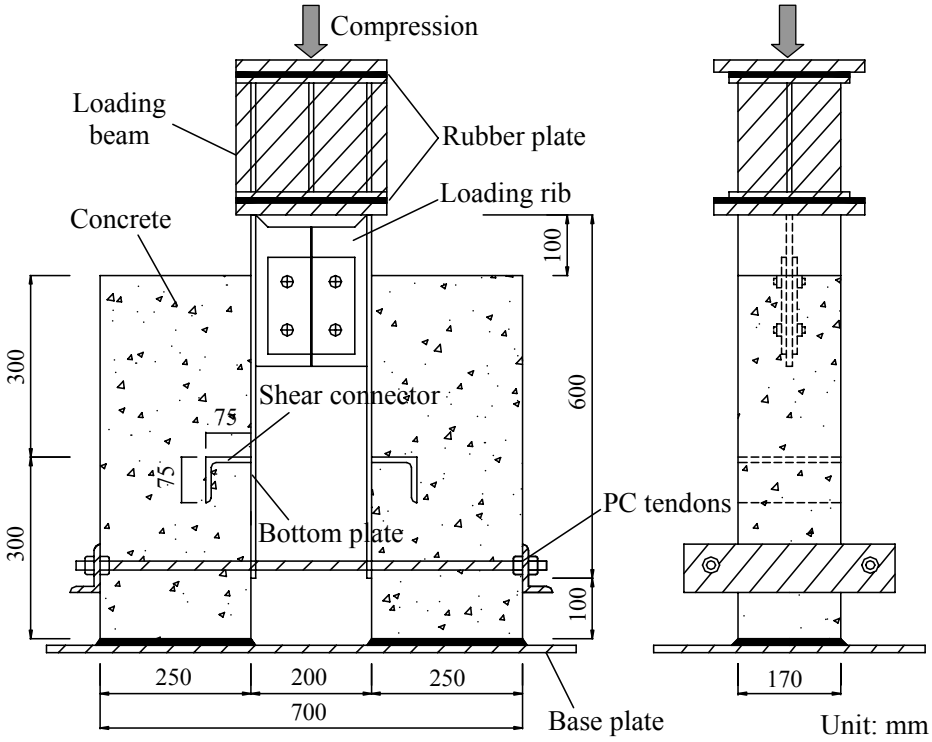

Fig. 3.2 Configurations and dimensions of specimen

the specimens to constrain the horizontal movement.

In the same way as large-scale plate specimen, push-out specimens were manufactured by assuming the worst condition that the bond was completely lost due to the numerous repeated loads in long-term service. The remover was used to eliminate the bond between steel and concrete. During casting concrete, the material was poured from the top of the specimen with following the actual construction process. Before casting the concrete, the remover was provided on the steel panel surfaces. The mechanical properties and chemical compositions of steel used in the specimens are given in **Table 3.1**. The compressive strength, modulus of elasticity, and Poisson's ratio for the concrete are evaluated through compression tests. The test results are listed in **Table 3.2**. **Fig. 3.3** illustrates the arrangement of strain gauges. Electrical-resistance strain gauges were attached on shear connector and outer surface of bottom plate, and the LVDTs were positioned under the loading rib of the specimen to monitor the relative slip between the steel and the concrete.

Table 3.1 Mechanical properties and chemical compositions

	Mechanical properties			Chemical compositions (%)				
	Yield stress (MPa)	Ultimate strength (MPa)	Elongation (%)	C	Si	Mn	P	S
Steel plate (SM400A)	302	452	28	0.15	0.16	0.86	0.018	0.003
Angle shape steel (SS400)	294	420	31	0.09	0.11	0.49	0.020	0.042

Table 3.2 Compression test results of concrete

No.	Compressive strength (MPa)	Modulus of elasticity (MPa)	Poisson's ratio
1	33.4	2.75×10^4	0.221
2	32.7	2.76×10^4	0.202
3	32.0	2.75×10^4	0.237

Fig. 3.4 gives manufacturing process of push-out specimens. Firstly shear connector was welded on bottom plate, then before casting concrete strain gauges were attached on inner surface, and grease was provided on steel plate as explained previous above. Finally, concrete was casted.

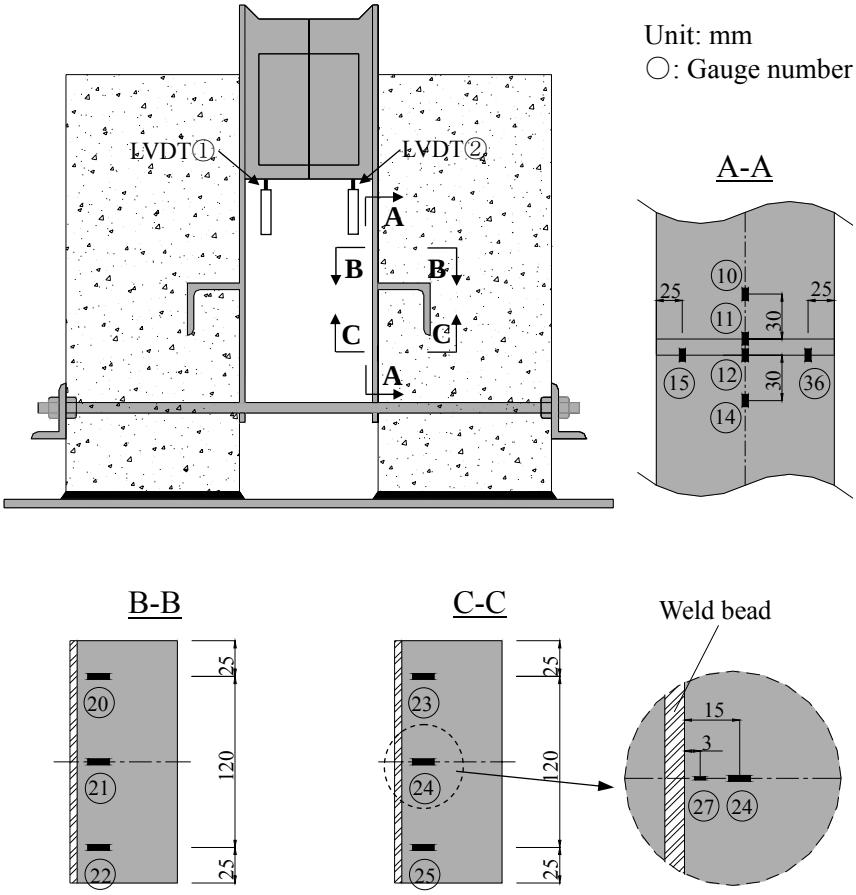

Fig. 3.3 Arrangement of strain gauges

(a) Attaching gauges

(b) Form working

(c) Curing concrete

(d) Finishing each specimen block

Fig. 3.4 Manufacturing process of specimen

3.2.2 FE model

The finite element analysis on the test specimen was conducted in order to identify the stress behavior around the welded joint. ABAQUS Ver.6.7 was used. **Fig. 3.5** gives an example of FE model. Due to the symmetry of the cross-sectional geometry and of the boundary conditions, only one quarter of the specimen was modeled. The eight-node brick elements were employed to model the concrete and steel members. In the same way as large-scale plate model, contact condition was assigned on the interface between the steel and the concrete so that they could behave separately. The tangential friction between them was ignored. The bottom of the specimen was constrained completely, and a compressive load was applied on the top of the specimen. PC tendons for tying the specimens were not modeled.

The modulus of elasticity of steel material was applied as 206,000MPa, and the Poisson's ratio was assumed as 0.3. Concrete material properties were determined based

on the results of cylinder compression tests. The modulus of elasticity and Poisson's ratio were assumed 27,500MPa and 0.220, respectively. The values are the average of three test results listed in **Table 3.2**.

In Chapter 2, the FEA on large-scale specimens has been tried to simulate concrete damage. However, the results revealed that it is difficult to demonstrate the concrete damage in the investigated composite slab due to the concrete meshing problem and the presence of contact problem. Moreover, the stress behavior of steel member was significantly influenced by the concrete damage. From the test results described later, concrete damage was not observed under loads of 120kN and 160kN at static test. Therefore, the concrete material was simplified by increasing tensile strength of concrete in FE models on push-out specimens. The stress-strain curve for the concrete was taken as indicated in **Fig. 3.6**.

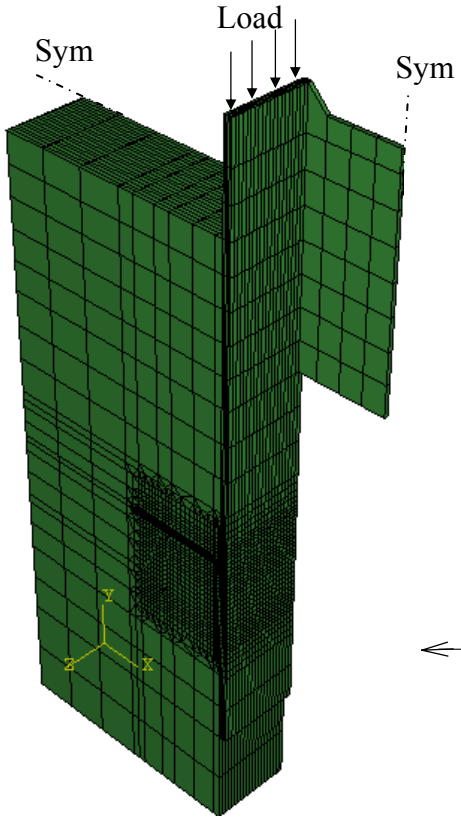

Fig. 3.5 FE model

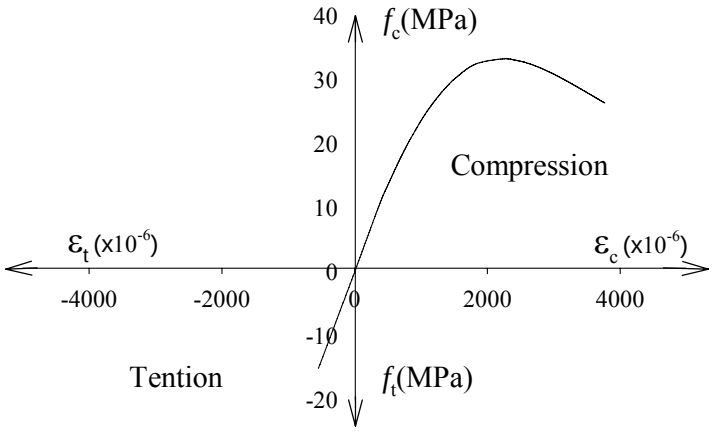

Fig. 3.6 Stress-strain curve for concrete

3.2.3 Test and FEA results

Fig. 3.7 shows the stress distributions on bottom plate in *x*-direction along the three reference lines noted in the figure when the compressive load of 150kN was loaded to a pair of specimens. The stresses were measured at three positions near the welded joint. The stresses are almost uniform in horizontal direction. Therefore, it can be said that the stress turbulence generated by loading ribs has no influence on the stress behavior around the welded joint.

Fig. 3.8 shows the stress distribution on the bottom plate in *y*-direction along the centerline. Lines and marks indicate the analysis results and the measured test results, respectively. Both results are in good agreement. Stress is suddenly changed near the shear connector. On the inner surface contacting with the concrete, high compressive and tensile stress are generated at the end-side and the center-side weld toe, respectively. The symmetrical distribution can be seen on the outer surface, but the absolute stress value of the outer surface is less than that of inner surface. This unique behavior is originated by local bending deformation of the bottom plate around the shear connector. **Fig. 3.9** represents the deformed shape of the bottom plate around the shear connector obtained by FEA. The stress concentration is observed at the weld toe due to the local bending deformation. The stress distribution on shear connector is given in **Fig. 3.10**. Although the stress on upper and lower surface represents also symmetrical distribution, the absolute value is less than the stress on bottom plate. It means that the weld toe on the bottom plate becomes further critical condition when the shear connector is subjected to shear force.

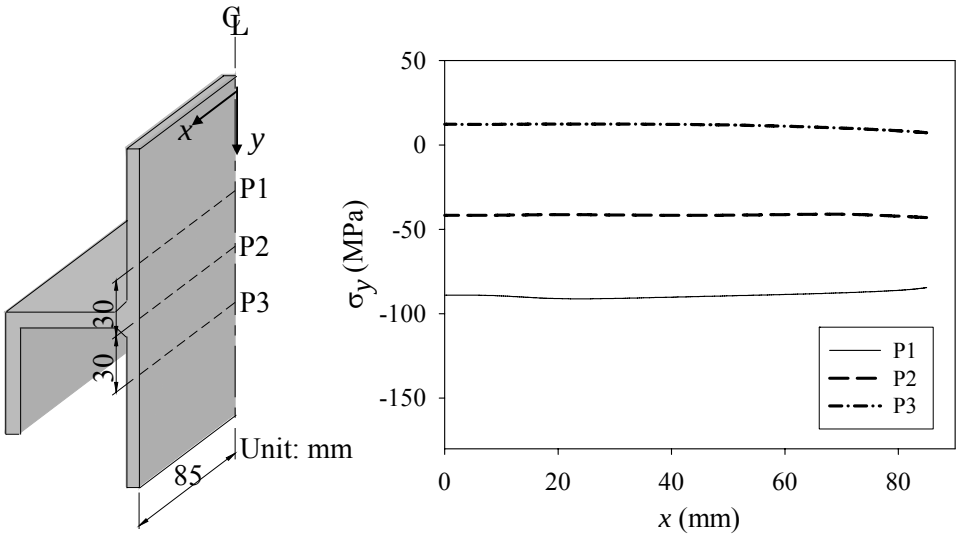

Fig. 3.7 Stress distribution of bottom plate in *x*-direction

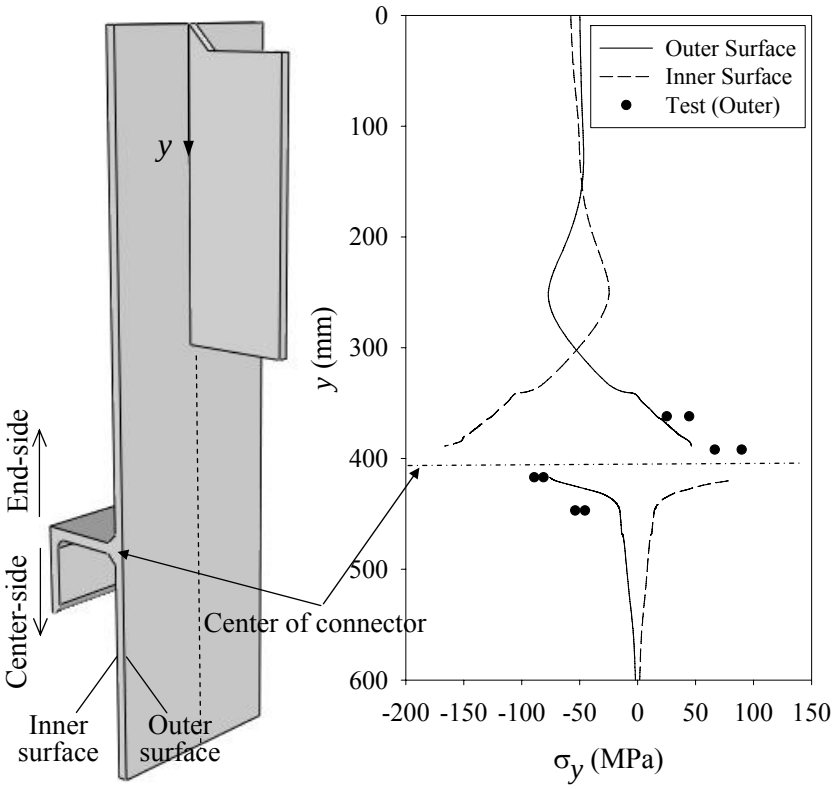

Fig. 3.8 Stress distribution on bottom plate in *y*-direction

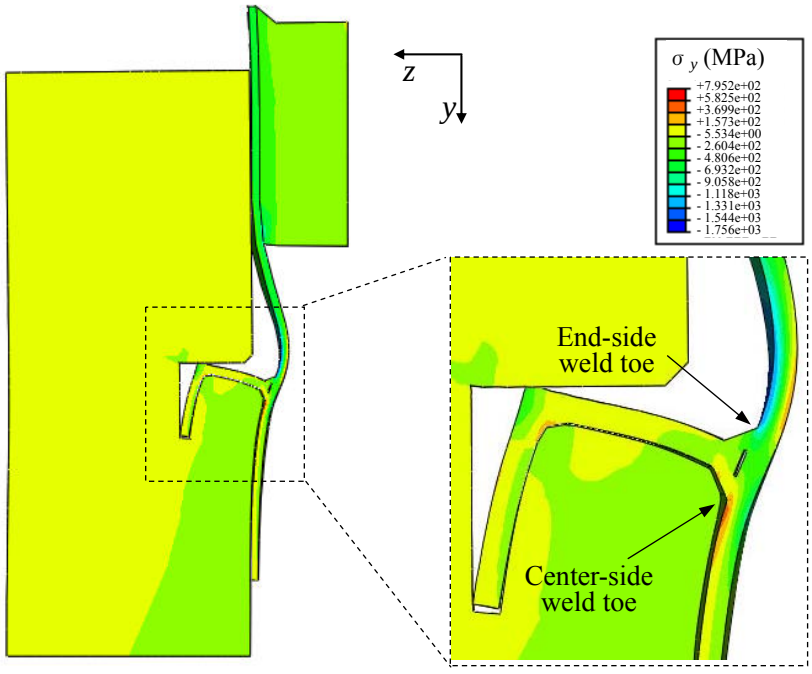

Fig. 3.9 Deformed shape of push-out model (×100)

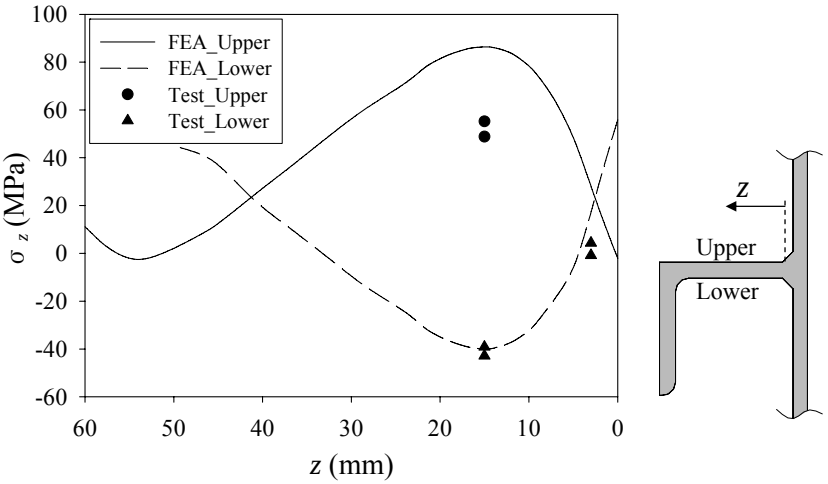

Fig. 3.10 Stress distribution on shear connector

3.3 Fatigue test

3.3.1 Test program

Two specimens were tested. The minimum load was 10kN in both specimens. The maximum load was 120kN, and 160kN. Hereafter, the specimen is named S-120 and S-160, respectively. The minimum and maximum loads are compressive load. The rate of load repetition was 5Hz.

Nominal shear stress of shear connector can be used to assess fatigue strength of the present welded joint. The nominal shear stress can be calculated as following equation:

$$\tau_n = S \times \frac{W_L}{D_L} \tag{3-1}$$

where, S is shear force, W_L is width of shear connector, and D_L is thickness of shear connector.

The nominal shear stresses calculated by Eq. (3-1) are 35.9MPa and 49.0MPa in S-120 and S-160, respectively. These values are less than the cut off limit of 67.0MPa under constant amplitude proposed in JSSC. According to the results, the possibility of fatigue damage at this type of welded joint is very low. However, it should be noticed that the nominal shear stress disregards the local stress of the welded joint.

3.3.2 Fatigue test results

In S-160, a fatigue crack appeared on the side surface of the specimen as shown in **Fig. 3.11** at 7.5 millions cycles. This crack was initiated along the center-side weld toe on the bottom plate where the high tensile stress was observed in **Fig. 3.8** and propagated to thickness direction.

According to the FEA results, high compressive and tensile stresses are generated at the end-side and the center-side weld toe, respectively. Moreover, the absolute value of the stress at the end-side weld toe is larger than that of the center-side weld toe. Therefore, after breaking the concrete, fatigue crack inspection was conducted on the exposed weld toe with a magnetic particle inspection technique. As a result, fatigue crack was detected at the end-side weld toe. It was about 140mm in surface length. The depth of crack was only 0.72mm as shown in **Fig. 3.13 (a)**.

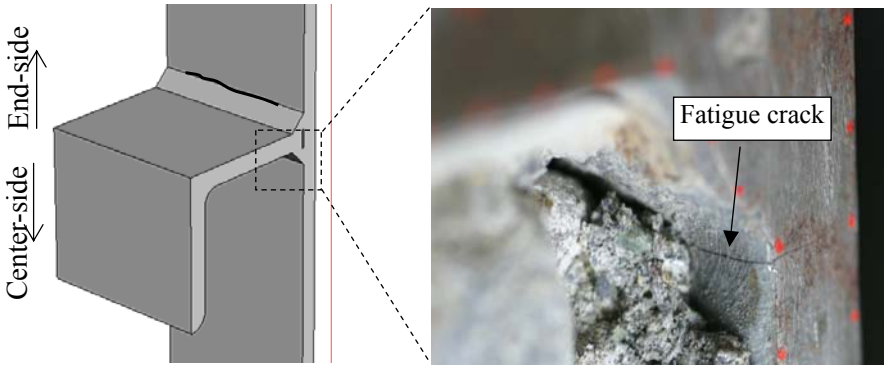

(a) at center-side weld toe (Tension)

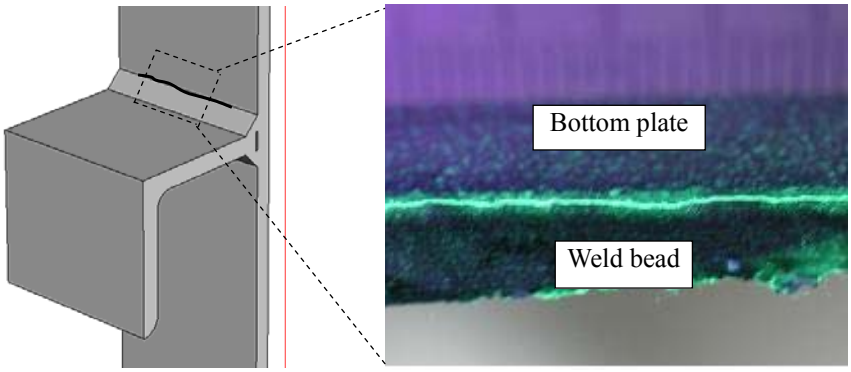

(b) at end-side weld toe (Compression)

Fig. 3.11 Fatigue crack (S-160)

In S-120, no crack was detected until 15.0 millions cycles. Therefore, after quitting the test at the cycle, the magnetic particle inspection was carried out on welded toes in the same way as S-160. A crack was observed at the end-side weld toe shown in **Fig. 3.12**. The crack was 90mm in surface length and 0.44mm in depth. However, no crack was detected at the center-side weld toe. **Fig. 3.13** gives the crack depth of bottom plates at the end-side weld toe.

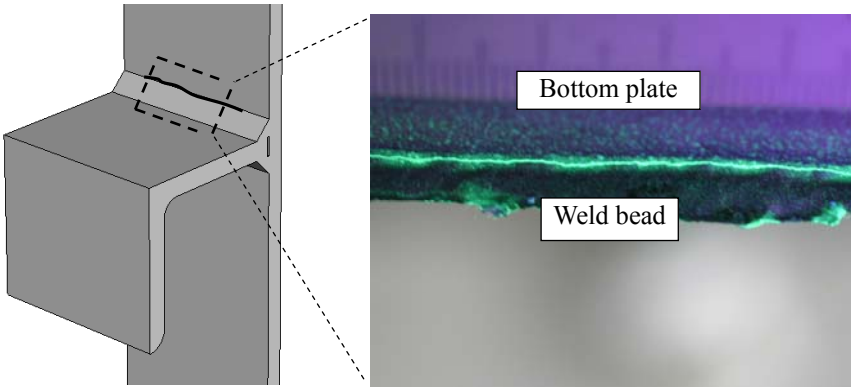

Fig. 3.12 Fatigue crack at the end-side weld toe (S-120)

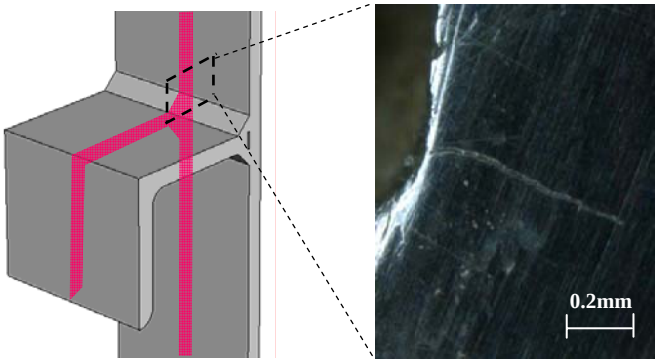

(a) S-160 (depth: 0.72mm)

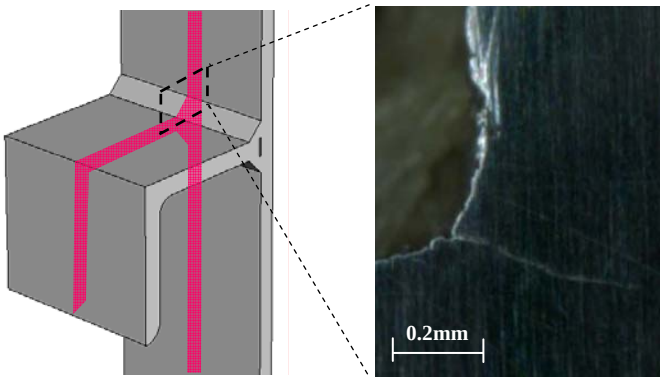

(b) S-120 (depth: 0.44mm)

Fig. 3.13 Crack depth of bottom plate at the end-side weld toe

For the welded joint used in this study, it is impossible to know the crack initiation life visually because the welded joint is embedded in the concrete. Therefore, the fatigue life is deduced from the strain change near the weld toe monitored by the strain gauges. The strain history of S-160 is shown in **Fig. 3.14**. The gauge numbers shown in the figure are consistent with those in **Fig. 3.3**. The strains on bottom plate shown in **Fig. 3.14 (a)** are changed sharply at 4.6 millions cycles at the end-side weld toe, and the strains at the center-side weld toe are changed at 5.2 millions cycles. These cycles are taken as the fatigue lives in S-160. The strain on shear connector and the relative slip between steel and concrete vary sharply at 4.6 millions cycles as given in **Fig. 3.14 (b)** and **Fig. 3.15**. On the other hand, in S-120, no noticeable strain change could be seen until 15.0 millions cycles. The strain histories were summarized in Appendix B.

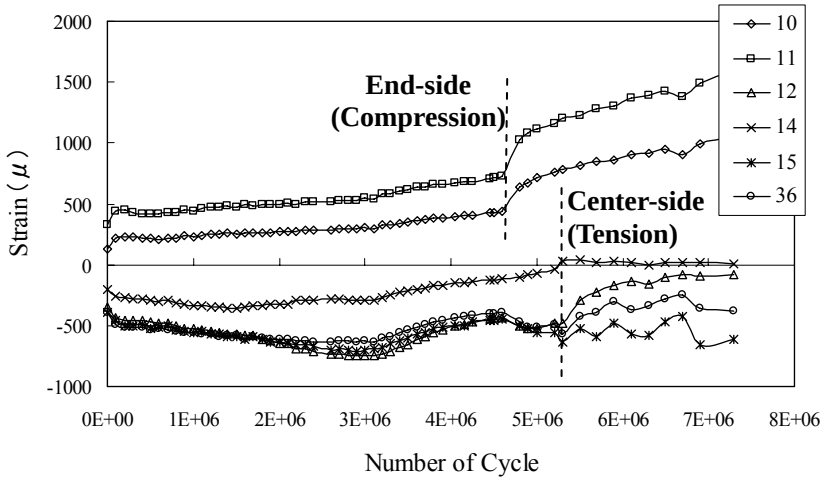

(a) on bottom plate

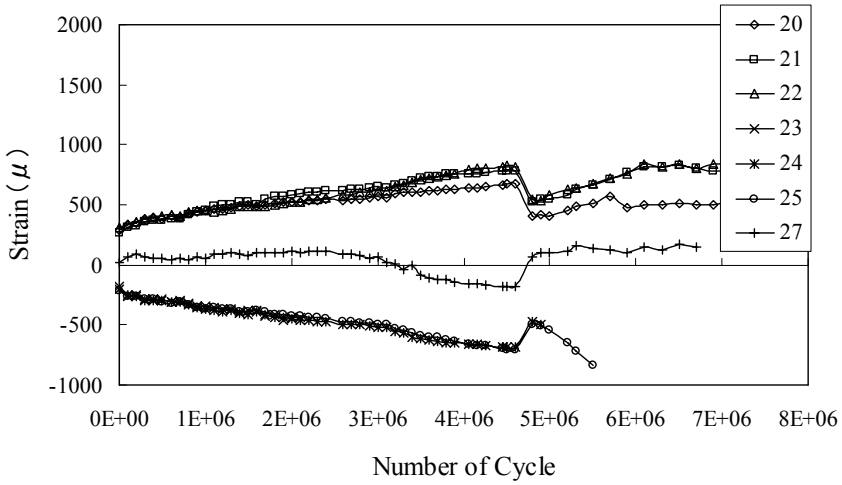

(b) on shear connector

Fig. 3.14 Strain histories in S-160

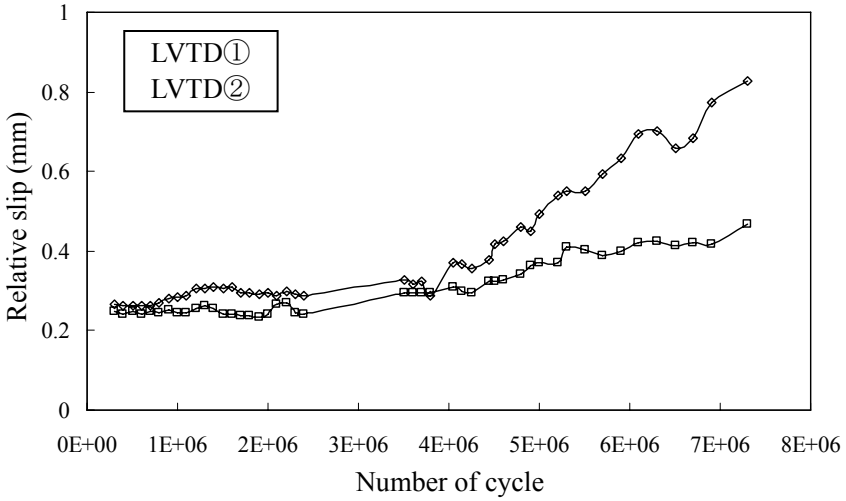

Fig. 3.15 Relative slip in S-160

Table 3.3 Summary of test results

Specimen	Min. load (kN)	Max. load (kN)	Fatigue crack	Fatigue life ($\times 10^6$)
S-160	10	160	End-side weld toe	4.6
			Center-side weld toe	5.2
S-120	10	120	End-side weld toe	15.0

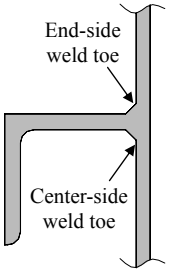

The fatigue test results on push-out shear specimens are summarized in **Table 3.3**. As mentioned above, in this study, fatigue lives were deduced by strain histories. In S-160, the fatigue life is 4.6 millions cycles at the end-side weld toe, and 5.2 millions at the center-side weld toe, and the 15.0 millions cycles is taken as the fatigue life in S-120, which is cycles at the end of test. It should be noticed that the fatigue lives include some errors.

3.4 Fatigue strength estimation

In this study, hot spot stress (HSS) concept is used for fatigue assessment because it is difficult to estimate the nominal stress for the welded joint of shear connector. The location of reference points and the extrapolation method to evaluate the HSS were

decided according to the IIW recommendation as shown in **Fig. 3.16**. The stresses at the reference points were calculated from the analysis results.

Fig. 3.17 shows the fatigue test results arranged with the HSS. In this study, the effect of compressive mean stress was ignored so as to get the conservative assessment results. In the figure, the curve of FAT100 recommended as the reference curve of fatigue strength in IIW is also shown. Even though the number of test results is limited, the fatigue test results satisfy the class FAT100. Therefore, it is confirmed that the fatigue strength of the welded joints between the angle shape shear connector and the bottom plate can be conservatively assessed by using the hot spot stress and the design curve of FAT100.

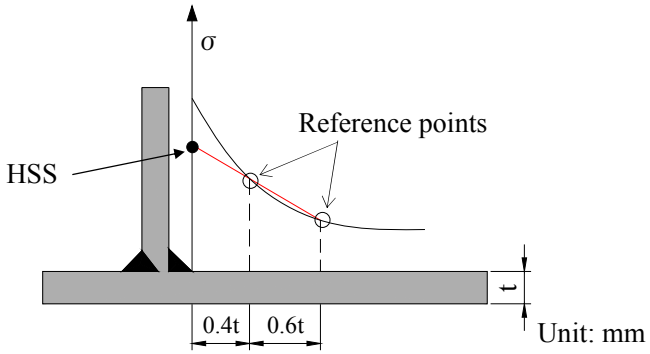

Fig. 3.16 Definition of HSS

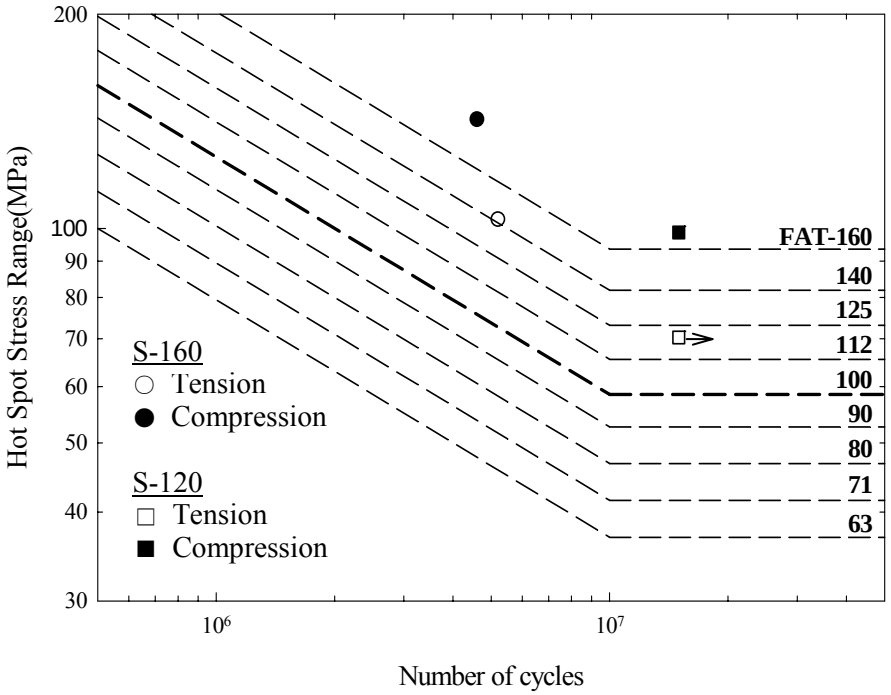

Fig. 3.17 Fatigue strength of shear connector (Push-out specimen)

3.5 Concluding remarks

In this chapter, the fatigue strength of welded joints between bottom plate and shear connector was investigated on push-out specimens, and the fatigue strength was examined. The results are as follow:

1) From the results of experiment and FEA, the local bending deformation of bottom plate occurred around the welded joint of shear connector. Moreover, the FE analysis provided a good agreement with the measured test results.

2) Fatigue cracks initiated from the weld toe under the tensile stress by the local bending deformation, and propagated in thickness direction. Fatigue cracks were also observed at the weld toe under high compressive stress, but the crack length in the thickness direction was very small.

3) Fatigue strength estimation was performed based on hot spot stress. The welded joints satisfied with the FAT100 curve which is reference curve of fatigue strength in using HSS. Therefore, fatigue strength of the welded joint of shear connector can be assessed by using the hot spot stress and the FAT100 curve proposed by IIW.

On the other hand, after finishing concrete surface, concrete defect was observed around the edge of shear connector, as shown in **Fig. 3.18**. This defect of concrete can affect to the local stress behavior around shear connector. Even though there was no influence in the present test specimens, the defect in-situ construction can be larger than that of test specimen because the amount of concrete is considerably large and casting condition is more severe. Therefore, special attention should be paid to the vibrating work in casting concrete.

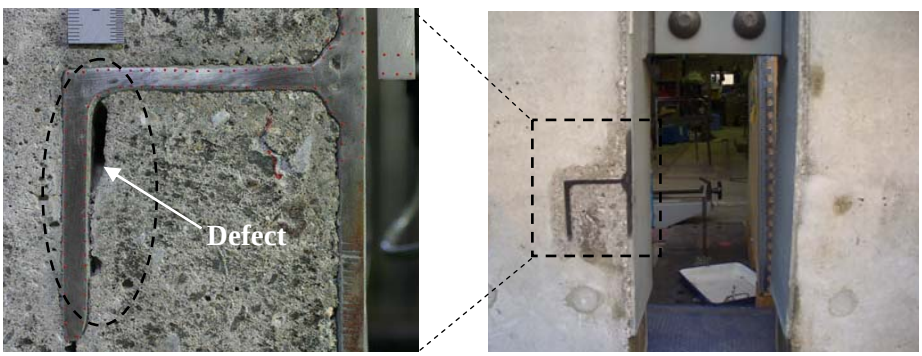

Fig. 3.18 Concrete defect

CHAPTER 4

FATIGUE TEST ON BEAM MODEL

4.1 Introduction

In the previous chapter, the fatigue strength of welded joints of shear connectors was verified on, and also its estimation method was established by push-out fatigue test. In addition, FE analysis was validated by comparing with test results.

In general, the fatigue resistance of shear connectors has been identified by a simple push-out test. However, as illustrated in **Fig. 4.1**, the push-out shear specimen is subjected to only horizontal force. Whereas, in actual composite slabs, the shear connector is under the combined action of vertical and horizontal force. Therefore, for more credible fatigue assessment, the fatigue strength should be evaluated considering the load condition of actual structures.

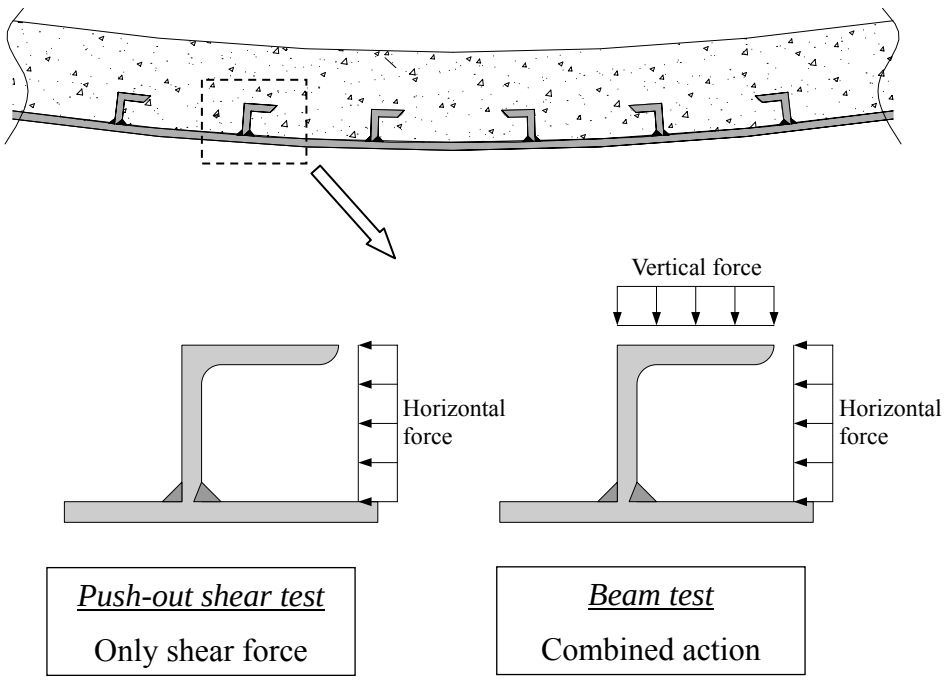

Fig. 4.1 Load condition around shear connector

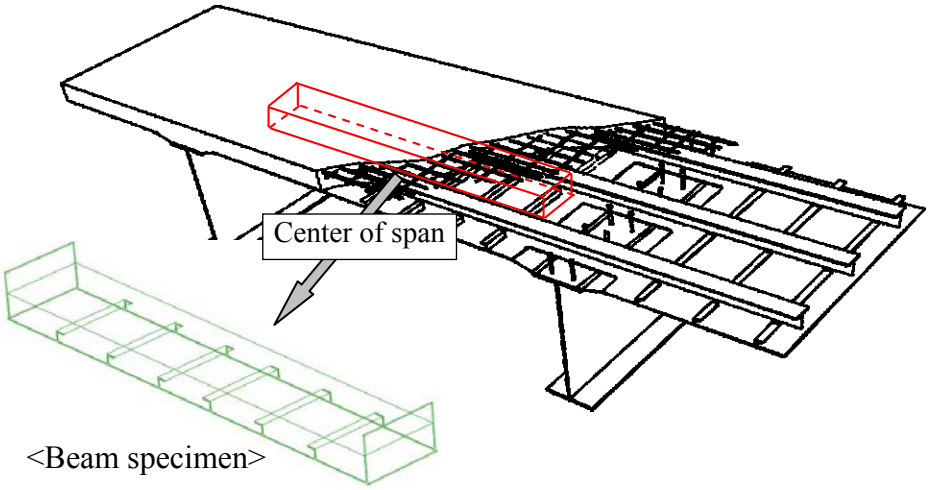

Fig. 4.2 Schematic view of beam specimen

In this chapter, fatigue test and FE analysis are carried out on beam specimens. In the same way as the push-out shear test, fatigue strength is examined, and FE analysis is validated through the comparison with measurement results of test. In static loading test, the relationship between local stress behavior at welded joints and loading position is also investigated.

The shear connectors are welded on bottom plate discontinuously due to the presence of CT-shape steel. Thus, the stress behavior can be fluctuated at the center and end portion of shear connector because the structural detail is different. However, according to the test results on large-scale plate specimens in Chapter 2, the stress behavior is nearly constant regardless the center and end portion of shear connector. Therefore, beam specimens are made picking up the center of composite slab as shown in **Fig. 4.2**.

4.2 Static loading test and FEA

4.2.1 Test program

The mechanical properties and chemical compositions of steel used in the specimens are given in **Table 4.1**, and compression test results of concrete are given in **Table 4.2**. The configurations and dimensions of the specimen are illustrated in **Fig. 4.3.** The specimen was 3m spanning, and the bottom plate was 8mm in thickness. Six shear

connectors were welded on the bottom plate by fillet weld through the whole width of specimen at intervals of 500mm.

In the same way as the push-out shear specimen, the remover was provided on the steel plate to simulate the no-bond condition between steel and concrete. Reinforcements were arranged in compression zone of the beam.

Fig. 4.4 shows an overview of test setup. The specimen was simply supported and loaded at the mid-span. The test was carried out with a three point bending condition. The load was applied through the whole width of the beam by using a computer-controlled servo-hydraulic 35 ton MTS actuator. Between the loading plate and specimen, rubber was placed to apply the load uniformly. The width of rubber is 100mm.

Table 4.1 Mechanical properties and chemical compositions

	Mechanical properties			Chemical compositions (%)				
	Yield stress (MPa)	Ultimate strength (MPa)	Elongation (%)	C	Si	Mn	P	S
Steel plate (SM400A)	339	431	31	0.14	0.15	0.63	0.014	0.006
Angle shape steel (SS400)	290	441	30	0.16	0.15	0.87	0.017	0.008
Rebar (D16)	320	448	28	0.10	0.18	0.47	0.027	0.034
Rebar (D19)	393	549	24	0.20	0.12	0.98	0.034	0.035

Table 4.2 Compression test results of concrete

No.	Compressive strength (MPa)	Modulus of elasticity (MPa)	Poisson's ratio
1	35.2	2.64×10^4	0.187
2	34.1	2.32×10^4	0.161
3	34.6	2.56×10^4	0.168

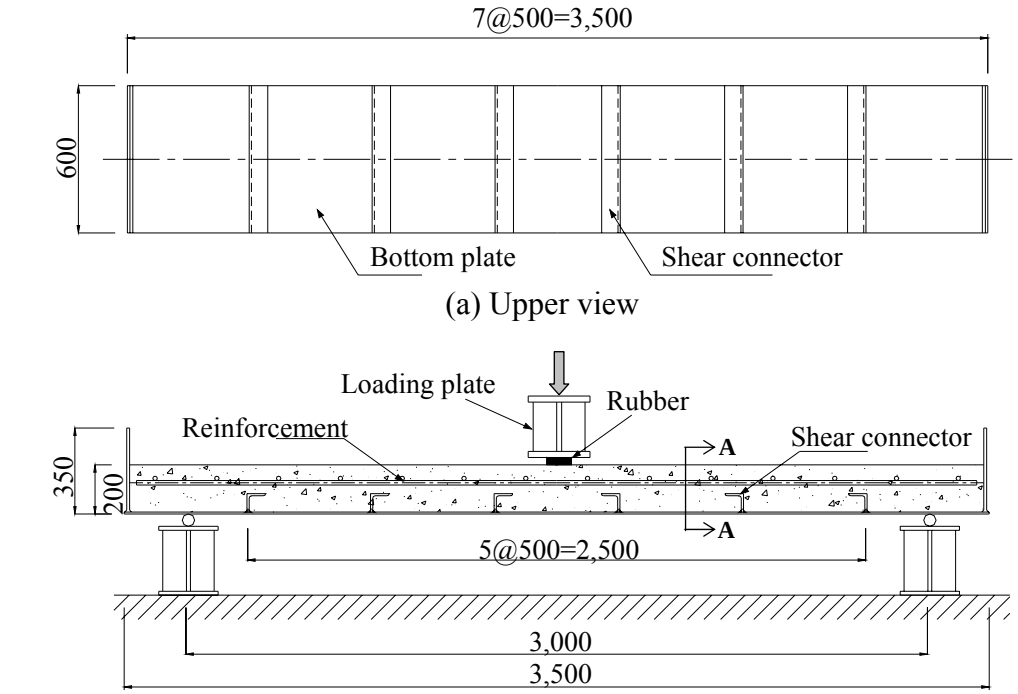

Fig. 4.3 Configurations and dimensions of specimen

Fig. 4.4 Overview of test setup

Strain gauges were arranged on the inner and outer surface of the bottom plate as shown in **Fig. 4.5**. Those positions and numbers were determined for measuring the hot spot stress at welded joints of shear connectors.

Manufacturing process of beam specimen is illustrated in **Fig. 4.6**. After assembling the steel member by welding, strain gauges were attached on inner surface and protected. As mentioned above, grease was provided on steel, and then concrete was casted.

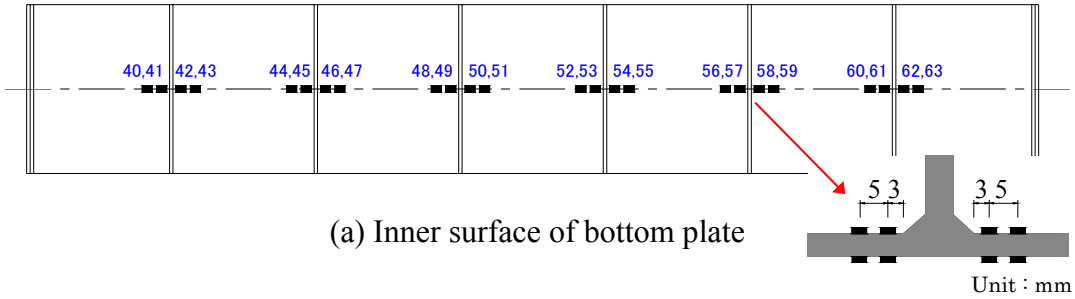

(a) Inner surface of bottom plate

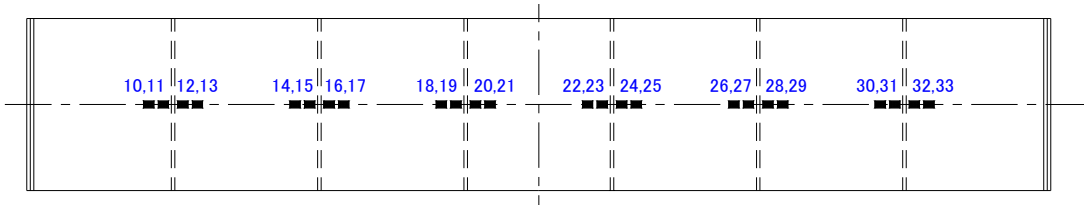

(b) Outer surface of bottom plate

Fig. 4.5 Arrangement of strain gauges

(a) Attaching gauges on inner surface

(b) Gauge protection

Fig. 4.6 Manufacturing process of specimen

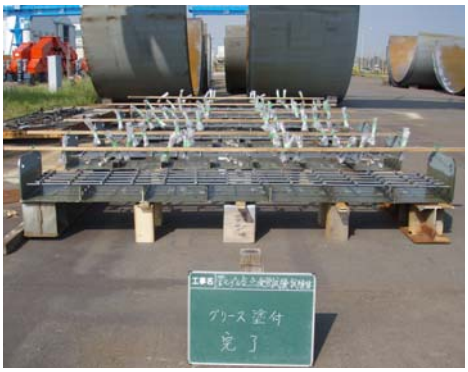

(c) Providing grease (d) Curing concrete

Fig. 4.6 Manufacturing process of specimen (Continue)

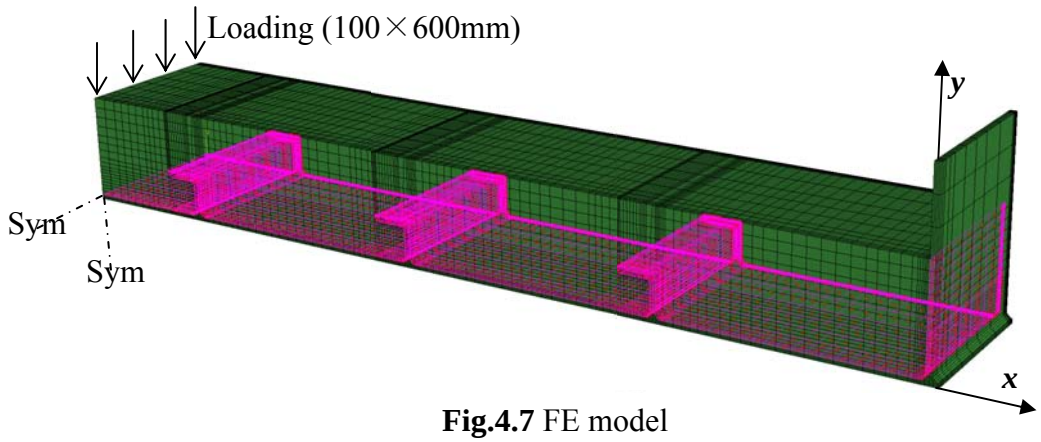

Fig.4.7 FE model

4.2.2 FE model

Fig. 4.7 shows FE model of the specimen. ABQUS version 6.7 was used to analyze the stress behavior of beam specimen. Due to the symmetry of the cross-sectional geometry, and of the boundary condition, only one-quarter model was created. The eight-node brick elements (C3D8) were employed to model the steel members and concrete solid. The contact condition was assigned to the interface between the steel and the concrete, but the bond between them was ignored in the same way as push-out shear model. The modulus of elasticity steel material was applied as 206,000MPa, and the Poisson's ratio was assumed as 0.3. Concrete material properties were determined based on the results of compression tests. The modulus of elasticity and Poisson's ratio were assumed 25,100MPa and 0.172, respectively. The values are the average of three test results in **Table 4.2**. **Fig. 4.8** indicates the stress-strain curve for concrete used in this analysis.

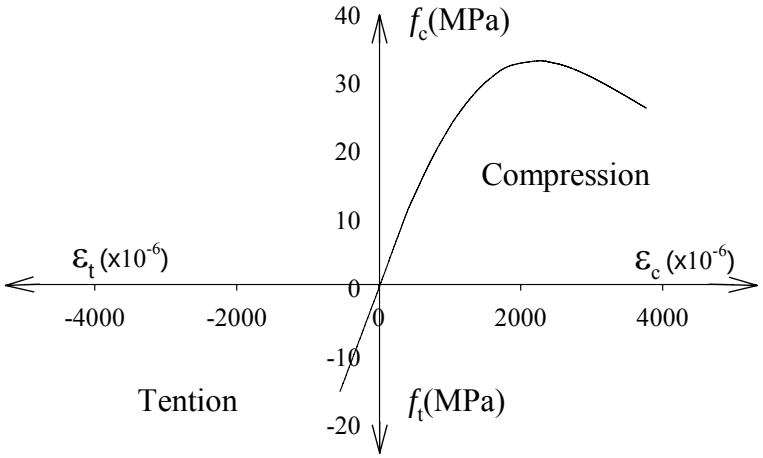

Fig. 4.8 Stress-strain curve for concrete

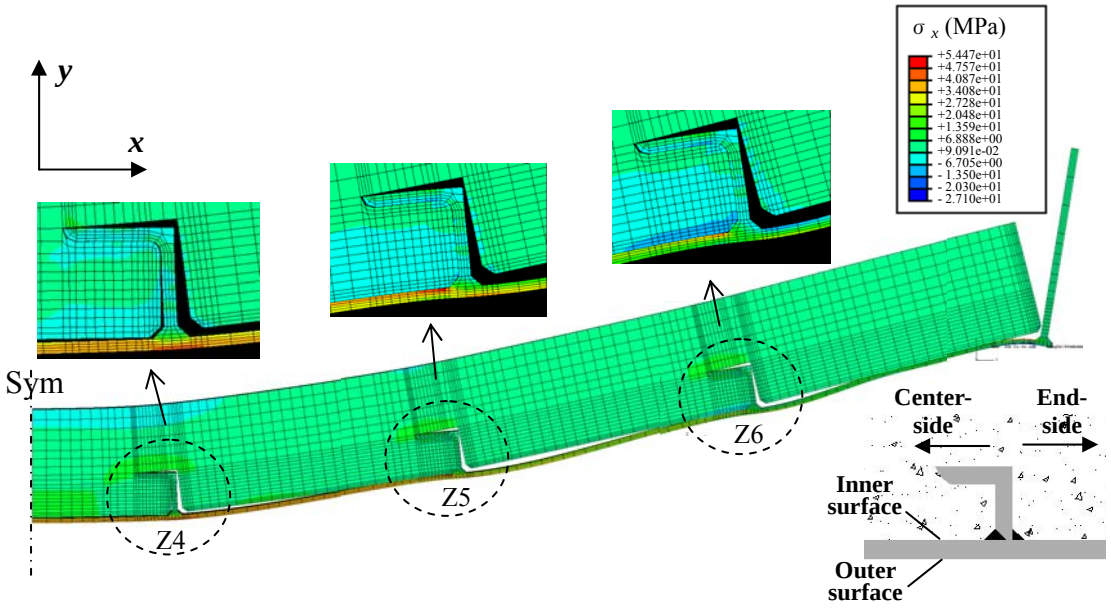

Fig. 4.9 Deformed shape and stress contour of beam model (×100)

4.2.3 Test and FEA results

Fig. 4.9 shows the deformed shape and stress contour of the beam specimen under the load of 50kN. Stress concentration at the welded toes due to the local bending deformation of the bottom plate can be seen around Z5 and Z6 connectors, while the stress concentration around Z4 occurs on the outer surface of bottom plate just below shear connector. This is due to the fact that the vertical force acting on the shear connector becomes larger when the load is placed around the shear connector. These stress behavior will be discussed experimentally in next section.

Fig. 4.10 represents the stress distribution on bottom plate. Lines and marks indicate the analysis results and the measurements, respectively. On the inner surface contacting with the concrete, stress is sharply increased at the center-side weld toe, and suddenly decreased at the end-side of shear connectors except Z4 connector. The maximum stress appears around Z5 connector. On the other hand, the symmetrical distribution can be seen on the outer surface. These stress manners are matched with the push-out shear specimen. Additionally, it can be found from the figure that the analyzed curves obtained by the finite element method are in good agreement with the measured results of test.

Fig. 4.11 presents the average stress distribution of the inner and the outer surface of bottom plate. From the figure, a unique stress behavior is observed in FE model, which is clearly different from the calculated values by beam theory. The stress distribution is obviously separated at the positions of shear connectors, and the stress is nearly constant between shear connectors. Even taking into account the presence of the bond between steel and concrete, it is considered that the unique behavior can be also generated in an actual composite slab. It will be discussed further in chapter 5.

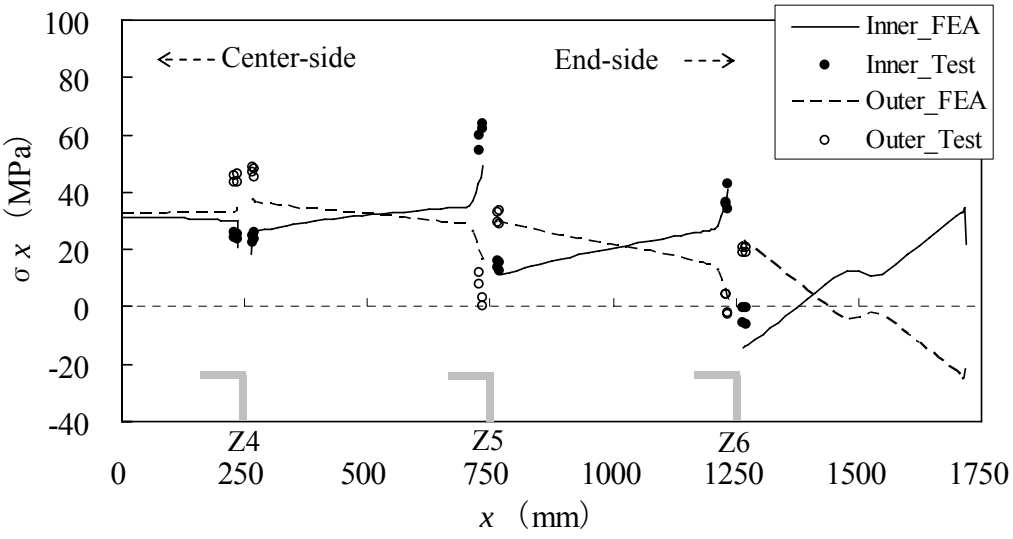

Fig. 4.10 Stress distribution on bottom plate (Surface stress)

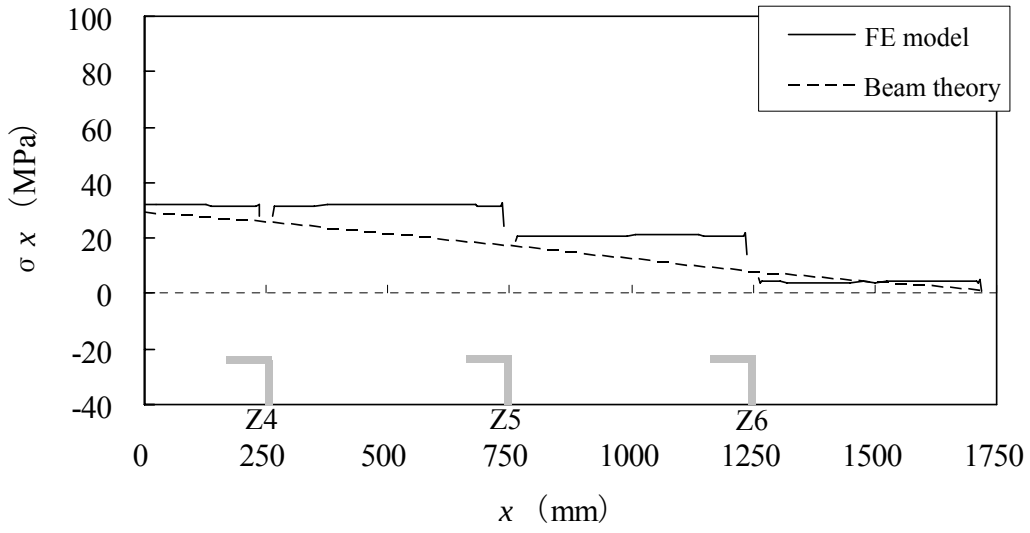

Fig. 4.11 Stress distribution on bottom plate (Average of surface stresses)

4.2.4 Effect of loading position

In the same way as the large-scale plate specimens, to investigate the local stress behavior in detail, the static loading test was carried out by changing the loading position in 5 places at 100mm intervals as shown in **Fig. 4.12**. Applied load was 20kN. The change of HSS at weld toes was monitored for each load case. HSS was calculated by the measured strains.

Hot spot stress with respect to loading position is shown in **Fig. 4.13**. HSS was calculated by the measured value of strain gauges. Firstly, it can be found from the **Fig. 4.13 (a)**, at Z3, the HSS at center-side weld toe becomes the minimum value when the load is placed at mid-span (Case①), while the maximum HSS appeared at Case③. At the center-side weld toe at Z5 (**Fig. 4.13 (b)**), HSS is also recorded the maximum value in Case③. HSS at the end-side weld toe represents the opposite trend in both Z3 and Z5 connector. On the other hand, there is no certain change of HSS at Z4 connector as shown in **Fig. 4.13 (c)**. It is for this reason that the load cases are placed around Z4 connector. This stress manner was also observed on large-scale specimen in Chapter 2.

Summing up the above results, the local bending deformation around shear connector becomes larger when the load is placed just beside connectors, while becomes smaller when the applied load is close to the target shear connector.

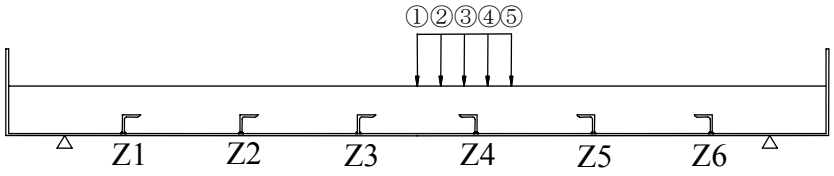

Fig. 4.12 Load cases

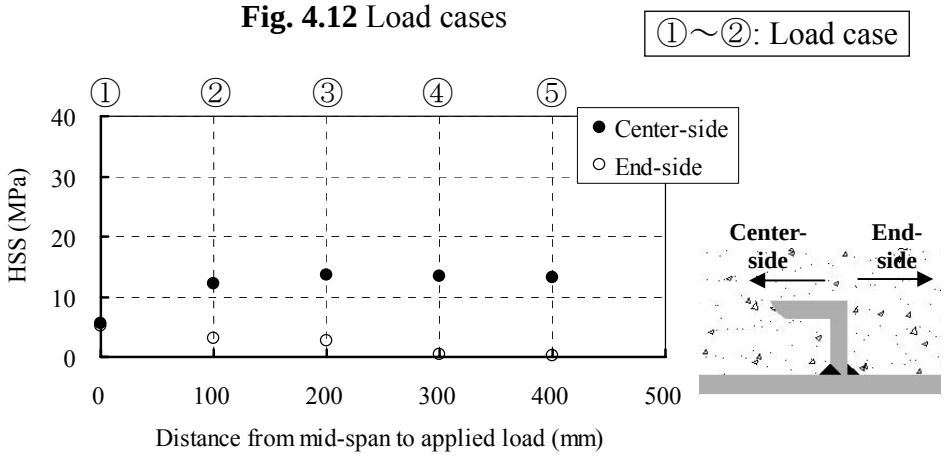

(a) at Z3

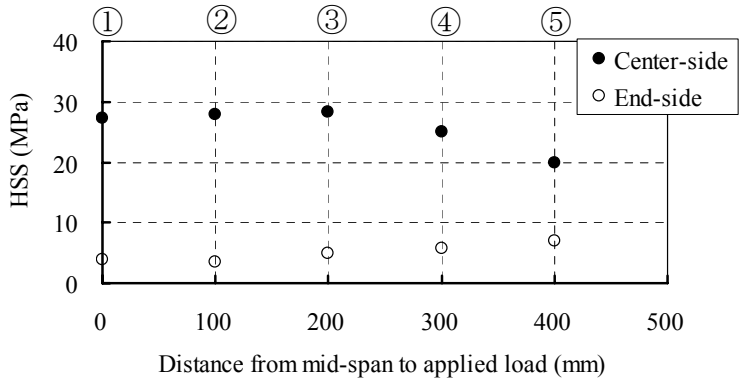

(b) at Z5

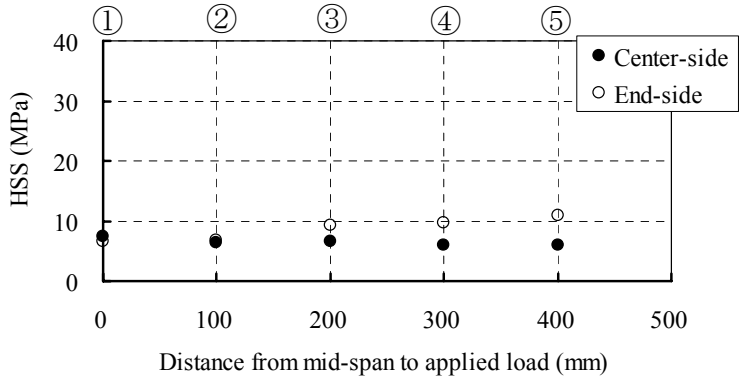

(c) at Z4

Fig. 4.13 HSS with respect to loading position

4.3 Fatigue test

4.3.1 Test conditions

Table 4.3 indicates fatigue test conditions. Two specimens were tested. The minimum load was 2kN in both specimens. Concrete cracks generated from the edge of shear connector have influence on the stress distribution around shear connectors. Therefore, in order to minimize the damage of the concrete, the fatigue test was started with the small load range. Hereafter, the specimens are named L-70 and L-100, respectively.

4.3.2 Fatigue test results

As mentioned above, the fatigue test was started with the small load range of 35kN. However, since no crack was found, the load range was increased up to 50kN after 5.7 millions cycles, and 70kN after 10.0 millions cycles. After that a fatigue crack about 500mm in length was found on the outer surface of the bottom plate at 4.9 millions cycles (15.6 millions cycles in total). **Fig. 4.14** shows the fatigue crack. The crack appeared on the outer surface of bottom plate just below the center-side weld toe of Z5, where the high tensile stress concentration was observed in **Fig. 4.10**. For the specimens used in this study, it is impossible to know the crack initiation life visually. Therefore, in the same way as the push-out specimen, the fatigue life is deduced from the strain change near the weld toe monitored by strain gauges. **Fig. 4.15** shows the strain histories near the weld toe of Z5. The numbers in **Fig. 4.15** indicate the gauge numbers shown in **Fig. 4.5**. The strains near the weld toe were fluctuated sharply at 4.0×10^6 cycles under the load range of 70kN. Therefore, the crack initiation life was supposed to be 4.0×10^6 cycles (14.7 millions cycles in total).

On the other hand, L-100 specimen under the load range of 100kN was failed by concrete cracks from the edge of shear connectors at 13,000 cycles. It will be discussed in section 4.5.

Table 4.3 Fatigue test conditions

Spec.	Min. load (kN)	Max. load (kN)	Frequency (Hz)
L-70	2	37/52/72	2.1
L-100	2	102	1.5

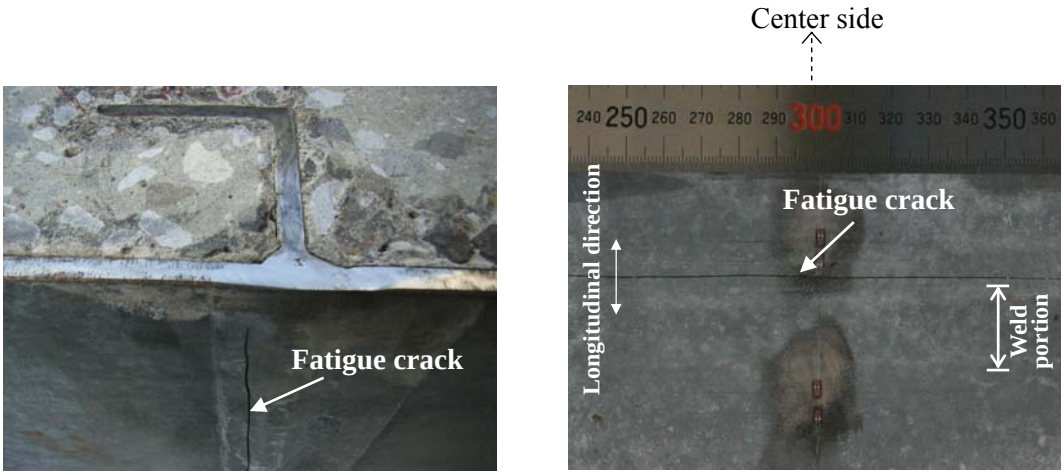

(a) Side view (b) Lower view

Fig. 4.14 Fatigue crack on bottom plate

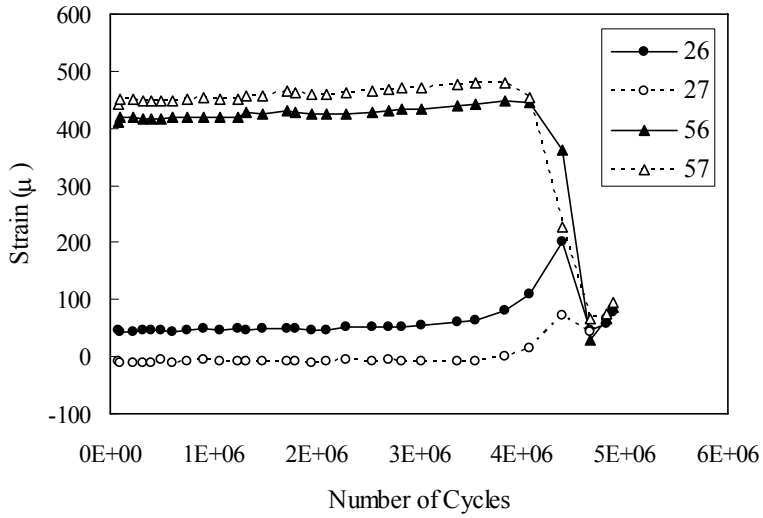

Fig. 4.15 Strain histories around Z5-shear connector

4.4 Fatigue strength estimation

Since it is difficult to determine the nominal stress for the welded joint, HSS concept is used for fatigue assessment. The location of reference points and the extrapolation method to evaluate the HSS were decided according to the IIW recommendations as shown in **Fig. 3.16**. The stresses at the reference points were calculated from the measured strains. Linear damage accumulation rule was applied in order to combine the damage at three different load ranges.

Fig. 4.16 shows the fatigue test results of the beam specimen arranged by the HSS with the results of the push-out shear specimens. The curve of FAT100 which is reference design curve in case of using HSS recommended in IIW is also given in the figure. Although the fatigue strength of beam specimen is assessed slightly lower than that of push-out specimens, the fatigue test results satisfy the class FAT100.

Based on the fatigue tests on push-out shear specimens and beam specimen, it is confirmed that conservative fatigue assessment can be performed by comparing HSS with the FAT100 curve.

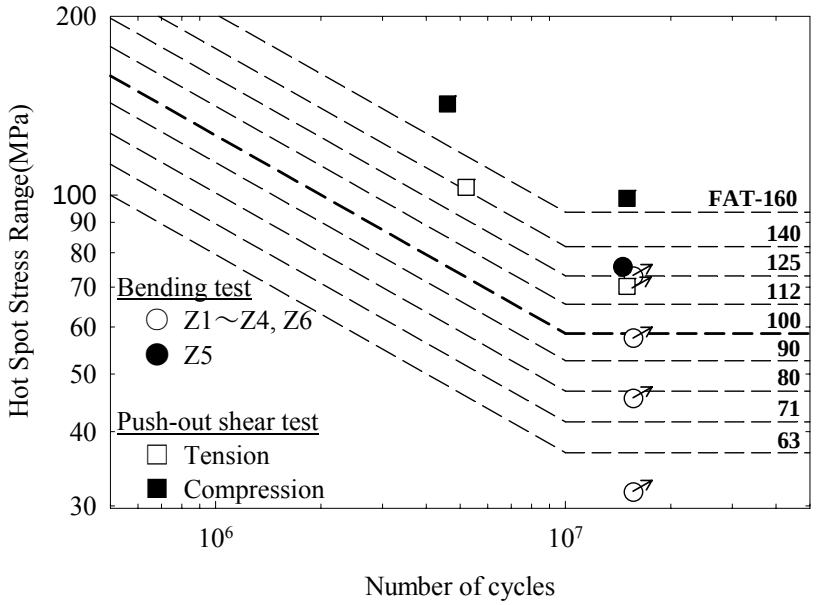

Fig. 4.16 Fatigue strength of shear connector

4.5 Concrete fracture

In both beam specimens, concrete cracks were observed from the edge of the shear connectors, and propagated toward mid-span with about 45° during the fatigue test. However, in L-70 beam, the concrete cracks were delayed around the reinforcements, and the beam was fractured by fatigue crack on the welded joint of shear connector. **Fig. 4.17** shows the concrete crack from edge of shear connector at the end of fatigue test.

In L-100 specimen, the concrete cracks at the edge of shear connectors were propagated continuously toward the loading position as can be seen in **Fig. 4.18**. Finally, the beam specimen was fractured at 13,000 cycles.

In **Fig. 4.19**, the propagation of concrete crack is illustrated. Even though the possibility of this like concrete crack occurrence is very low in actual slab under service load, this result indicates that concrete cracks initiated from the edge of shear connectors can be a critical damage in composite slabs when relatively large load is applied to the slab.

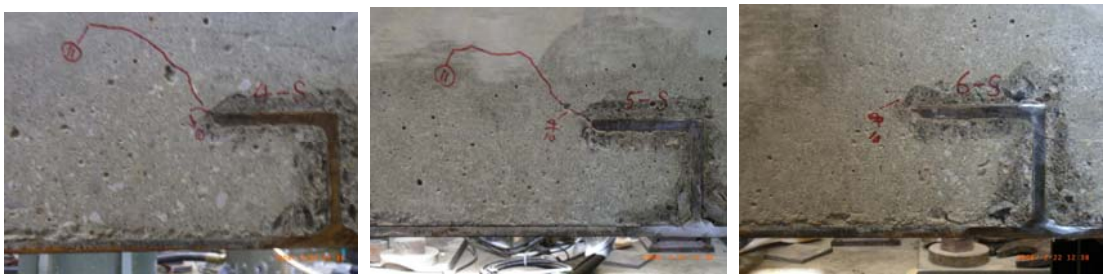

(a) near Z4 (b) near Z5 (c) near Z6

Fig. 4.17 Concrete crack from edge of shear connector (L-70)

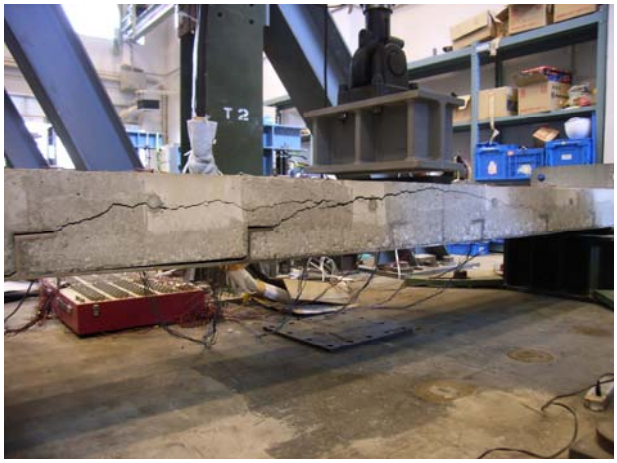

Fig. 4.18 Concrete fracture (L-100)

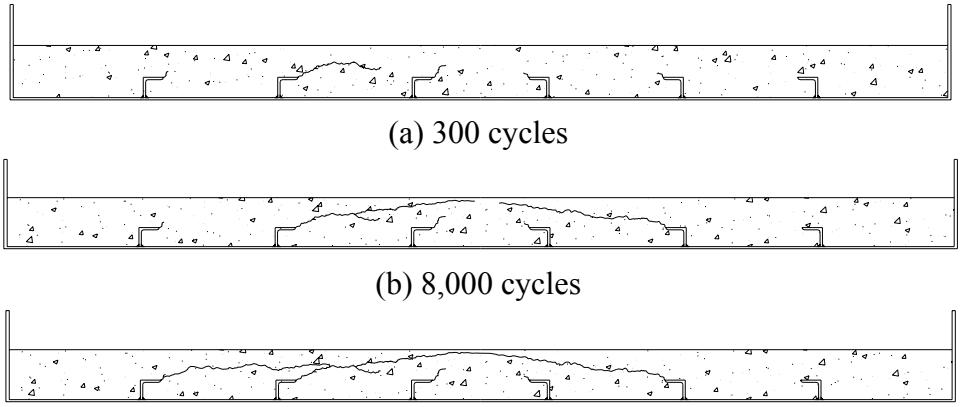

(a) 300 cycles

(b) 8,000 cycles

(c) 13,000 cycles

Fig. 4.19 Concrete crack propagation

4.6 Concluding remarks

From the fatigue test and FEA on push-out specimen, the fatigue strength of welded joints of shear connectors was verified, and also its estimation method was established. In addition, FE analysis was validated by comparing with test results. However, the push-out shear specimen is subjected to only shear force, whereas in actual composite slabs, the shear connector is under the combined action of bending and shear force. Therefore, for more credible fatigue assessment, fatigue test and FE analysis were carried out on beam specimens. In the same way as the push-out shear test, the bond action between steel and concrete was ignored.

The following main conclusions can be stated as follows:

1) The stress concentration occurred at the welded joint of shear connectors in test and FEA as the same to the push-out specimen. This is due to the fact that the local bending deformation of bottom plate occurs around the welded joint of shear connector. From the fatigue test result, fatigue crack was initiated at the welded toe, and propagated to the thickness direction. In addition, the FE analysis results represented a good agreement with the test results.

2) Fatigue strength of beam specimen was also satisfied with the class FAT100. Therefore, it can be confirmed that conservative fatigue estimation can be performed by comparing HSS and FAT100 curve.

In actual composite slab, the possibility of fatigue damage on steel member is relatively low. However, if the fatigue cracks occur at welded joints and penetrate bottom plate, it leads to a considerable decrement in load-carrying capacity of composite slab because the detection of the fatigue crack is very difficult in service due to the structural detail. Therefore, researchers and engineers should pay attention to the fatigue damage of steel members.

CHAPTER 5

LOCAL STRESS BEHAVIOR AROUND ANGLE SHAPE SHEAR CONNECTOR

5.1 Introduction

In chapters 3 and 4, it was confirmed that conservative fatigue assessment can be performed on welded joints of shear connectors by comparing HSS with the FAT100 curve proposed in IIW. It means that if HSS is estimated, a simple fatigue assessment can be carried out by comparing with the design curve of FAT100. However, it is widely known that laboratory tests are time-consuming and very expensive.

The finite element method has become a powerful and useful tool for the analysis of a wide range of engineering problems. It contributes to provide a satisfactory solution for economic requirements. From the stress analysis for large-scale plate model, beam model, and push-out shear model, the FE models were validated for the no-bond condition between steel and concrete.

In this chapter, the finite element analysis is conducted on two actual composite slabs to investigate HSS at welded joint between the shear connector and the bottom plate under the design truck load. Then simple fatigue assessment is carried out by comparing HSS with the FAT100 curve. Moreover, based on the analysis results, the relationship between HSS at the welded join and stress components on shear connectors is examined.

5.2 FE model

The 3D-FEA was performed on two actual composite slabs. **Table 5.1** represents the outline of investigated bridges. Two bridges have different size of shear connector and different intervals of shear connectors and CT-shape steels. Among them, A-bridge has the same size of shear connector to the test specimens.

Table 5.1 Investigated bridges

Unit: mm

	A-Bridge	B-Bridge
Main girder	I-plate girder	Box girder
Width of slab	8,700	9,500
Thickness of bottom plate	8	8
Transverse span of deck	5,500	5,300
Angle shape shear connector	75×75×9×642 Interval ; 562	100×75×10×625 Interval ;442.5
CT shape steel	150×150×6.5×9×8600 Interval ; 812	150×150×6.5×9×9400 Interval ; 775

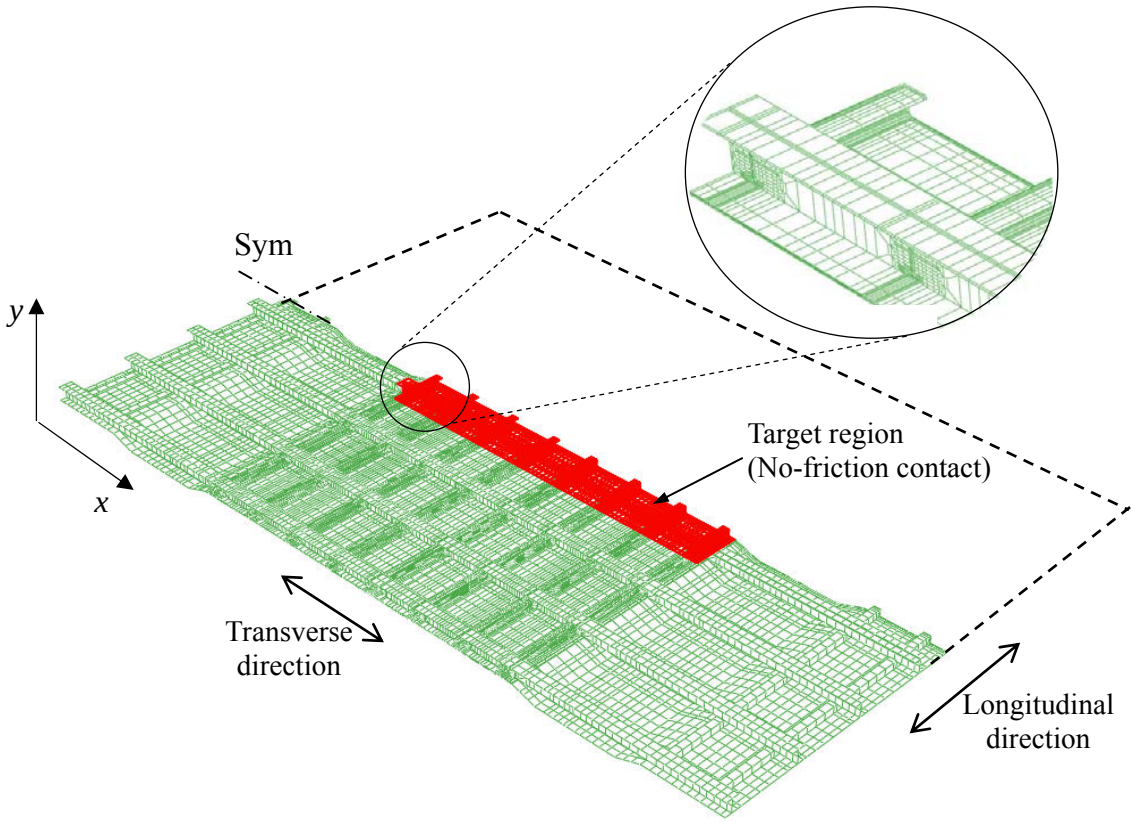

(a) Steel members

(b) Cross section of slab

Fig. 5.1 FE model

As an example, **Fig. 5.1** illustrates the FE model of A-bridge. The full-width of the slab was modeled in transverse direction, and seven panels were modeled in longitudinal direction. ABAQUS version 6.7 was employed to simulate actual composite slabs. Due to the symmetry of the cross-sectional geometry and of the boundary conditions, only half model was created in longitudinal direction. **Table 5.2** shows employed elements in the model. Eight-node solid elements were employed to the concrete, shear connector, and bottom plate in the target region as shown in **Fig. 5.1 (a)**. Besides the target region, four-node shell elements were utilized to model concrete and steel members. The minimum element size was 2×2×3.2mm. Reinforcements have little influence to the stress behavior of steel members under the design truck load because those are embedded in compressive zone. Therefore, considering the convergence problem and analyzing time of FEA, reinforcements were created by truss element.

Contact surface between the steel and the concrete were connected completely. However, in the target region besieged with outline as shown in **Fig. 5.1 (a)**. The contact elements were applied to the interface so that the steel and the concrete can behave independently. The bond between them was ignored. The slab was simply supported at the position of main girder web. The modulus of elasticity and Poisson's ratio of steel and concrete were assumed as listed in **Table 5.3**.

According to the results of FEA mentioned later, the maximum principle stress on concrete portion was below 3.0MPa even in case of the most severe load case. The stress value is affected by mesh size and shape. Moreover, there is a possibility of local concrete fracture near the edge of shear connector. However, the present model assumed that the effect of concrete fracture is small. For the reasons, both steel and concrete are assumed as elastic body.

Table 5.2 Employed elements

Slab member	Element
Concrete, shear connector and bottom plate in the target region	Solid
CT-shape steel, shear connector and bottom plate besides the target region	Shell
Reinforcement	Truss

Table 5.3 Material properties

Material	Modulus of elasticity (MPa)	Poisson's ratio
Steel	206,000	0.3
Concrete	28,300	0.182

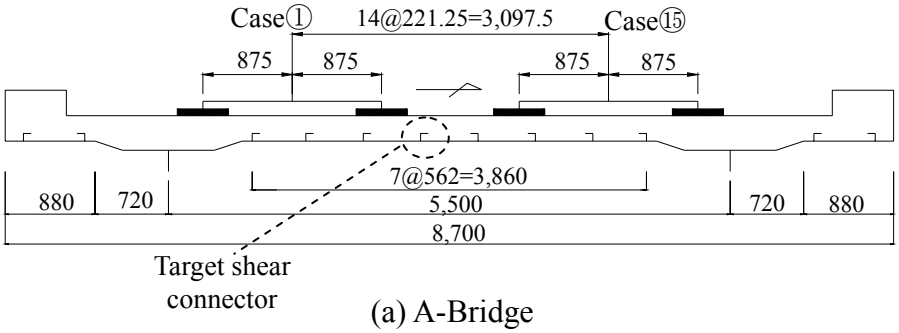

(a) A-Bridge

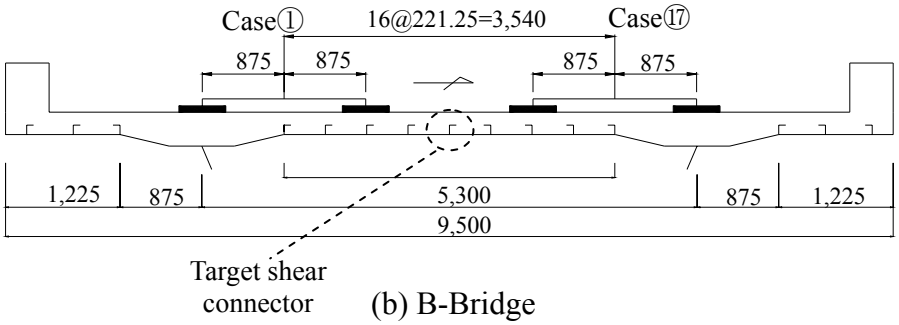

(b) B-Bridge

Fig. 5.2 Target shear connectors and load cases

5.3 Stress behavior under design truck load

5.3.1 Loading conditions

The stress behavior was analyzed for two actual bridges when the design truck load was applied on slab. **Fig. 5.2** shows the target connectors and load cases. Loading position was changed in 15 places (A-bridge) and 17 places (B-bridge). The contact area of the load is 200×500mm^2 rectangles, which represents the contact area of a rear tire of heavy truck. In this section, analysis results were mainly summarized for target shear connectors located around the mid-span as shown in **Fig. 5.2**.

5.3.2 Analysis results

As examples, stress distributions of the bottom plate along the center of model (symmetric surface in **Fig. 5.1**) around the target shear connector are shown in **Fig. 5.3**. In the transverse axis, the value of 0 indicates the center of target shear connector. There is a sudden change of stress around the shear connector symmetrically on the inner and outer surface of bottom plate, and the local bending deformation can be observed similar to the test models. Similar phenomenon was observed around other shear connectors. **Fig. 5.4** shows the HSS of target shear connectors with respect to loading position. It is found from the figure that the maximum HSS in both bridges are less than the cut-off limit of FAT100 category (58MPa). Therefore, it can be said that the possibility of fatigue damage at the welded joint in this type of composite slab is very low.

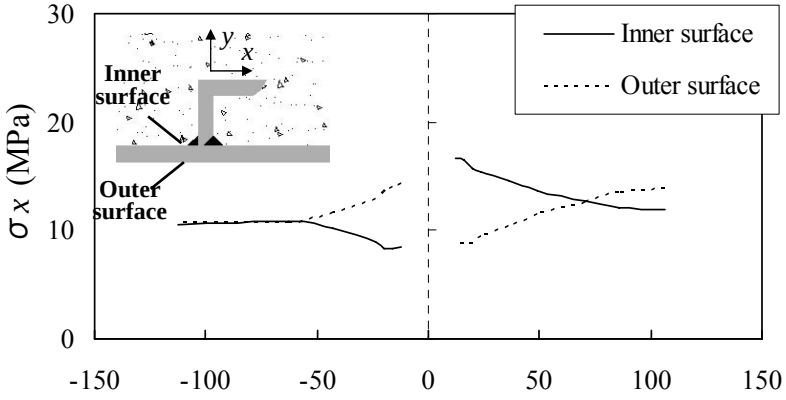

(a) A-bridge (load case⑪)

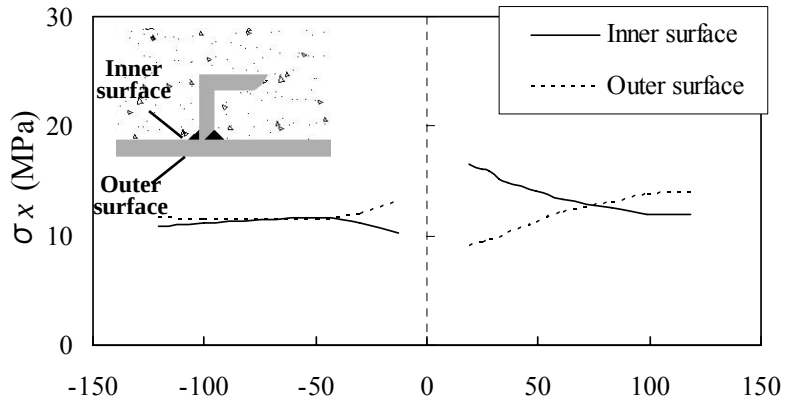

(b) B-bridge (load case⑬)

Fig. 5.3 Stress distribution on bottom plate

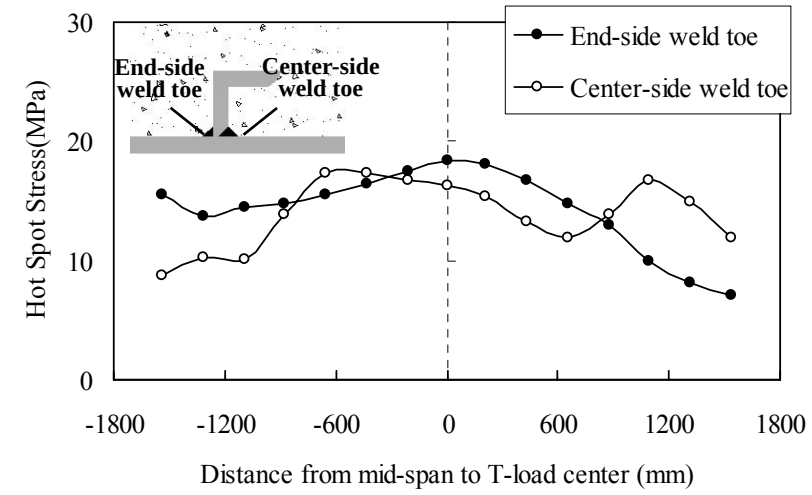

(a) A-bridge

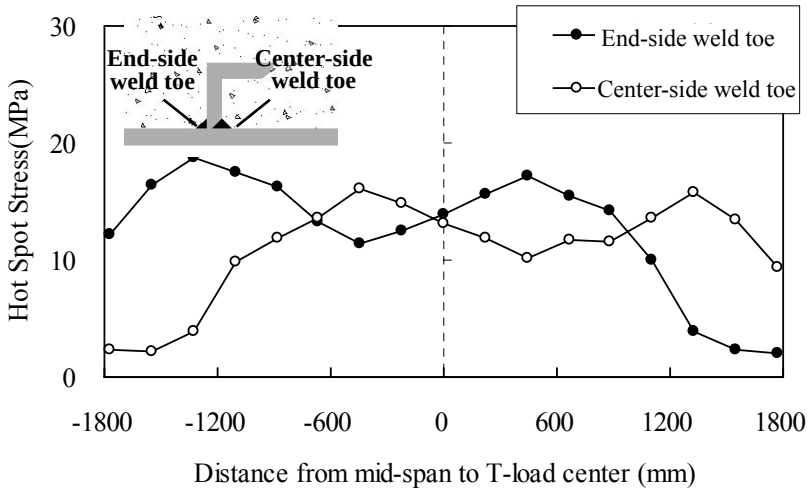

(b) B-bridge

Fig. 5.4 HSS with respect to loading position

5.4 Local stress behavior around welded joints

The FEA results on actual composite slab revealed that the possibility of fatigue damage at the welded joint in this type of composite slab is very low under the design truck load. It means that the slab section can be designed more economically by reducing the number of shear connector or CT-shape steel. However, it is difficult to perform this like of 3D-FEA for each case of slab section in design step. Therefore, local stress behavior around welded joints was examined in detail to establish a simple estimating method of HSS.

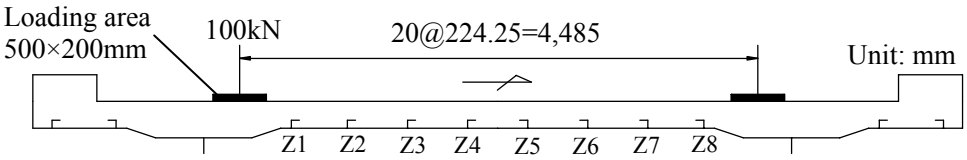

Fig. 5.5 Load cases

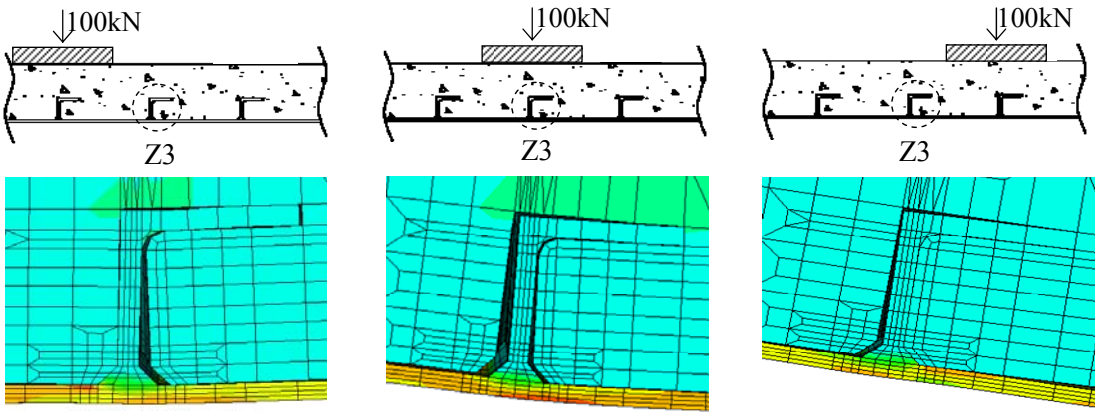

Fig. 5.6 Deformed shape and stress contour with respect to loading position

5.4.1 Loading conditions

For more detailed analysis of local stress behavior, the single design truck load with 100kN was applied on the composite slab as shown in **Fig. 5.5**. This analysis was carried out on A-bridge given in **Table 5.1**. Load position was changed in 21 places in transverse direction. In the figure, from Z1 to Z8 indicate each position of shear connector.

5.4.2 Stress distribution on bottom plate

Fig. 5.6 gives examples of deformed shape and stress contour around shear connector with respect to loading position. The local bending deformation of the bottom plate is occurred around shear connectors, and varied in accordance with the loading position. As similar to test results, when the applied load is located just beside connectors from a target connector, stress concentration is occurred at both sides of weld toe due to the local bending deformation.

Fig. 5.7 represents examples of the stress distribution on the bottom plate along the center of model (symmetric surface in **Fig. 5.1 a)**) under the load of 100kN. Stresses on the inner and outer surface are sharply changed around welded joints of shear

connectors due to the local bending deformation. On the other hand, the average stress of inner and the outer surface is nearly constant between shear connectors, and suddenly varies around shear connectors like a stepped distribution. It means that the forces between bottom plate and concrete are transferred by only shear connectors. This stress manner was also observed on beam models.

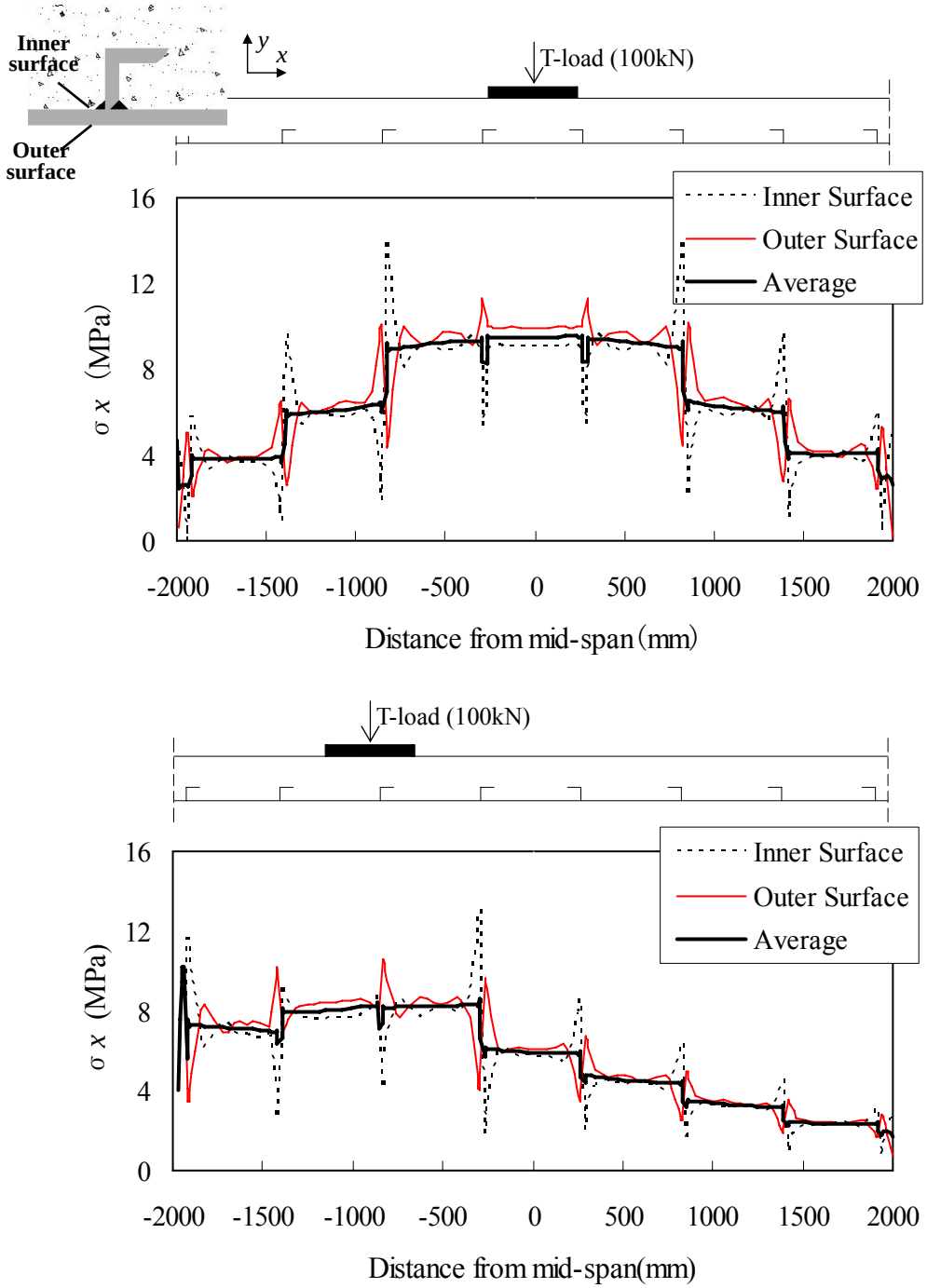

Fig. 5.7 Stress distribution on the bottom plate

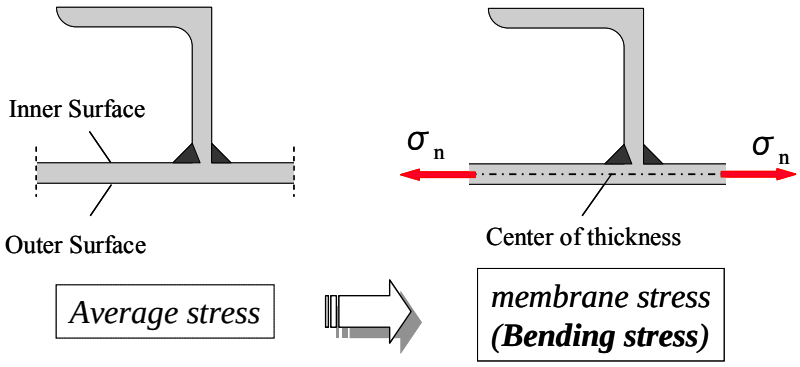

5.8 Definition of bending stress

The average stress of the inner and the outer surface is the same to the stress at center of thickness. And, the stress can be said as membrane stress of bottom plate. In this study, the stress at the center of thickness (σ_n) was called as the bending stress of the composite slab at the position of bottom plate as shown in **Fig. 5.8**.

5.4.3 Hot spot stress at welded joints

Influence lines for HSS and bending stress were calculated to investigate the relationship between stress concentration and loading position in detail.

Fig. 5.9 shows influence lines for HSS and bending stress near Z3 connector. There are two weld toes on the welded joint of a shear connector. HSS was calculated for each weld toe, and the relationship was investigated between loading positions. The bending stress means the stress at center of thickness just below shear connectors.

At the center-side weld toe, HSS tends to become larger than bending stress when the load is placed in center side from the target shear connector (Z3), and the maximum HSS occurs when the load lies near Z4. In contrast, as the load moves to the end side from Z3, HSS becomes smaller than bending stress due to the effect of compression. At the end-side weld toe, influence lines for HSS and bending stress represent the opposite trend to the center-side weld toe. These stress manners were also observed on other shear connectors, and the results were summarized in Appendix C.

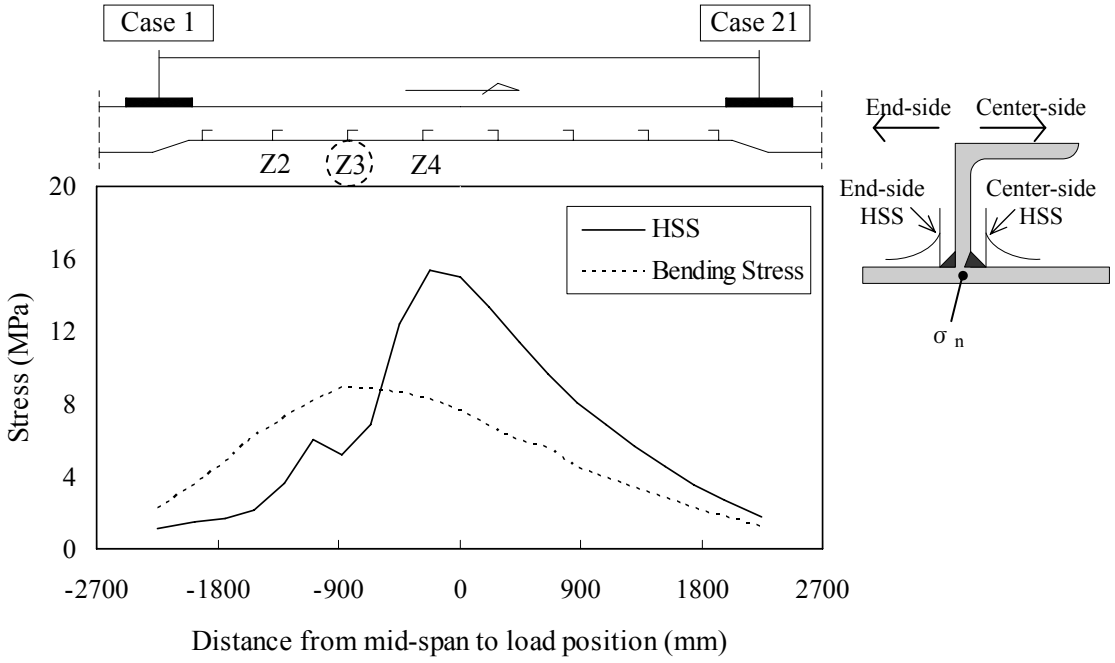

a) Center-side weld toe

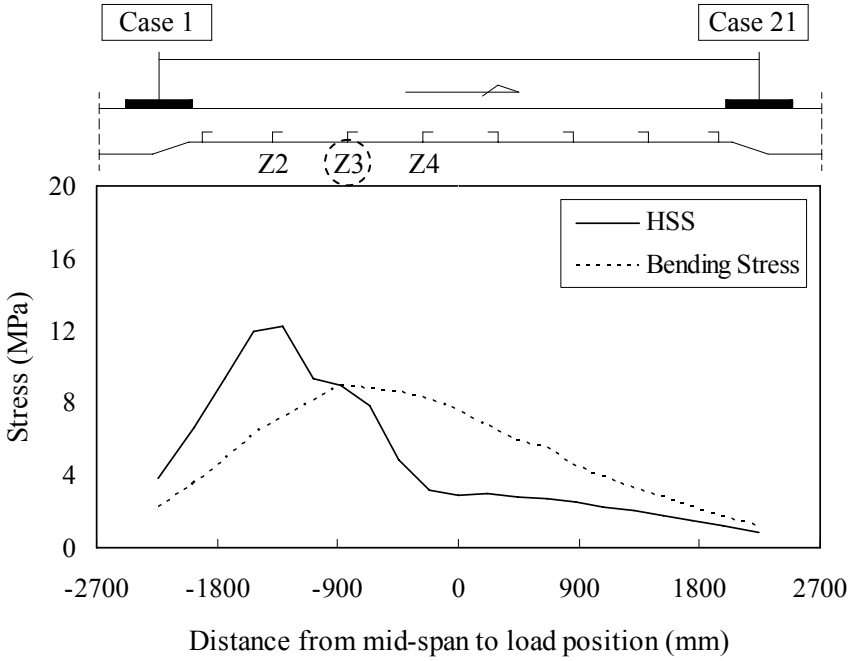

b) End-side weld toe

Fig. 5.9 Influence lines for HSS and bending stress

5.5 Relationship between hot spot stress and shear stress

As illustrated in **Fig. 5.10**, axial stress (σ) and shear stress (τ) are generated on the shear connector because the angle shape shear connector is subjected to horizontal and vertical forces due to the deflection of composite slab.

It is considered that the bending moment transmitted from the shear connector to the bottom plate has an influence on the local bending deformation of the bottom plate. Therefore, the dominant stress component was investigated through the comparison of bending moment induced by axial stress (σ) and shear stress (τ). The comparison was conducted on Z3 connector.

As an example, bending moments were calculated at **A** point indicated in **Fig. 5.10**. The results shows that the bending moments by σ and τ were 15.2N·mm and 76.6 N·mm, respectively. Therefore, shear stress is the dominant stress component in the local bending deformation of bottom plate. For other analysis cases, similar phenomena were also observed. For this reason, the local stress behavior around welded joints was examined focusing on the shear stress of shear connectors.

In addition, there are two possible cross-sections for estimating shear stress. One is the cross-section passing through upper weld bead (in **Fig. 5.10** Ⅰ - Ⅰ), and the other is passing through lower weld bead (in **Fig. 5.10** Ⅱ - Ⅱ). In calculating shear stress along the Ⅰ - Ⅰ cross-section, it is difficult to reflect the direct force acting on weld bead. However, based on the analysis results, shear stress distribution along the Ⅱ - Ⅱ cross-section was very complicated. Furthermore, the correlation with stress concentration factor described later was highly variable and scattering. Therefore, in this study, shear stress was estimated along the cross-section passing through upper weld bead.

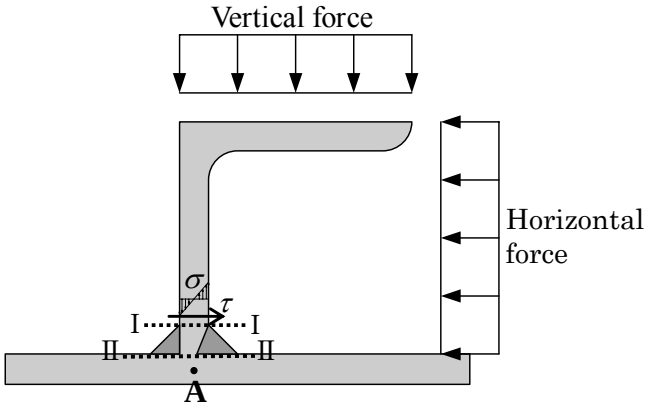

Fig. 5.10 Stress components of shear connector

Fig. 5.11 shows the influence line for average shear stress of Z3. The average shear stress means an averaged value of shear stresses on shear connector along the center of model (symmetric surface in **Fig. 5.1 a)**). Compared with the influence lines for HSS in **Fig. 5.9**, for the cases that HSS is larger than bending stress, the maximum positive and negative shear stresses appear when HSS at the center-weld toe and the end-weld toe become the maximum value, respectively. This trend shows a close agreement with the increase and decrease manners of the difference value between HSS and bending stress. Similar phenomena were also observed on other shear connectors, and the results were summarized in Appendix C.

From the above results, it is considered that the local bending deformation of bottom plate is originated by the horizontal shear force acting on shear connector. Therefore, this study paid attention to the correlation between stress increments and shear stresses occurred at shear connectors. The stress increment means the difference value between HSS and bending stress. The results were plotted in the cases that HSS is larger than bending stress for all load cases and shear connectors. The results are shown in **Fig. 5.12**. In here, since the thickness of shear connector is constant, it is possible to replace shear stress to shear force. It is found from the figure that there is a strong correlation between stress increments and shear stresses regardless of the position of load, shear connector, and weld toe.

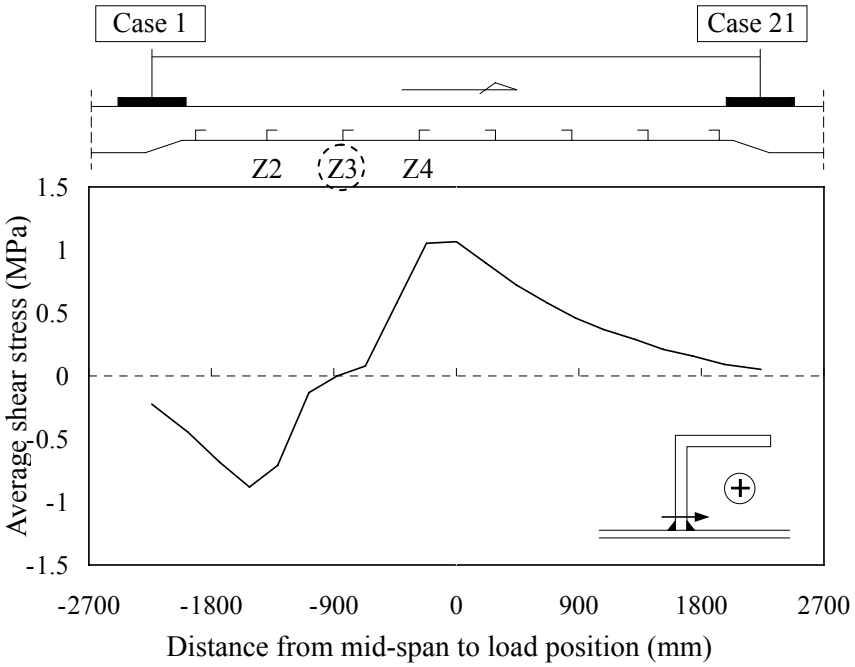

Fig. 5.11 Influence line for average shear stress (Z3)

In a practical fatigue design, it is more convenient to represent the correlation into stress concentration factor (SCF). The SCF (k_t) was calculated by following equation.

$$k_t = \frac{\sigma_{HSS}}{\sigma_n} \tag{5-1}$$

where: σ_{HSS} is hot spot stress, σ_n is bending stress of bottom plate.

Fig. 5.13 shows the result. The shear stresses were normalized by bending stresses. It is found from the figure that high correlation can be observed.

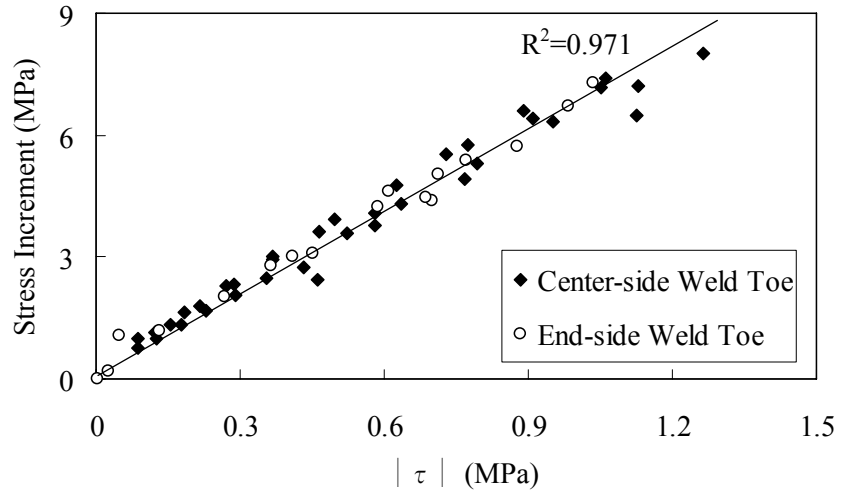

Fig. 5.12 Correlation between stress increment and average shear stress

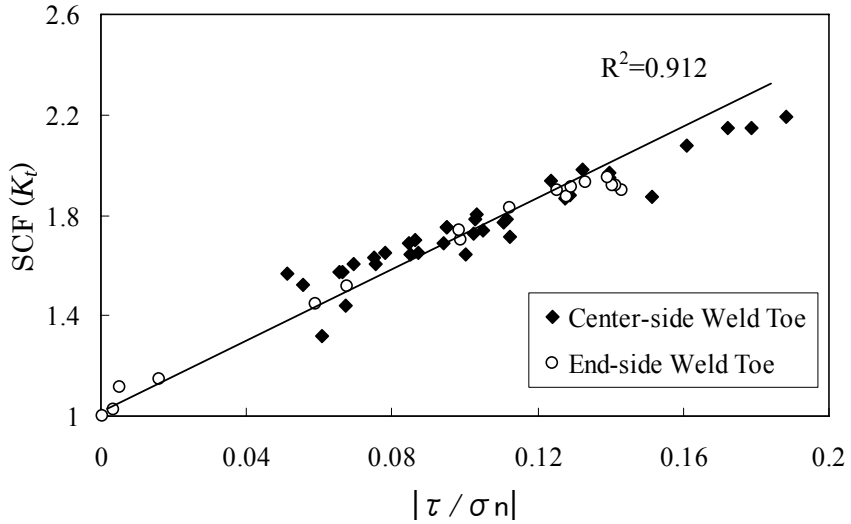

Fig. 5.13 Correlation between SCF and average shear stress

However, it is not clear whether the shear stress and the SCF have a high correlation even in different slab sections because the result shown in **Fig. 5.13** is for only one type of slab section. Therefore, parametric study was carried out by 2D-FEA on various type of slab section.

Fig. 5.14 illustrates an example of 2D-FE model. Four-node shell elements employed to model. Applied material property is the same to 3D-FE model listed in **Table 5.3**. Slab span was unified as 4m. Several parameters were considered, such as slab thickness, bottom plate thickness, and internal of shear connectors and size of shear connector. **Table 5.4** lists the parameters of slab section. These parameters were determined on the basis of the actual composite slabs using angle shape shear connector. In the same way as 3D model, the contact condition was applied to the interface between the steel and the concrete. The slab is simply supported and loaded at the mid-span.

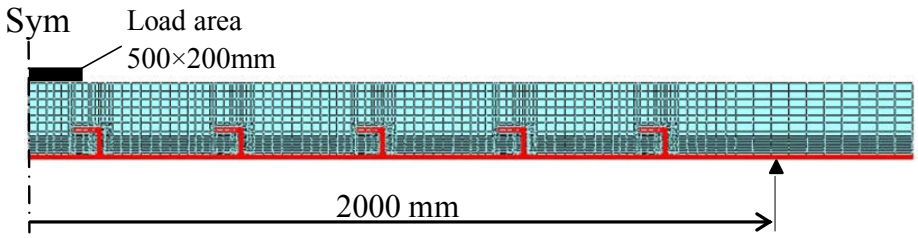

Fig. 5.14 2D-FE Model

Table 5.4 Parameters of slab section

Unit: mm

No	Thickness of Slab	Thickness of bottom plate	Interval of shear connector	Size of shear connector
1	210	8	400	75×75×9
2	260	8	500	100×75×7
3	310	9	600	75×75×9
4	270	8	600	100×75×7
5	250	8	600	75×75×9
6	240	8	500	100×75×10
7	280	8	700	75×75×9
8	310	9	800	75×75×9

Focusing on shear stress normalized by bending stress and stress concentration factor, the results of 2D-FEA are plotted in **Fig. 5.15** with the results of 3D-FEA. It can be found from the figure that there is a high correlation between SCF and shear stress regardless of slab sections.

Consequently, for the slab sections examined in this study, it is possible to estimate stress concentration factor regardless of slab section. The stress concentration factor can be estimated by following equation:

$$K_t = 1 + 7.042\left(\frac{\tau}{\sigma_n}\right) \tag{5-2}$$

In Eq. (5-2), k_t is stress concentration factor shown in Eq. (5.1). σ_n is bending stress of bottom plate, and τ is average shear stress of shear connector.

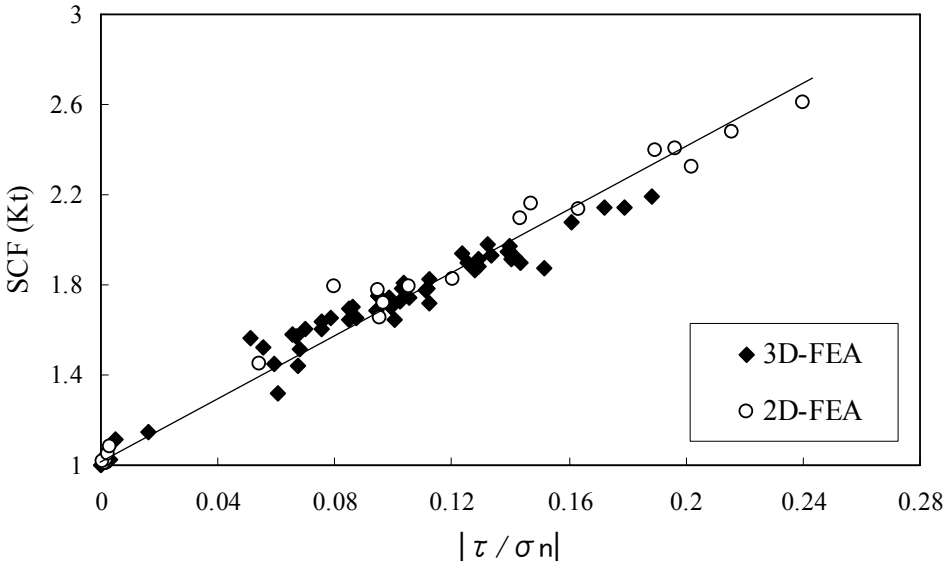

Fig. 5.15 Correlation between SCF and average shear stress

5.6 Concluding remarks

From the fatigue tests on push-out specimens and beam specimens, it was confirmed that conservative fatigue assessment can be performed on welded joints of shear connectors by comparing HSS with the FAT100 curve proposed in IIW. It means that if HSS is estimated, a simple fatigue assessment can be carried out by comparing with the design curve of FAT100. However, experimental study is time consuming and expensive, especially in steel-concrete composite slabs. Therefore, the numerical approach for estimating HSS was examined by FEA on actual composite slabs.

As the results of FEA on actual composite slabs, local bending deformation of bottom plate was also originated around shear connector in actual composite slabs. But, under the design truck load, the maximum hot spot stress at welded joints was about 20MPa which is less than the cut-off limit of FAT100 curve (58MPa). It means that the possibility of fatigue damage is very low in this kind of welded joint.

According to above result, the slab section can be designed more economically in terms of fatigue. But, it is difficult to perform this like of 3D-FEA for each case of slab section in design step. Therefore, a simple estimating method of HSS was examined based on the results of 3D-FEA.

Stress concentration factor and shear stress normalized by bending stress had a high correlation regardless of slab section and loading position, and the correlation equation was establish. Therefore, the correlation between stress concentration factor and shear stress can be base information to estimate HSS at the welded joint of shear connector in the investigated composite slab.

CHAPTER 6

SIMPLE FATIGUE DESIGN METHOD

6.1 Introduction

The preceding chapter has provided the correlation equation between shear stress and stress concentration factor. It can be used to perform the simple fatigue assessment on the investigated composite slab. However, further study is still required to apply the equation to a practical fatigue design because the current design method cannot estimate bending stress and shear stress for each position of shear connectors, which are essential stress components in the correlation equation.

In this chapter, evaluating methods of bending stress and shear stress for each position of shear connectors are examined by numerical analysis.

6.2 Current design method

6.2.1 Bending stress

At present, Japan Society of Civil Engineers has proposed design equations for bending moment for investigating load-carrying capacity. But, using these formulas we can not calculate bending moment for each position of shear connector because only section force of slab is obtained from theses formulas. For the reason, to apply the correlation equation presented in Chapter 5 to practical fatigue assessment, it is essential to establish a new estimating method of bending stress.

6.2.2 Shear stress

The current design method for shear stress has employed bond shear stress between steel and concrete, and effective width has been utilized to replace a slab with a beam. Using these concepts, shear force acting on shear connector is estimated through

multiplying the bond shear stress by the burdened area per single shear connector. Finally, shear stress of shear connector can be calculated by dividing the area of shear connector into the shear force. The shear force is estimated by assuming that steel and concrete are completely composited, while shear connector is burdened the whole shear force. That is to say, the approach disregards the bond between steel and concrete.

Fig. 6.1 shows the comparison of shear stresses calculated by the current design method and 3D-FEA for all of shear connector and load case as shown in **Fig. 5.5**. It is found that shear stresses of the current design method are estimated conservatively in comparison with 3D-FEA results. However, the correlation between both values is very weak because the influence of the local stress behavior around shear connector observed in 3D-FEA is not reflected in the current design method. Moreover, big divergences are also observed for several cases. This is due to the fact that the shear stress by 3D-FEA is almost zero when the load is located near the target shear connector as shown in **Fig. 5.11**, while the shear stress by the current design method becomes large under the same load case. Therefore, it is irrelevant to apply the shear stresses calculated by the current design method to the proposed correlation equation obtained in Chapter 5.

From the above results, it is obvious that a new estimating method for bending stress of bottom plate and shear stress of shear connector should be established to carry out a simple fatigue assessment by using the correlation between shear stress and stress concentration factor.

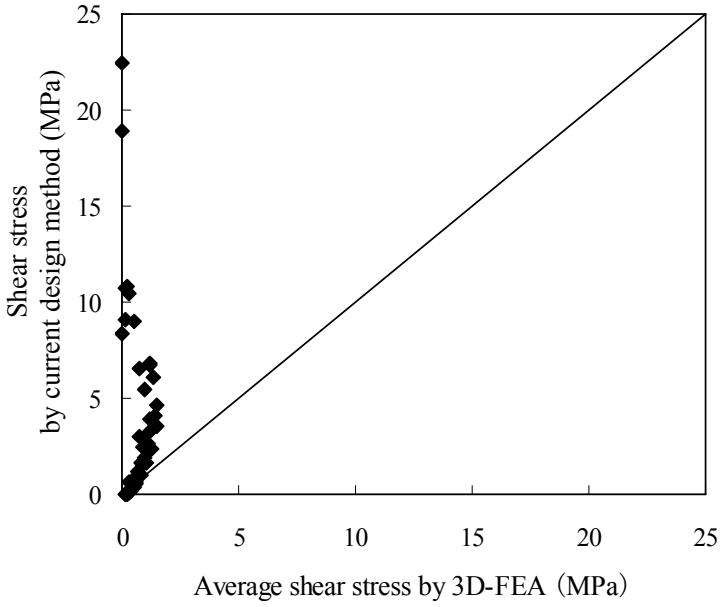

Fig. 6.1 Comparison of shear stresses

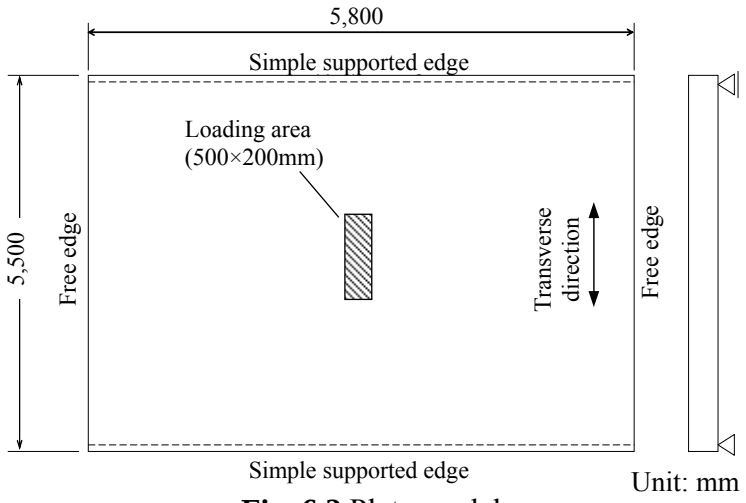

Fig. 6.2 Plate model

6.3 Bending stress of bottom plate

The bending moment of a plate can be calculated by a series solution. But, it is not feasible to carry out the plate analysis in practical design. Therefore, this study also employs the concept of replacing a plate with a beam by applying effective width for bending moment. If the effective width of plate is estimated properly, the maximum bending moment can be evaluated as the same value of a plate by beam theory.

On the other hand, the moment distribution of a beam is different from that of a plate. To obtain more accuracy bending moments, it is needed to correct the moment distribution. This like approach has been also used in the existing design method for calculating shear stress. Therefore, the plate analysis was performed by a series solution to correct bending moment distribution of a beam. The plate model is 5,500mm spanning, 5,800mm of width, and 250mm of slab thickness which are the same dimensions to 3D-FE model. The plate was simply supported under the load of 100kN at the center of plate. **Fig. 6.2** illustrates the plate model.

Fig. 6.4 shows the bending moment distributions obtained from plate analysis and beam theory. The effective width was calculated from plate analysis. The value was 3,605mm. It is found from the figure that bending moments by plate analysis and beam theory behave differently. In the plate analysis, the bending moment varied sharply with increasing distance from loading position. Therefore, bending moments calculated by beam theory was corrected as following equation (Refer **Fig. 6.3**):

$$M'(x) = \begin{cases} \dfrac{x}{a} M(x) & (x \le a) \\ \dfrac{l-x}{b} M(x) & (a \le x) \end{cases} \tag{6-1}$$

The bending moment distribution corrected as Eq. (6-1) is given in **Fig. 6.4**. Although the corrected bending moments are somewhat underestimated around supporting points, the distribution shape and values are very similar to the results of plate analysis. If the corrected equation becomes more complicated, the further close value can be obtained. But, in this study Eq. (6-1) is adopted in terms of simplicity.

In addition, another correction is added to Eq. (6-1). From the stress distribution of bottom plate by 3D-FEA shown in **Fig. 5.7** in Chapter 5, the average stress (bending stress) of bottom plate is nearly constant between the shear connectors, and varies at shear connectors like a step pattern. This is due to the fact that since the bond between

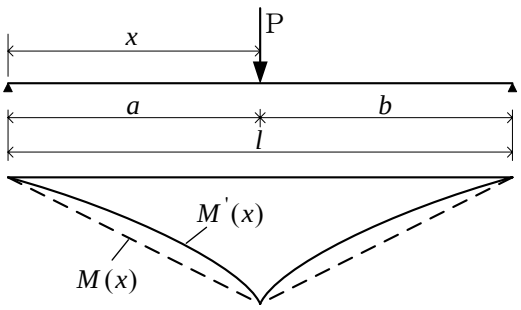

Fig. 6.3 Correction of bending moment

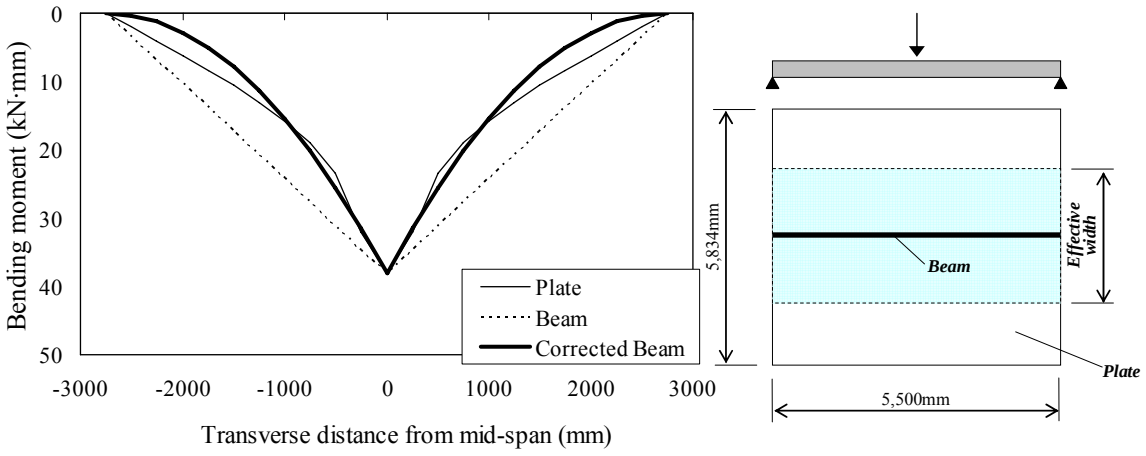

Fig. 6.4 Bending moment distribution

the steel and the concrete is neglected, the force is transmitted between steel and concrete only through shear connectors. It means that the bottom plate between shear connectors acts as a tensile member. Therefore, the bending moment of bottom plate between shear connectors is estimated by averaging bending moments of both side shear connectors, and then bending stress is calculated assuming that the whole section of slab is available.

Fig. 6.5 indicates the comparison of bending stresses calculated by the 3D-FEA and the proposed method stated above. Bending moments by the proposed method are slightly overestimated near the loading position. The reason may lie in the fact that the behavior of shear connector just below the applied load becomes very complicated. It is difficult to evaluate the complicated behavior as a simplified method. However, it is

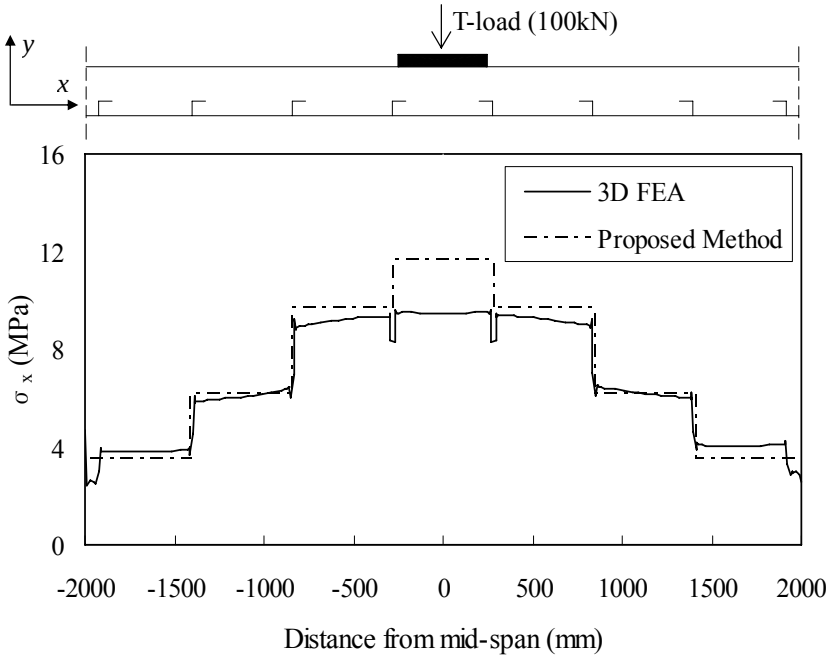

Fig. 6.5 Stress distribution on bottom plate

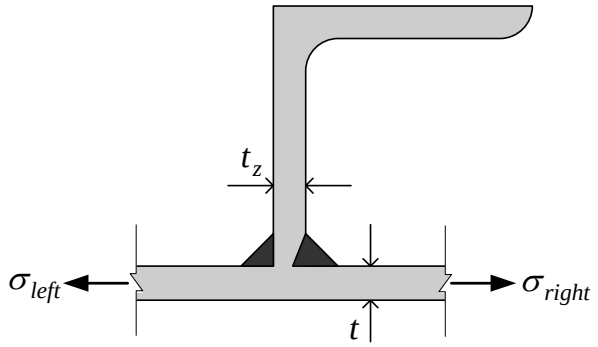

Fig. 6.6 Bending moment on bottom plate

considered that the error can be allowable because the proposed method provides conservative values even in the most critical case that the maximum bending stress occurs.

Even though there are some errors as mentioned above, the proposed method reflects well the local stress behavior of 3D-FEA. Therefore, after evaluating a stepped distribution of bending stress as the above method, the bending stress just below shear connector is estimated as the average value of bending stresses on the right and left side of bottom plates as following equation (Refer **Fig. 6.6**):

$$\sigma_n = \frac{1}{2}\left(\sigma_{left} + \sigma_{right}\right) \tag{6-2}$$

6.4 Shear stress of shear connector

It is predicted that the shear stress of shear connector is strongly related to the difference value between the right and left side bending stresses of bottom plate as shown in **Fig. 6.6**. Therefore, the shear stress per unit length of shear connector can be obtained as following equation:

$$\tau = \frac{t}{t_z}(\sigma_{left} - \sigma_{right}) \tag{6-3}$$

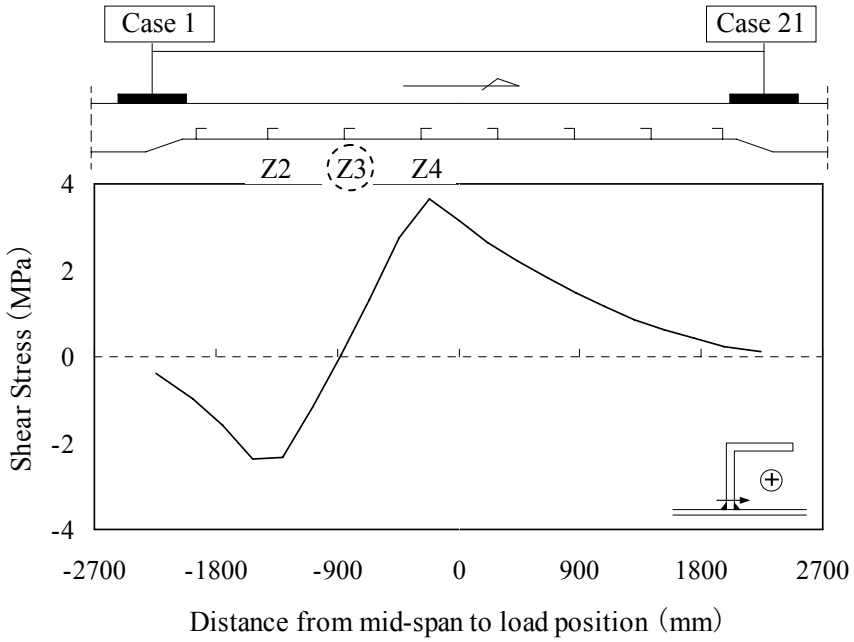

Fig. 6.7 Influence line for shear stress estimated by Eq. (6-3)

As an example, **Fig. 6.7** shows the influence line for shear stress on Z3 connector, which was estimated by Eq. (6-3). The effective width of 3,600mm was used for estimating shear stress. It can be seen that the shape of influence line coincides with the results of 3D-FEA shown in **Fig. 5.11**. However, the values are quite different. For other shear connector, similar phenomenon was also observed, and the results were summarized in Appendix D.

Shear stresses estimated by Eq. (6-3) were compared with the results of 3D-FEA for all shear connectors and load cases. The result is given in **Fig. 6.8**. The proposed method evaluates shear stresses about 3 times larger than 3D-FEA. A possible reason of that is the evaluating section of shear stress. Since the proposed method is based on the average shear stress along I - I section shown in **Fig. 5.10**, the force acting on weld bead could not be reflected. And also, the value of effective width for bending can be another reason.

However, compared with **Fig. 6.1**, the high correlation is observed. It means that the proposed method reflects well the nature of stress behavior. For the reason, this study proposes the estimating method for shear stress by correcting Eq. (6-3), as follow:

$$\tau = 0.299 \frac{t}{t_z} (\sigma_{left} - \sigma_{right}) \tag{6-4}$$

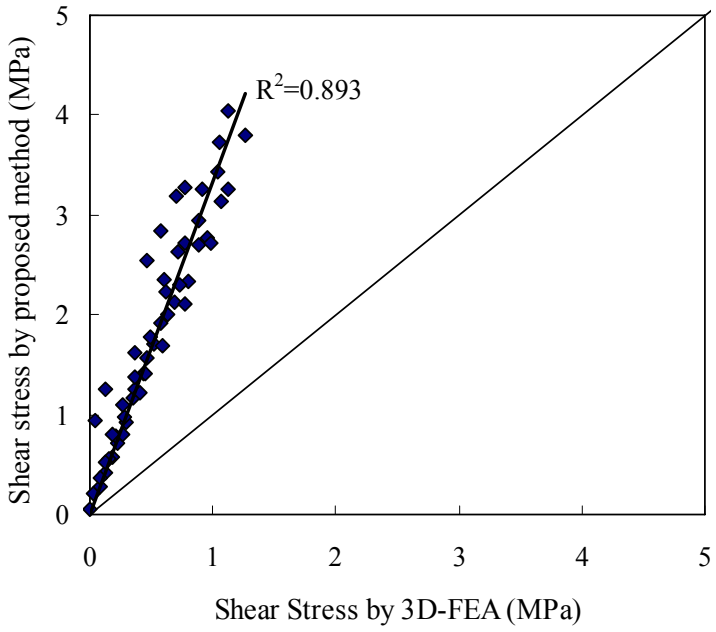

Fig. 6.8 Comparison of shear stress

6.5 Hot spot stress estimation

In the previous section, the simple estimating methods of shear stress and bending stress for each position of shear connectors was proposed. In this section, HSS is estimated by substituting the shear stress and the bending stress obtained from the proposed method into Eq. (5-1).

As an example, influence lines for HSS and bending moment at Z3 connector is given in **Fig. 6.9**. It can be observed two peaks in the figure. This is due to the fact that the estimating equation of stress concentration factor was obtained regardless the center-side and the end-side weld toe. The influence line represents good agreement with **Figs. 5.9 (a)** and **(b)**. Similar stress manners were also observed, and the results were summarized in Appendix D. **Fig. 6.10** shows the comparison of HSS for all load cases. Taken as a whole, both results are in good agreement.

Even though the proposed method is remarkably simple, it is possible to calculate shear stress of shear connector and bending stress of bottom plate when the bond between concrete and steel plate is lost. Furthermore, using the proposed method, stress concentration factor and HSS at welded joints can be estimated. **Fig. 6.11** illustrates the conceptual overview of the HSS estimation method.

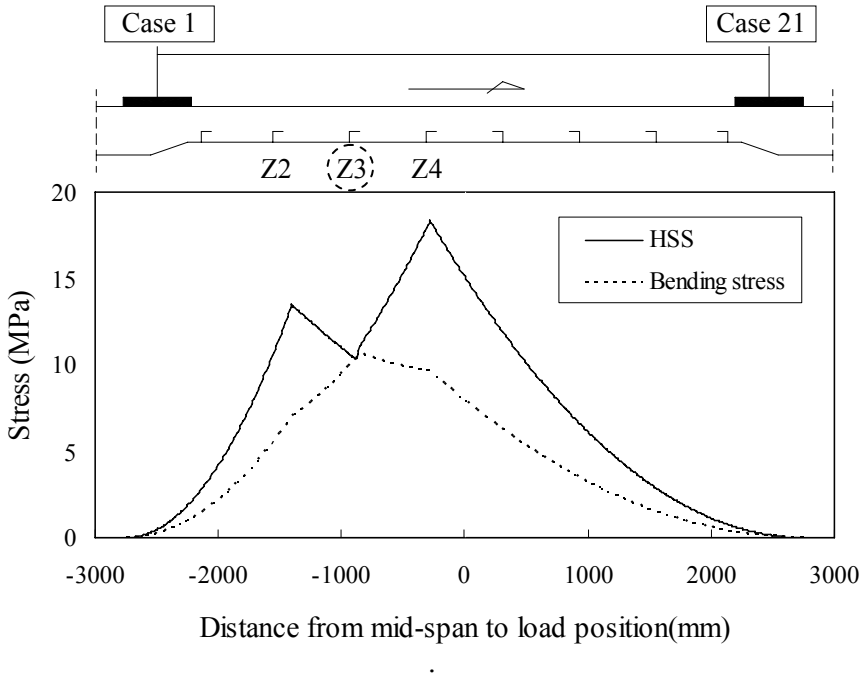

Fig. 6.9 Influence lines for HSS and bending moment by proposed method

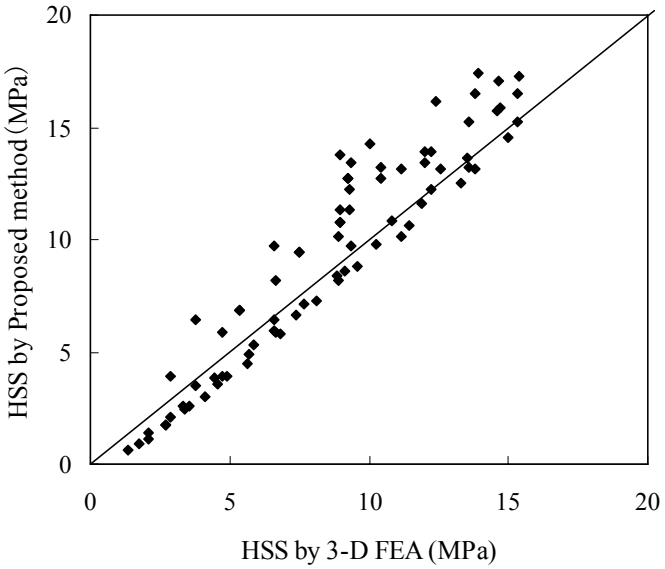

Fig. 6.10 Verification of proposed method

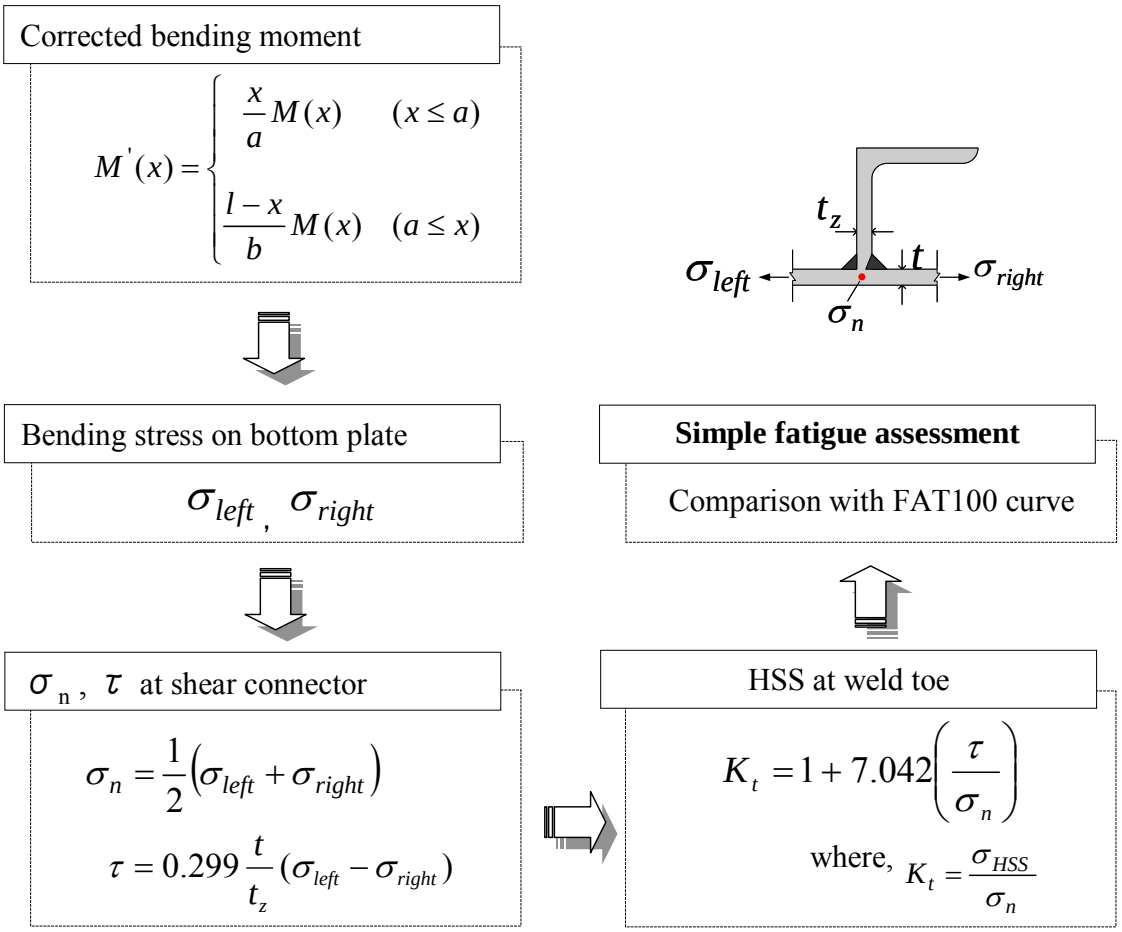

Fig. 6.11 HSS estimation method - conceptual overview

6.6 Concluding remarks

In chapter 5, it has been confirmed that HSS at the welded joint of shear connector is highly correlated to the shear stress on shear connector. The correlation is useful to estimate HSS, and the simple fatigue assessment can be performed on the investigated composite slab. On the other hand, in order to utilize the correlation equation for fatigue assessment, bending stress and shear stress for each position of shear connectors are essential factors. However, the current design methods cannot estimate bending stress and shear stress for each position of shear connectors.

In this chapter, evaluating methods of bending stress and shear stress for each position of shear connectors were proposed based on the unique stress behavior in the investigated composite slab. Consequently, combining with the correlation between stress concentration factor and shear stress presented in chapter 5, HSS can be estimated.

CHAPTER 7

SUMMARIES AND CONCLUSIONS

In steel-concrete composite slabs, it is difficult to detect fatigue cracks at welded joints at an early stage because welded joints of steel members are embedded in concrete. Therefore, if the fatigue cracks occur at welded joints and penetrate bottom plate, it leads to a considerable decrement in load-carrying capacity of composite slab. In addition, repairing work of the fatigue cracks is not feasible due to the complicated structure of composite slab. For the reasons, even though the possibility is relatively low, researchers and engineers should pay more attention to the fatigue damage of steel members.

In this dissertation, fatigue resistance of angle shape shear connector used in steel-concrete composite slabs was examined through experimental study and numerical analysis. Furthermore, a simple method of fatigue assessment on the welded joint of angle shape shear connector was proposed by 3D-FEA results on actual composite slab. In actual composite slabs, the bond action is expected between steel and concrete. However, this study assumed the worst condition that the bond was completely lost due to the numerous repeated loads in long-term service life. The following is summary of the research findings.

In chapter 2, the local stress behavior of the composite slab using angle shape shear connector was investigated by experimental and numerical study on large-scale plate specimens to identify the possible weak point against fatigue. Moreover, by comparing the flexural strength for two specimens having different interval of shear connectors, the possible economic design of slab section was identified. Based on the results, the following conclusions are reached.

1) Local bending deformation of bottom plate occurred around the welded joints of shear connectors in test and FEA results, and the local bending deformation caused the stress concentration at weld toe.

2) Below the load of 300kN, a relatively good agreement between FEA and test

results was identified. Considering that the single truck load is 100kN, it can be said that this FE model is useful to simulate the investigated composite slab in terms of fatigue problem.

3) The fracture loads of two specimens with different interval of shear connectors were almost same level as 1050kN and 1120kN, respectively. Stress behavior and fracture mode were also similar. Therefore, it can be said that there is possibility to extend the interval of shear connectors in terms of flexural strength. However, fatigue assessment should be required for more economic design of slab section.

4) Composite slabs are fractured by punching shear failure of concrete plane. Moreover, concrete cracks initiated from the edge of shear connectors were also observed. Even though the possibility is low that this like concrete crack occurs in actual composite slab, the cracks can be further critical damage than the punching shear fracture under the fluctuating load.

In chapters 3 and 4, from the FEA and test results on large-scale plate specimen, it was confirmed that the stress concentration occurs at welded joints. It means the welded joint is a weak point against fatigue. Therefore, fatigue tests on push-out specimen and beam specimen which can simulate the local stress concentration were carried out in order to examine fatigue strength of the welded joint of angle shape shear connector. It was demonstrated that:

1) Stress concentration due to the local bending deformation of bottom plate occurs at the welded joint of shear connectors, and it causes fatigue damage on the welded joint Fatigue crack was initiated at the welded toe, and propagated to the thickness direction. In addition, the present FE analysis results represented a good agreement with the test results.

2) The welded joint between bottom plate and angle shape shear connector satisfies with the FAT100 curve which is reference curve of fatigue strength in using HSS proposed by IIW. Therefore, the fatigue strength of the welded joint can be conservatively assessed by using the hot spot stress and the design curve of FAT100.

From the fatigue test on push-out specimens and beam specimens, it was confirmed that the fatigue assessment can be carried out by using HSS and FAT100 curve. It means that if HSS is estimated, simple fatigue assessment can be conducted by comparing HSS with FAT100 curve. However, laboratory tests are time-consuming and very expensive. From the stress analysis for large-scale plate model, beam model, and push-out shear model. The FE models were validated for the no-bond condition between steel and concrete.

In chapter 5, a numerical approach for estimating local stress concentration was examined on actual composite slabs by FEA. From the results, the following conclusions are reached.

1) Local bending deformation of bottom plate is also originated around shear connector in actual composite slab models. The maximum hot spot stress at welded joints was below 20MPa under the design truck load. Considering that the cut-off limit of FAT100 category is 58MPa, the possibility of fatigue damage at the welded joint in this type of composite slab is very low.

   The result represents that the composite slab section can be designed more economically by reducing the number of shear connector or CT-shape steel in terms of fatigue strength. However, it is difficult to perform this like of 3D-FEA for each case of slab section in design step. Therefore, a simple estimating method of HSS was examined based on the results of 3D-FEA.

2) Stress concentration factor and shear stress normalized by bending stress had a high correlation regardless of slab section and loading position. The correlation will provide the researchers and structural engineers with valuable tool for estimating HSS at welded joints of shear connectors in the investigated composite slab.

In chapter 6, evaluating methods of bending stress and shear stress for each position of shear connectors were proposed based on the unique stress behavior in the investigated composite slab using angle shape shear connector. Consequently, simple fatigue assessment can be carried out by substituting the bending stress and shear stress into the correlation equation between SCF and shear stress.

BIBLIOGRAPHY

Abe, H., Nakajima, A, and Horiuchi, H.: Effect of Division of Slabs in Composite Girder and Development of Flexible Connectors, *Journal of Structural Engineering, JSCE*, 35A, pp.1205-1214, 1989. (In Japanese)

Asano, K., Matsuda, H., Soga, A., Uchida, D., and Kobayashi, K.: Development of New Steel Deck-Concrete Composite Deck Girder Bridge of Higher Fatigue Durability, *Mitsui Zosen Technical Review*, No.199, pp39-46, 2010.2. (In Japanese)

Basker, K., Shanmugam, N.E., and Thevendran, V.: Finite-Element Analysis of Steel-Concrete Composite Plate Girder, *Journal of Structural Engineering*, Vol.128, No.9, pp1158-1168, 2002

Carreira, D.J., and Chu, K.H.: Stress-stain relationship for plain concrete in compression, *ACI., Proc.*, Vol.82, No.11, pp.797-804, 1985.

Choi, S.M., Tateishi, K., Uchida, D., Asano, K., and Kobayashi, K.: Fatigue Resistance for Welded Joint of Shear Connector used in Composite Slab, *Pacific Structural Steel Conference2010*, pp1043-1048, 2010.

Choi, S.M., Tateishi, K., Uchida, D., Asano, K., and Kobayashi, K.: Fatigue Strength of Angle Shape Shear connector used in Steel-Concrete Composite Slab, *International Journal of Steel Structures*, Vol.8, No.3, pp199-204, 2008.

Chuah, C.L., Shima, H., and Virach, R.: Load-Displacement Relationship of Plate Shape Shear Connector in Steel-Concrete Composite Structures, *Proceedings of the Japan Society of Civil Engineers*, Vol.15, No.433, pp.223-229, 1991.

Fukazawa, K., Sakai, M., Sudou, N., and Kobayashi, K.: Fatigue durability of steel-concrete composite slab, MELAB and application to continuous composite steel girder bridge, *Mitsui Zosen Technical Review*, I-456, pp8-18, 2002.6. (In Japanese)

Gattesco, N., Giuriani, E., and Gubana, A.: Low-Cycle Fatigue Test on Stud Shear connectors, *Journal of structural engineering*, Vol.123, pp. 145-150, 1997

Hobbacher, A.: Recommendations for fatigue design of welded joints and components, *International Institute of Welding*, IIW document XIII-2151-07/XV-1254-07, 2007.

Horikawa, T., and Sonoda, k.: Theoretical Analysis and Experiment for Shearing Force on Studs in a Steel Plate and Concrete Composite Slab for Bridge Deck, *Journal of Structural Engineering*, JSCE, Vol.33A, pp299-306, 1987. (In Japanese)

Japan Road Association (JRA): Fatigue design guidelines for steel highway bridges, 2002. (In Japanese)

Japan Society of Civil Engineers (JSCE): *Design Code for Steel Structures, PART B; Composite Structures*, 1997

Japan Society of Steel Construction (JSSC): *Fatigue Design Recommendation for Steel Structures*, 1995.

Kajikawa, Y. and Maeda, Y.: Fatigue Strength of Flange Plate with Stud Shear Connector subjected to Combined Tension and Shear, *Proceedings of the Japan Society of Civil Engineers*, No.362, pp285-292, 1985. (In Japanese)

Kakuta, Y, and Fujita, Y.: Fatigue Strength of Reinforced Concrete Slabs Failing by Punching Shear, *Proceedings of the Japan Society of Civil Engineers*, No.317, pp149-157, 1982. (In Japanese)

King, D.C., SLUTTER, R.G.., and Driscoll, G.C.: Fatigue Strength of 1/2-inch Diameter Stud Shear Connectors, *Highway Research Board*, No 103, pp.78-106, 1965.

Lee, P. G., Shim, C. S., and Chang, S. P.: Static and fatigue behavior of large stud shear connectors for steel–concrete composite bridges, *Journal of Constructional Steel Research*, Vol.61, pp. 1270-1285, 2005

Maeda, Y. and Matsui, S.: Experimental study on structural behavior and load carrying capacity of full-sized steel grating floors, *Proceedings of the Japan Society of Civil Engineers*, No.181, pp1-14, 1970. (In Japanese)

Maleki, S. and Bagheri, S.: Behavior of channel shear connectors, Part I: Experimental study, *Journal of Constructional Steel Research*, 64, pp.1333–1340, 2008.

Maleki, S. and Bagheri, S.: Behavior of channel shear connectors, Part Ⅱ: Analysis study, *Journal of Constructional Steel Research*, 64, pp.1341–1348, 2008.

Matsui, S., Hiragi, H., and Fukumoto, Y.: Derivation of Strength Equations of Headed Stud Shear Connectors, *Journal of Structural Engineering, JSCE*, Vol.35A, pp.1233-1243, 1989 (In Japanese)

Matsui, S., Sakaki, H., Fukumoto, Y., and Kajikawa, Y: Fatigue of Steel-Concrete Decks Subjected to A Moving Wheel Load, *Journal of Structural Engineering, JSCE*, Vol.34A, pp.409-420, 1988 (In Japanese)

Nakai, H., Matsui, S., Yoda, T., and Kurita, A.: Trends in Steel-Concrete Composite Bridges in Japan, *Structural Engineering International*, Vol.8, No. 1, pp. 30-34(5), 1998.

Research on Fatigue Durability Evaluation for Highway Bridge Slabs, National Institute for Land and Infrastructure and Transport, Japan, Technical Note of NILIM, No.472, 2008.

Ros, S. and Shima, H.: A New Beam Type test Method for Load-Slip Relationship of L-shape Shear Connector, *The 8th Symposium on Research and Application of Hybrid and Composite Structures*, 60,1-8, 2009.

Saidi, T., Furuuchi, H., and Ueda, T.: Relationship between Transferred Shear Force and Relative Displacement of Shear Connector in Steel-Concrete Sandwich Beam, , *Journal of Structural Engineering*, JSCE, 44(A), pp.1537-1545, 1998.

Saidi, T., Furuuchi, H., and Ueda, T.: The Transferred Shear Force-Relative Displacement Relationship of the Shear Connector in Steel-Concrete Sandwich Beam and its Model, *Proceedings of the Japan Society of Civil Engineers*, Vol.64, No.1, pp122-141, 2008.

Sawano, K., Hamada, S., Wakabayashi, T., and Nauoka, M.: Fatigue strength of 19mm Diameter Stud Shear, *Proceedings of the Japan Society of Civil Engineers*, No.174, pp.1-8, 1970 (In Japanese)

Slutter R.G. and Fisher J.W.: Fatigue Strength of Shear Connectors, *45th Annual Meeting of Highway Research Board*, No.316, 1966.

Sonoda, K., Horikawa, T., and Hirose, K.: Effective Width for the Design of Shear Connectors of Steel Deck and Concrete Composite Bridge Slabs, *Proceedings of the Japan Society of Civil Engineers*, No.338, pp1-9, 1983. (In Japanese)

Sonoda, K., Horikawa, T., Kitoh, H., and Kiso, S.: Shearing Force on Studs and Punching Shear Load of a Steel Plate and Concrete Composite Slab, *Proceedings of the Japan Society of Civil Engineers*, No.404, pp249-258, 1989. (In Japanese)

Tateishi, K., Choi, S.M., Uchida, D., Asano, K., and Kobayashi, K.: Fatigue Strength of Steel-Concrete Composite Slab using Angle Shape Shear Connector, *Steel Construction Engineering*, JSSC, Vol.14, No.55, pp.123-131, 2007. (In Japanese)

Tateishi, K., Choi, S.M., Uchida, D., Asano, K., and Kobayashi, K.: Local Stress Behavior around Welded Joint of Angle Shape Shear Connector used in Steel-Concrete Composite Slab, *Steel Construction Engineering*, JSSC, Vol.8, No.3, pp199-204, 2009. (In Japanese)

Thürlimann B.: Fatigue and Static Strength of Stud Shear Connectors, *ACI Journal*, 30, pp.1287-1302, 1959.

Toprac, A.A.: Fatigue Strength of 3/4-Inch Stud Shear Connectors, *Highway Research Board*, No.103, pp.53-77, 1965.

Yasumoto, S. and Sakuma, M.: A Study on the Effective Width of Concrete Slab Bridges, *Proceedings of the Faculty of Engineering of Tokai University*, 23(1), pp.69-87, 1983. (In Japanese)

APPENDIX A: Stress distribution on large-scale plate specimens

Following figures are stress distribution on bottom plate of large-scale plate specimens corresponding to **Fig. 2.11** and **2.12** in Chapter 2.

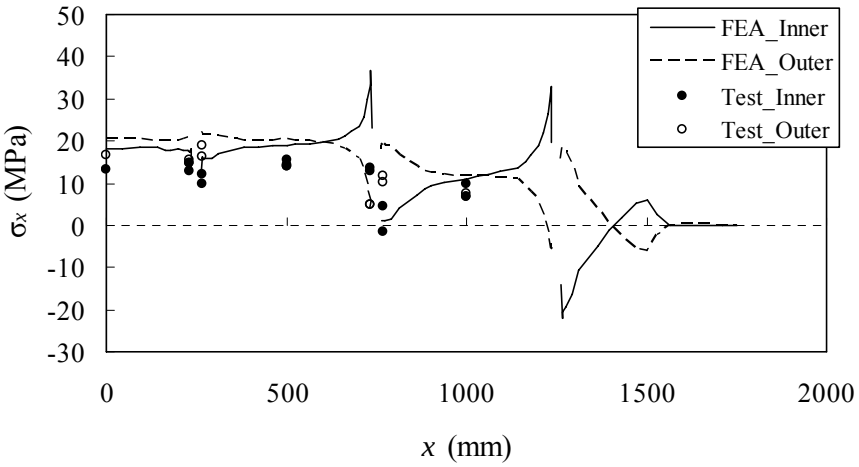

(a) 100kN

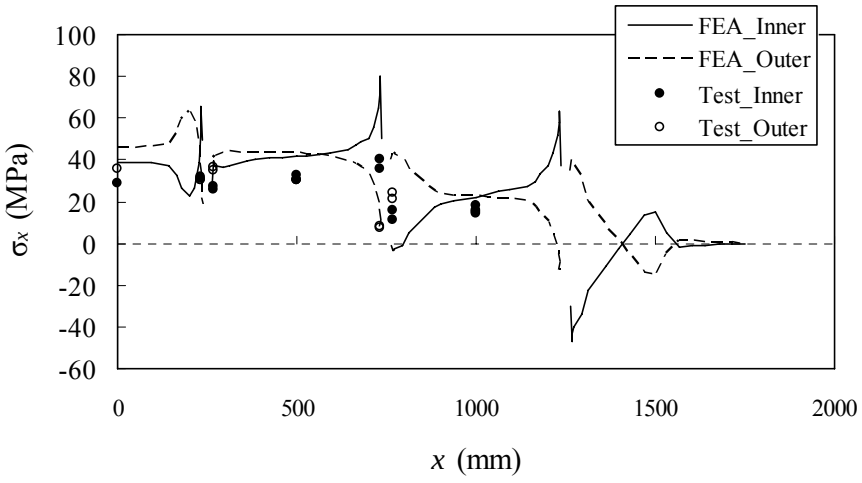

(b) 200kN

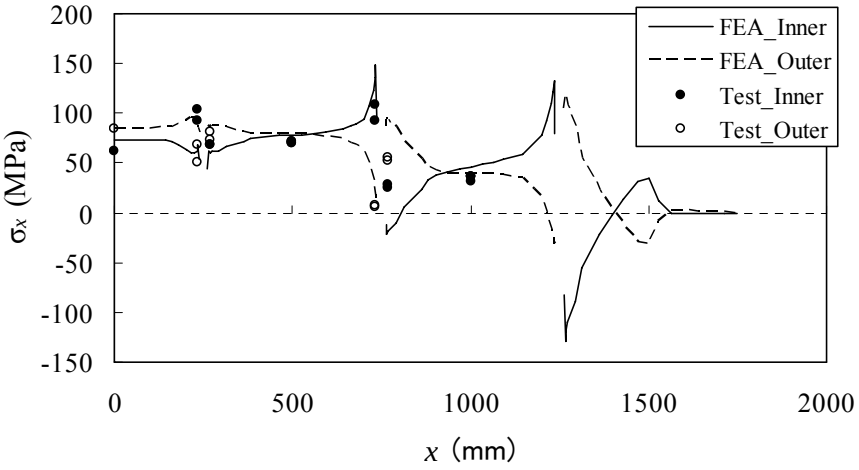

(c) 400kN

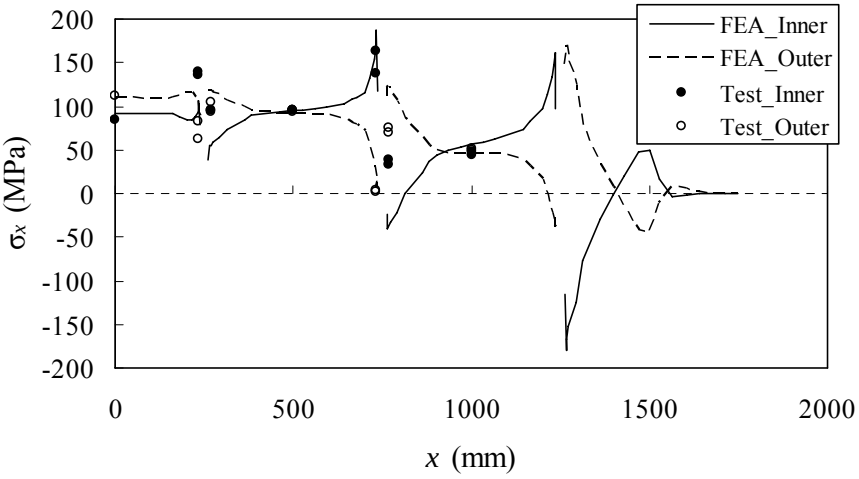

(d) 500kN

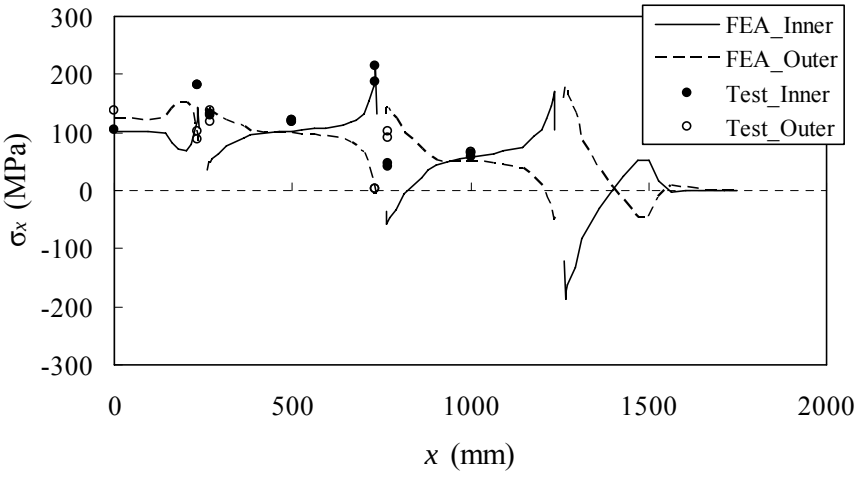

(e) 600kN

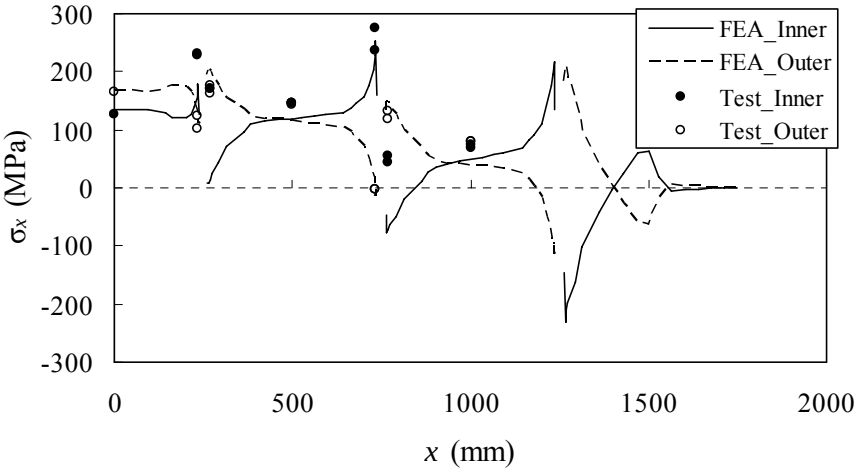

(f) 700kN

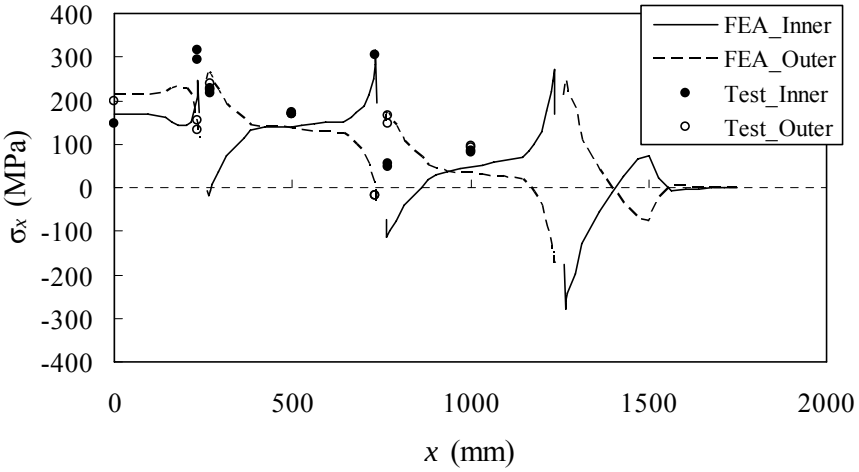

(g) 800kN

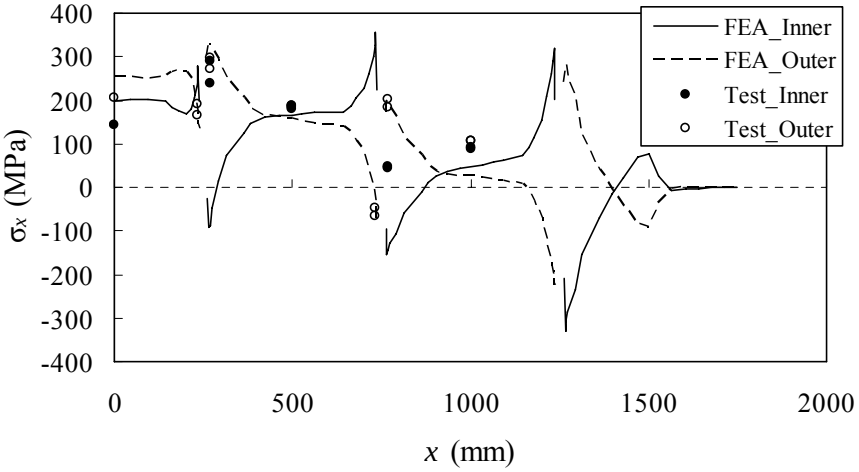

(h) 900kN

Fig. A.1 Stress distribution on bottom plate in *x*-direction (ST1)

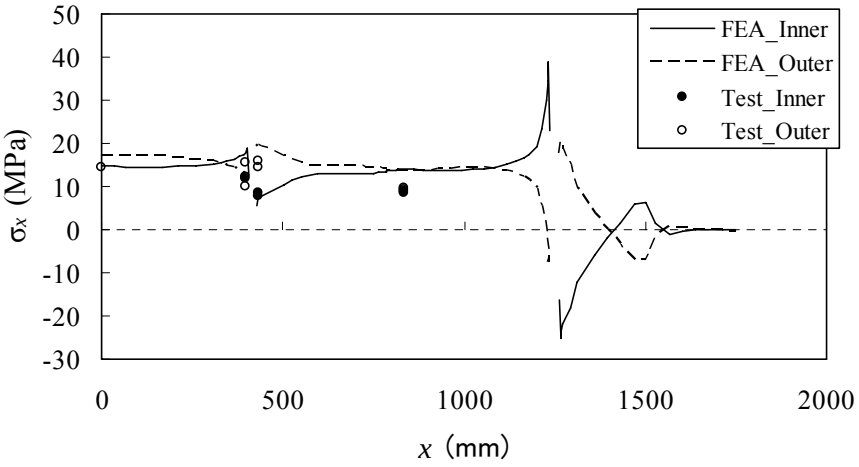

(a) 100kN

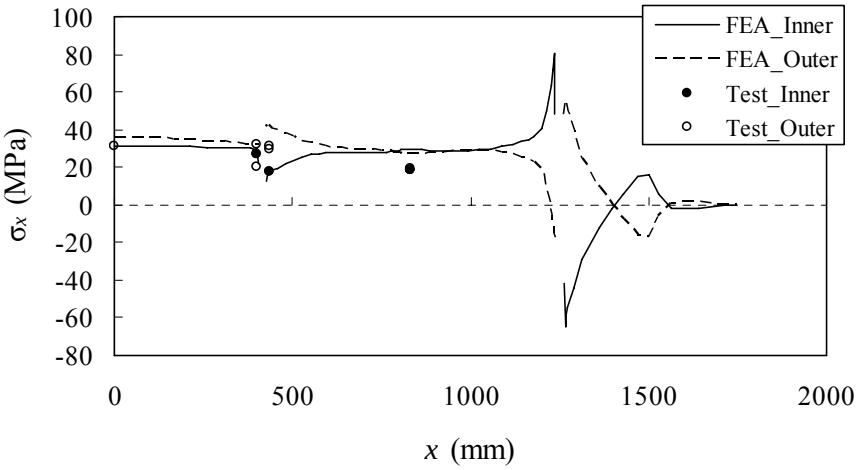

(b) 200kN

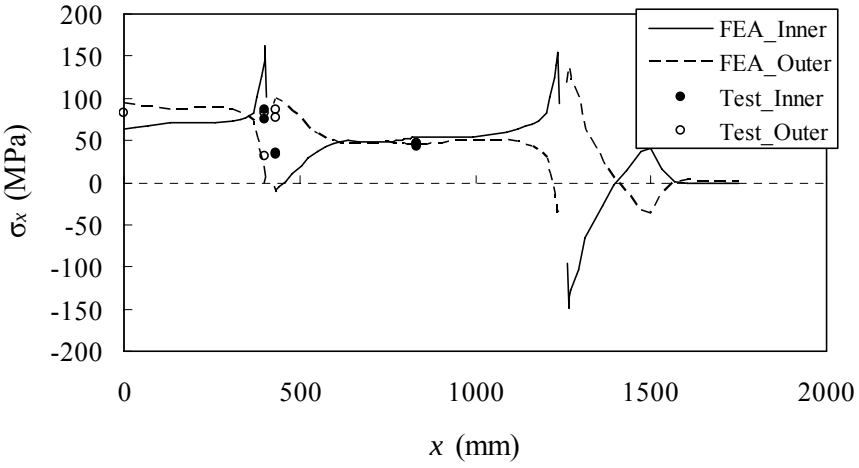

(c) 400kN

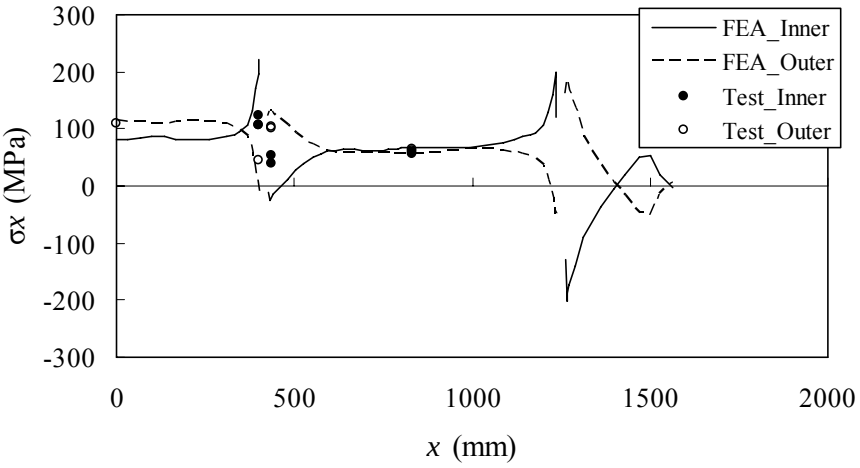

(d) 500kN

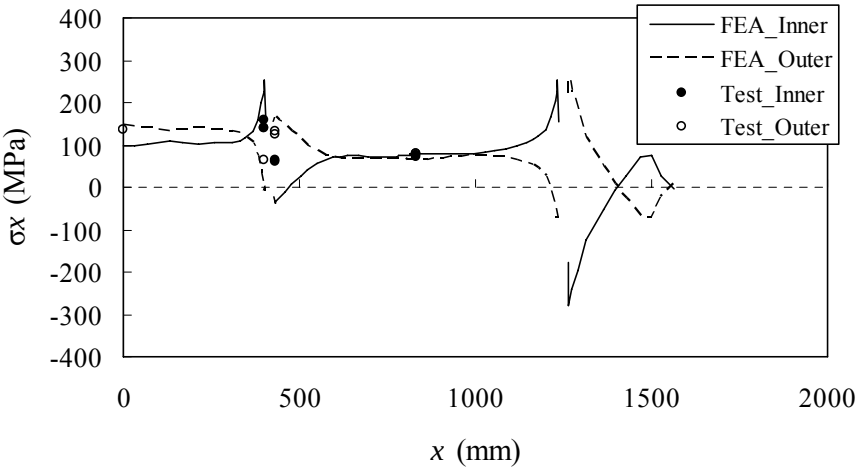

(e) 600kN

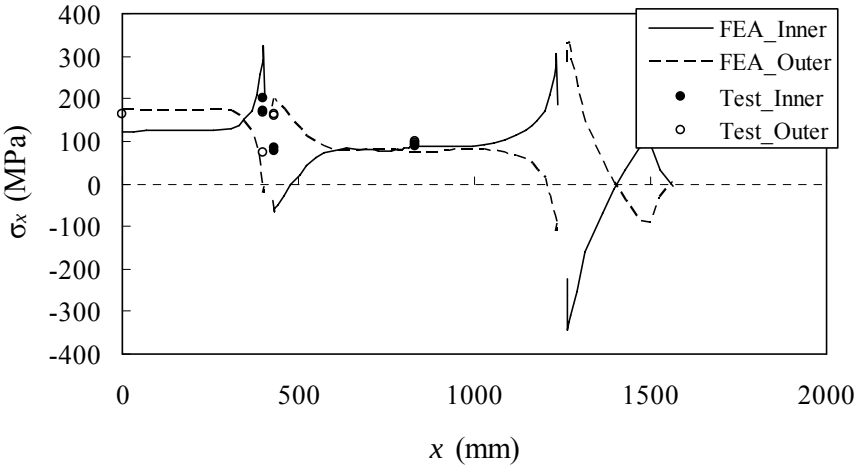

(f) 700kN

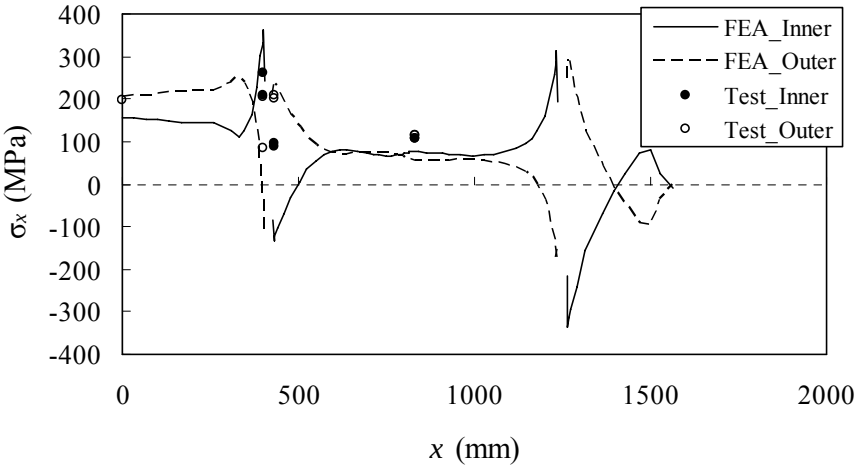

(g) 800kN

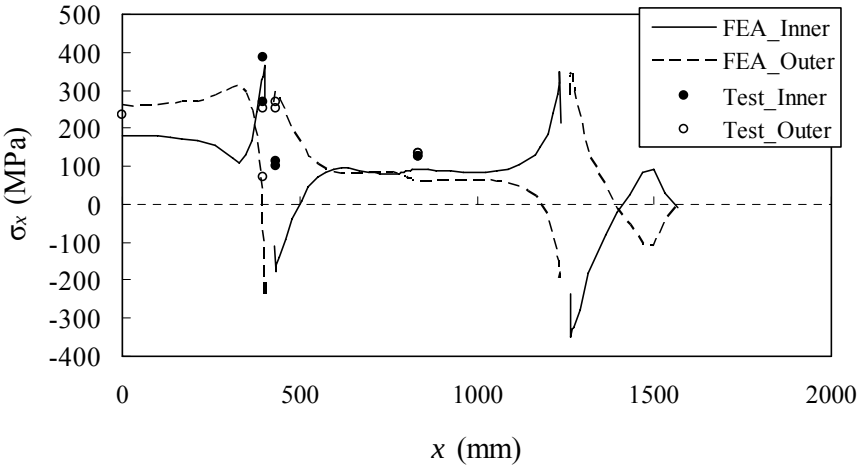

(h) 900kN

Fig. A.2 Stress distribution on bottom plate in *x*-direction (ST2)

APPENDIX B: Strain histories on push-out specimen (S-120)

Following figures are strain histories on push-out specimen in Chapter 3. The gauge numbers shown in the figure are consistent with those in **Fig. 3.3**.

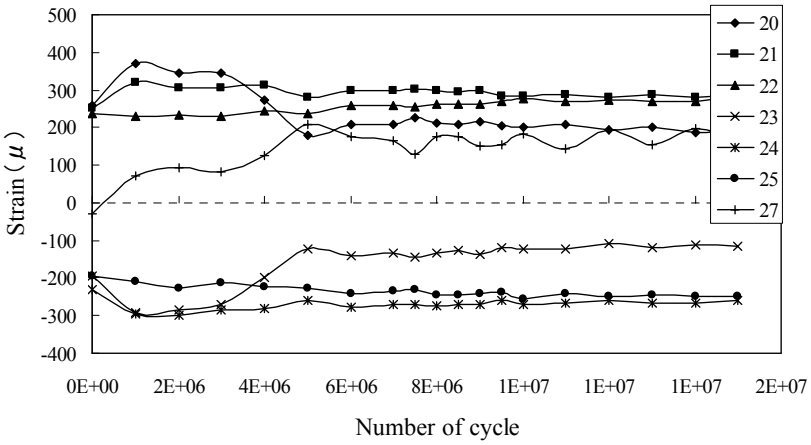

(a) on shear connector

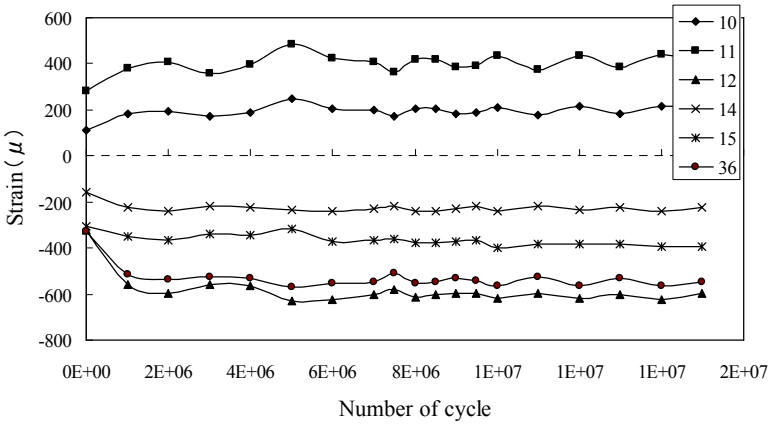

(b) on bottom plate

Fig. B.1 Strain histories in S-120

APPENDIX C: FEA results on actual composite slab

Following figures are FEA results on actual composite slab corresponding to **Fig. 5.9** and **5.11** in Chapter 5.

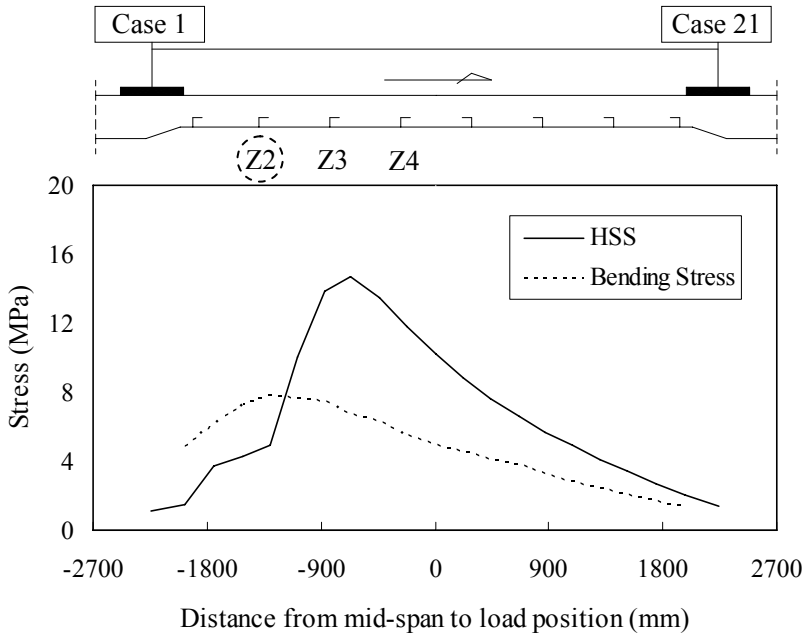

a) Center-side weld toe

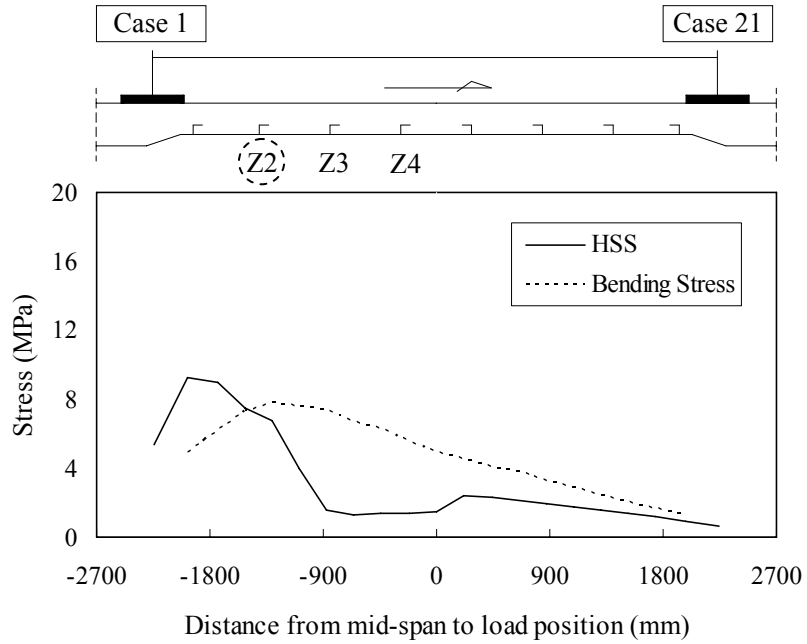

b) End-side weld toe

Fig. C.1 Influence lines for HSS and bending moment (near Z2)

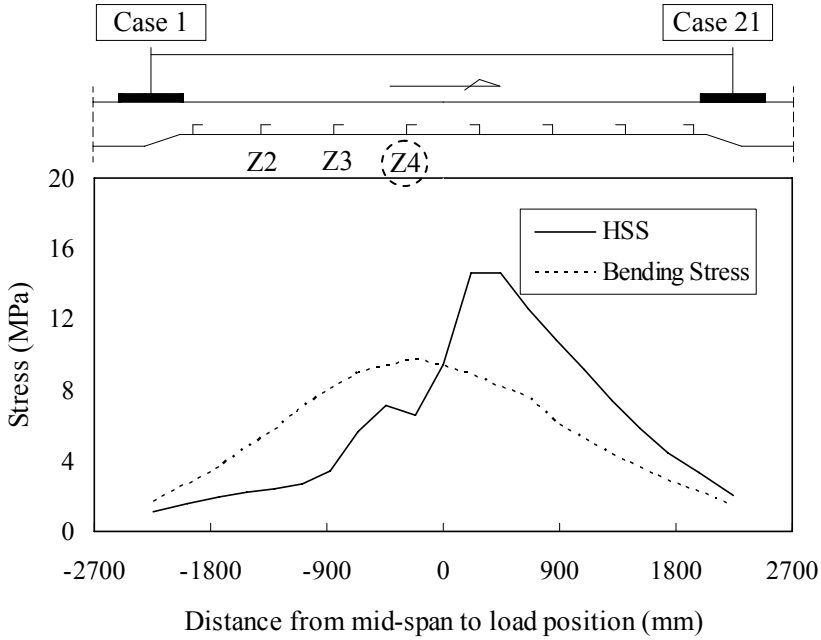

a) Center-side weld toe

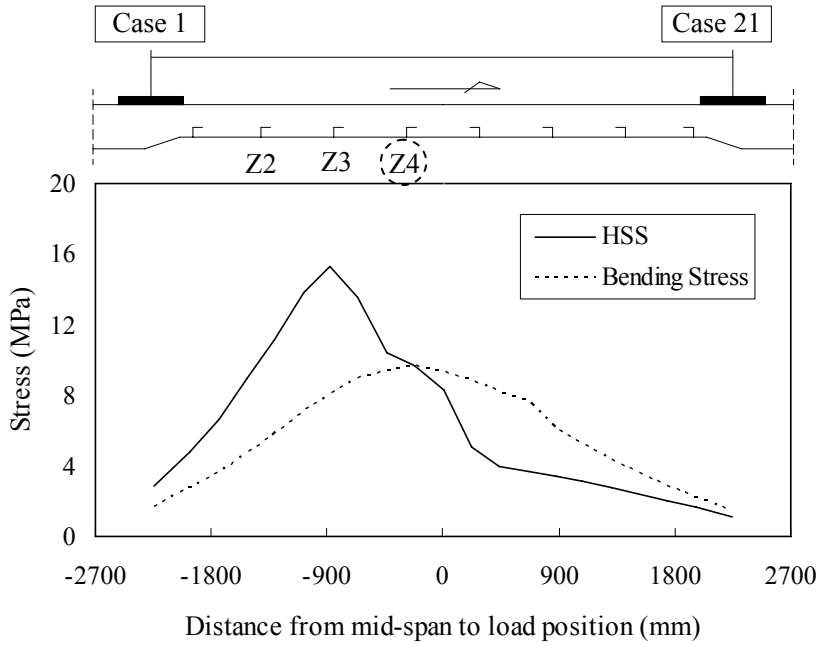

b) End-side weld toe

Fig. C.2 Influence lines for HSS and bending moment (near Z4)

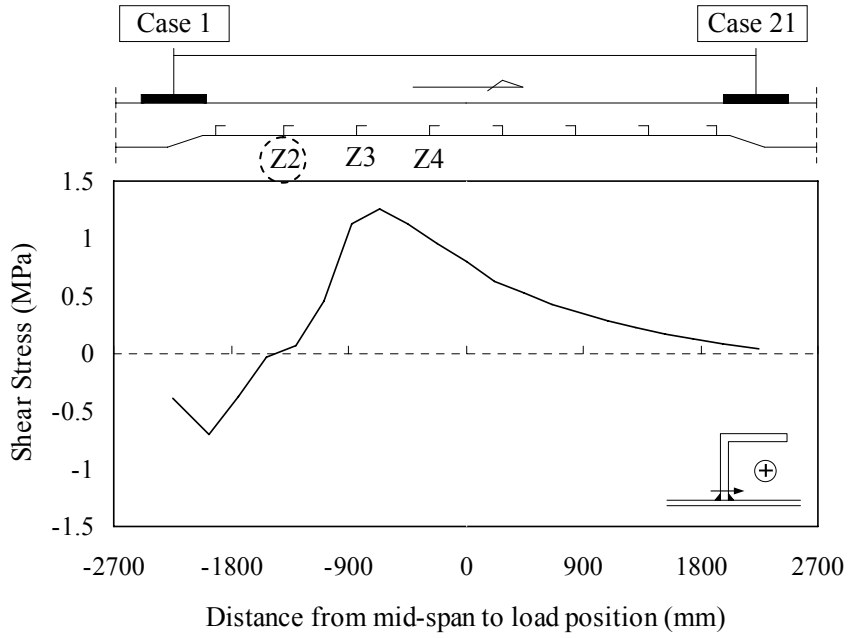

(a) on Z2

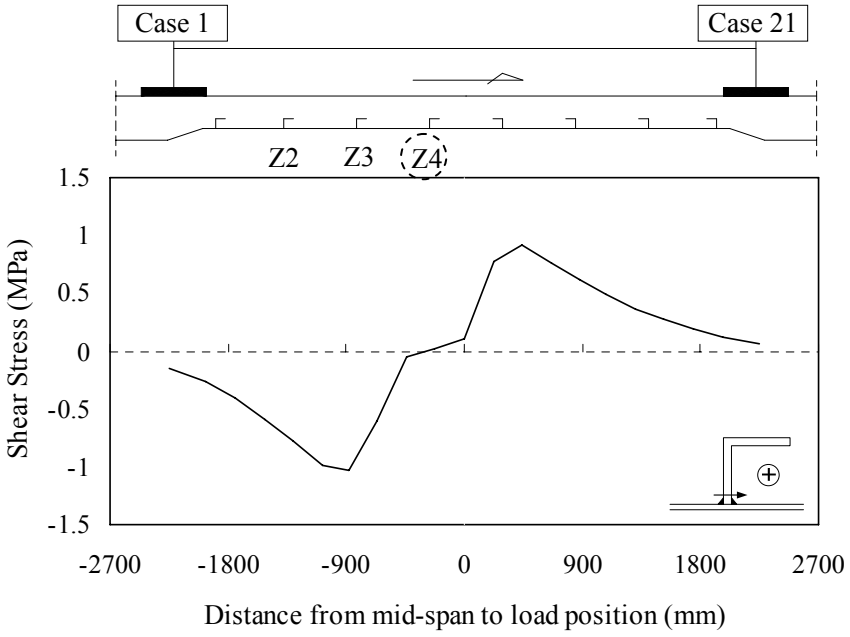

(b) on Z4

Fig. C.3 Influence line for average shear stress by FEA

APPENDIX D: Calculation results by proposed method

Following figures are calculating results by the proposed method corresponding to **Fig. 6.7** and **6.9** in Chapter 6.

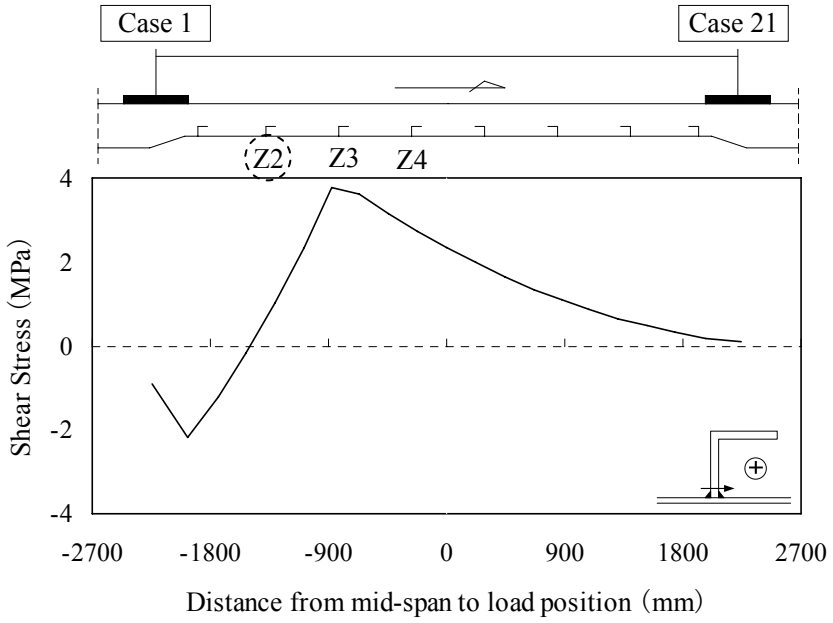

(a) Z2

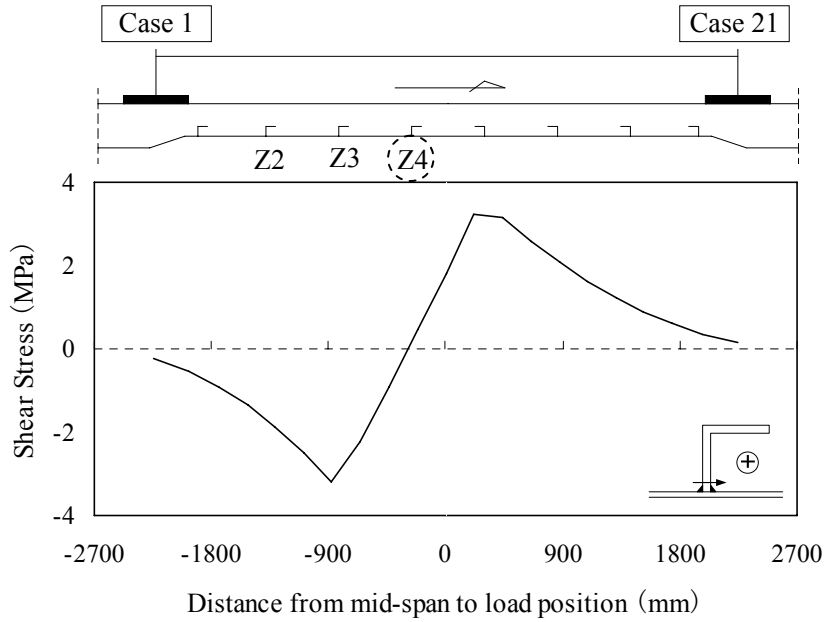

(b) Z4

Fig. D.1 Influence line for shear stress estimated by Eq. (6-3)

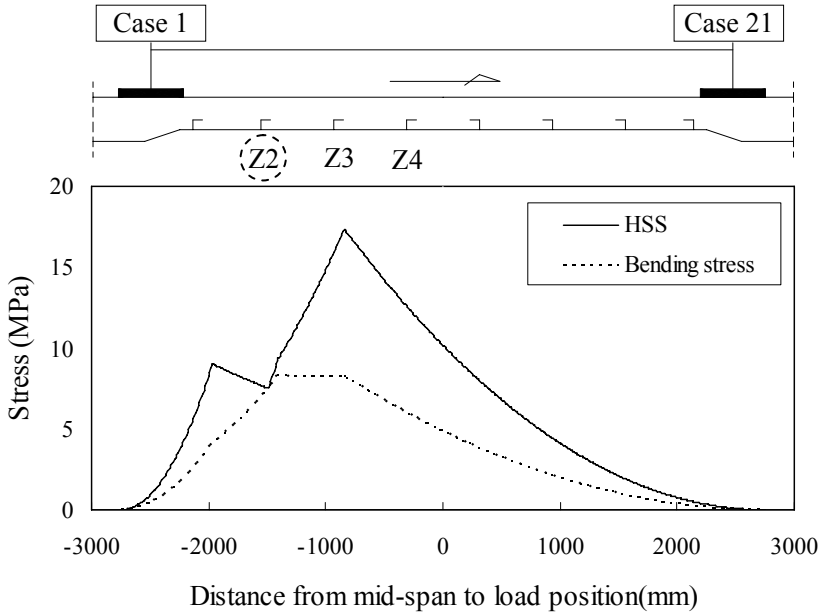

(a) near Z2

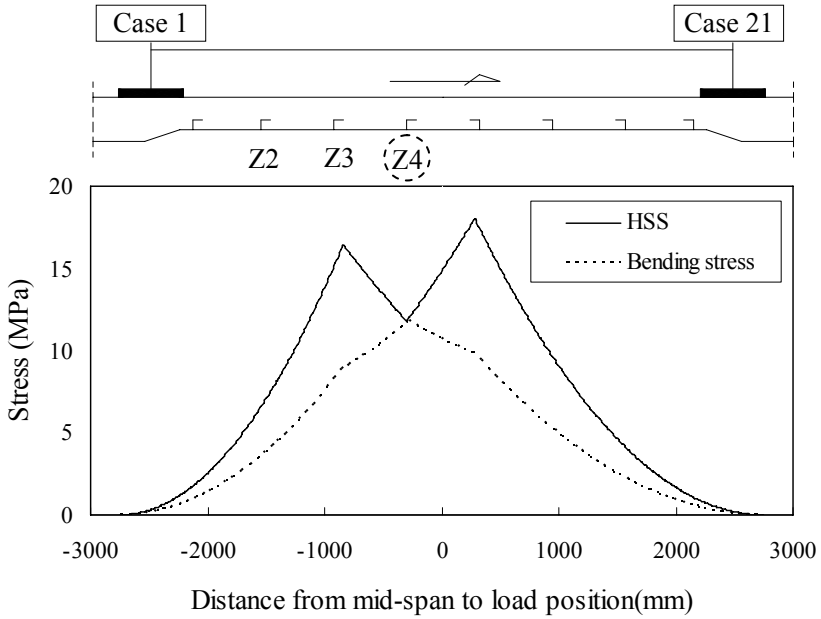

(b) near Z4

Fig. D.2 Influence lines for HSS and bending moment by proposed method

APPENDIX E: Fatigue test on perforated rib

Perforated rib is another type of shear connector used in composite slabs (Asano, K. et al., 2010). In the fatigue test on beam specimen described in Chapter 4, the fatigue strength of perforated rib was also investigated. Dimensions of specimen are the same as the beam specimen using angle shape shear connector.

Fig. E.1 illustrates the configurations and dimensions of specimen, and **Table E.1** presents the conditions and results of fatigue test. In the Table, fatigue life was deduced values by strain histories monitored by strain gauges.

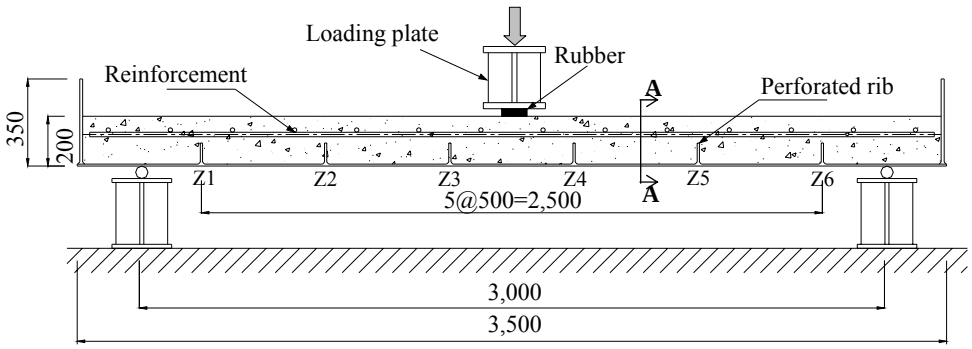

(a) Side view

Unit: mm

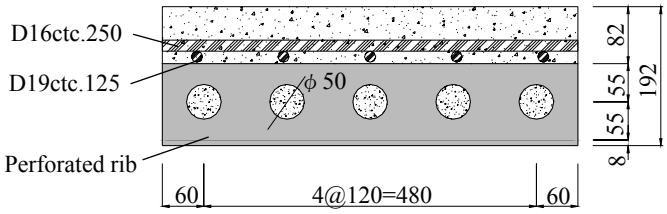

(b) A-A section

Fig. E.1 Configurations and dimensions of specimen

Table E.1 Fatigue test conditions and results

Spec.	Min. load (kN)	Max. load (kN)	Frequency (Hz)	Fatigue life ($\times 10^4$)	Fatigue crack
P-72	2	72	2	170	Z2
P57	2	57	2	790	Z2

The fatigue crack was detected on the outer surface of bottom plate just below the center-side weld toe at Z2 as shown in **Fig. E.2**.

Fig. E.3 is the fatigue test results arranged by the HSS with the results of angle shape shear connectors. Although the fatigue strength of perforated rib is assessed slightly lower than that of angle shape steels, the fatigue test results satisfy the class FAT100.

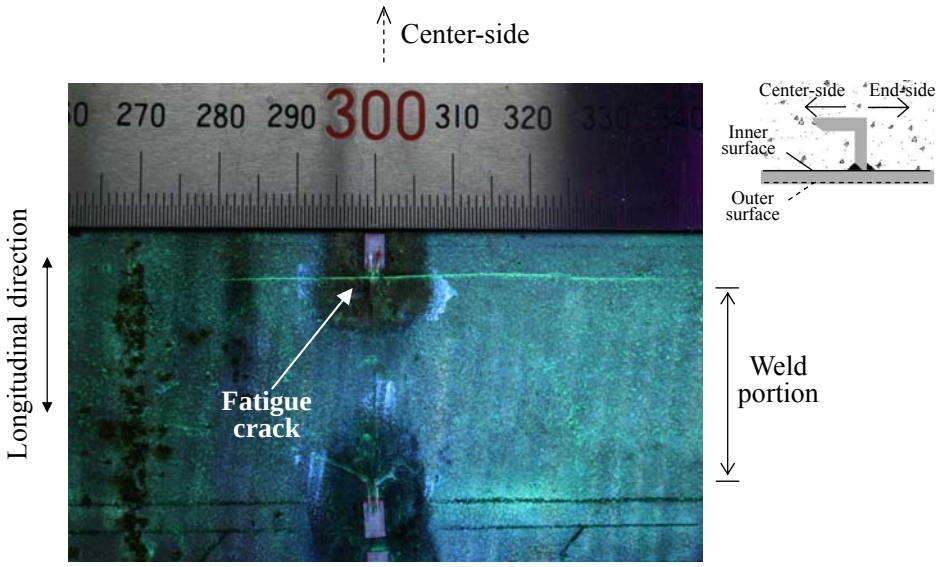

Fig. E.2 Fatigue crack on bottom plate (Lower view)

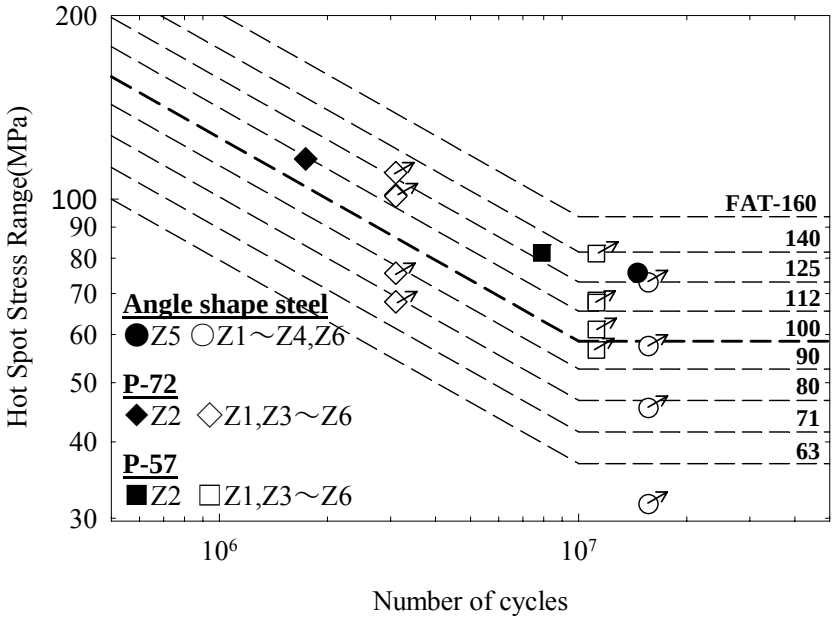

Fig. E.3 Fatigue strength of perforated rib